Modulation of protein expression in *Mycobacterium tuberculosis*-stimulated, TB-IRIS patient-derived PBMCs by n-3 polyunsaturated fatty acids

Marine Anne Barnabé

(BRNMAR077)

Submitted to the University of Cape Town

In fulfilment of the requirement for the degree:

MSc(Med) Chemical Biology

Faculty of Health Sciences

UNIVERSITY OF CAPE TOWN

10 January 2018

Supervisor: Professor Jonathan Blackburn

DECLARATION

I, Marine Anne Barnabé, hereby declare that the work on which this dissertation/thesis is based is my original work (except where acknowledgements indicate otherwise) and that neither the whole work nor any part of it has been, is being, or is to be submitted for another degree in this or any other university.

I have used the Nature convention for citation and referencing. Each contribution to, and quotation in, this thesis from the work(s) of other people has been attributed, and has been cited and referenced.

I empower the university to reproduce for the purpose of research either the whole or any portion of the contents in any manner whatsoever.

Signed by candidate

10 Jan 2018

Marine Anne Barnabé

Date

Acknowledgements

Thanks must go to the following persons for making noteworthy contributions to the current work.

To my supervisor Prof. Jonathan Blackburn, for enabling this work.

To Dr Janique Peyper, for her guidance and help in kick-starting this project, and her expertise in immunology amongst others.

To Dr Clemens Hermann, for his invaluable help in reading the thesis draft, and his pertinent insights.

To Dr Bridget Calder, for her help and incredible expertise in all things MS-related, and most of all her friendship.

To the Blackburn lab members and Nazla, for always creating a positive and friendly working environment.

To the NRF, for funding my Master's degree.

To my parents, for their support, both moral and financial, throughout these two (sometimes difficult) years.

And most of all, to my partner Lloyd without whom I would have no doubt given up. Thank you for your unwavering support and belief in me, I could not have done it alone.

Abstract

Tuberculosis-associated immune reconstitution inflammatory syndrome (TB-IRIS) is an inflammatory disorder which affects up to 54% of TB-HIV co-infected patients. Its pathogenesis remains unclear, and although treatment with the corticosteroid prednisone has shown some benefits, there is no specific treatment currently available for TB-IRIS. N-3 polyunsaturated fatty acids (PUFA) have safely and successfully been used in the treatment of other inflammatory diseases, and we hypothesized that they will have beneficial anti-inflammatory effects on TB-IRIS patient-derived immune cells.

To investigate this hypothesis, we used mass spectrometry (MS)-based proteomic methods to probe the secretome of peripheral blood mononuclear cells (PBMCs) re-stimulated *ex vivo* with *Mycobacterium tuberculosis* (*Mtb)* whole cell lysate (WCL), and treated with n-3 PUFA. Optimization experiments were performed on cells obtained from eight healthy donors to assess the secretome changes induced by re-stimulation with *Mtb* WCL and treatment with n-3 PUFA. In addition, experiments were repeated using PBMCs obtained from five non-IRIS and five TB-IRIS patients. The secretome was prepared via chloroform/methanol precipitation and overnight Trypsin digestion, and investigated via MS-based shotgun proteomics. MaxQuant was used for protein identification and Perseus for statistical analysis.

Stimulation with *Mtb* WCL shifted the secretome of healthy PBMCs towards an inflammatory state, and this was altered by treatment with EPA/DHA via changes in the regulation of several proteins. Preliminary results from TB-IRIS patient-derived PBMCs show the same trend. These promising early results suggest the potential benefits of n-3 PUFA dietary supplementation for patients with TB-IRIS, and warrant further studies with increased sample size to confirm findings, and the possible inclusion of n-3 PUFA in a future clinical trial on patients with TB-IRIS.

List of Abbreviations

AA	Arachidonic acid
ABC	Ammonium bicarbonate
ACN	Acetonitrile
AhpC	Alkyl hydroperoxide reductase
AIDS	Acquired immunodeficiency syndrome
ALA	α-linolenic acid
ANOVA	Analysis of variance
APCs	Antigen-presenting cells
ART	Antiretroviral therapy
BCA	Bicinchonic acid
BCG	Bacille Calmette-Guérin
BSA	Bovine serum albumin
BSL2	Biosafety level 2
CCR5	C-C chemokine receptor type 5
cDNA	Complimentary DNA
CFP-10	Culture filtrate protein 10kDa
CLR	C-typre lectin receptor
CID	Collision-induced dissociation
CO_2	Carbon dioxide
COX	Cyclooxygenase
c-PBMCs	Cryopreserved peripheral mononuclear cells
CRP	C reactive protein
CXCR4	C-X-C chemokine receptor type 4
DC	Dendritic cell
DHA	Docosahexaenoic acid
DMSO	Dimethyl sulfoxide
DNA	Deoxyribonucleic acid
DR-TB	Drug-resistant TB
DST	Drug susceptibility testing
DTT	Dithiothreitol

E	Ethambutol
ELISA	Enzyme-linked immunosorbent assay
ELISPOT	Enzyme-linked immunosorbent spot assay
EPA	Eicosapentaenoic acid
ESAT-6	Early secreted antigen target 6kDa
ESI	Electrospray ionization
FA	Formic acid
FASP	Filter-aided sample preparation
FCS	Fetal calf serum
FDR	False discovery rate
H	Isoniazid
HCL	Hydrochloric acid
HIV	Human immunodeficiency virus
HLA	Human leukocyte antigen
HPLC	High-pressure liquid chromatography
IAA	Iodoacetamide
IFN-γ	Interferon-gamma
IGRA	Interferon-gamma release assay
IL	Interleukin
iTRAQ	Isobaric tag for relative and absolute quantitation
HAART	Highly active antiretroviral therapy
HV	Healthy volunteer
KatG	Catalase-peroxidase
LA	Linoleic acid
LC-MS/MS	Liquid chromatography-tandem mass spectrometry
LFQ	Label-free quantitation
LOX	Lipoxygenase
LPA	Line-probe assay
LTBI	Latent TB infection
MALDI	Matrix-assisted laser desorption ionization
MDR-TB	Multi-drug-resistant TB
MMP	Matrix metalloproteinase

mRNA	Messenger ribonucleic acid
MS	Mass spectrometry
MS1	mass spectrometry (peptide ion level)
MS2	tandem mass spectrometry (fragment ion level)
Mtb	*Mycobacterium tuberculosis*
MTT	3-(4,5-dimethylthiazol-2-yl)-2,5-diphenyltetrazolium bromide
m/z	Mass-to-charge ratio
NAAT	Nucleic acid amplification test
NF-κB	Nuclear factor κB
NKT	Natural killer T cells
NNRTI	Non-nucleoside reverse transcriptase inhibitor
NRTI	Nucleoside reverse transcriptase inhibitor
PANTHER	Protein annotation through evolutionary relationships
PBMCs	Peripheral blood mononuclear cells
PBS	Phosphate buffered saline
PCA	Principal component analysis
PCR	Polymerase chain reaction
PEG	Polyethylene glycol
PEP	Posterior error probability
PI	Protease inhibitor
PPD	Purified protein derivative
POC	Point of care
PSM	Peptide-spectrum match
PTMs	Post-translational modifications
PUFA	Polyunsaturated fatty acids
R; RIF	Rifampicin
RIPA	Radioimmunoprecipitation assay
RNS	Reactive nitrogen species
ROS	Reactive oxygen species
RR-TB	Rifampicin-resistant TB
RT	Reverse transcriptase
SDS	Sodium dodecyl sulfate

SILAC	Stable isotope labeling with amino acids in cell culture
SSA	Sub-Saharan Africa
STRING	Search Tool for the Retrieval of Interacting Genes/Proteins
TB	Tuberculosis
TB-IRIS	TB-associated immune reconstitution inflammatory syndrome
TCA	Trichloroacetic acid
TGF-β	Transforming growth factor-beta
Th1	Type 1 helper T cell
Th2	Type 2 helper T cell
Th17	Type 17 helper T cell
TIC	Total ion chromatogram
TLR	Toll-like receptor
TNFα	Tumor necrosis factor-alpha
TOF	Time-of-flight
T_{reg}	Regulatory T cell
TST	Tuberculin skin test
UA	Urea buffer, 8M urea in 0.1 M Tris-Cl pH 8.5
WCC	White cell count
WCL	Whole cell lysate
WHO	World Health Organization
XDR-TB	Extensively drug-resistant TB
Z	Pyrazinamide

Table of Contents

List of Figures

List of Tables

List of Equations

Chapter 1

Literature review

1.1 Tuberculosis

1.1.1 Significance of disease

Tuberculosis (TB) is an infectious disease caused by the bacillus *Mycobacterium tuberculosis* (*Mtb*), and is especially common in low-resource settings. TB is the leading cause of death by infectious disease world-wide with 1.6 million deaths and an estimated 10.4 million new infections in 2016.[1] It is distributed primarily to low-income countries: the top six affected are India, Indonesia, China, Nigeria, Pakistan, and South Africa. Africa carries a large part of the burden with 25% of the total number of TB cases in this region, and South Africa has the highest incidence rate in the world with 781 cases per 100,000 people[2] (Figure 1). It is therefore a significant public health concern.

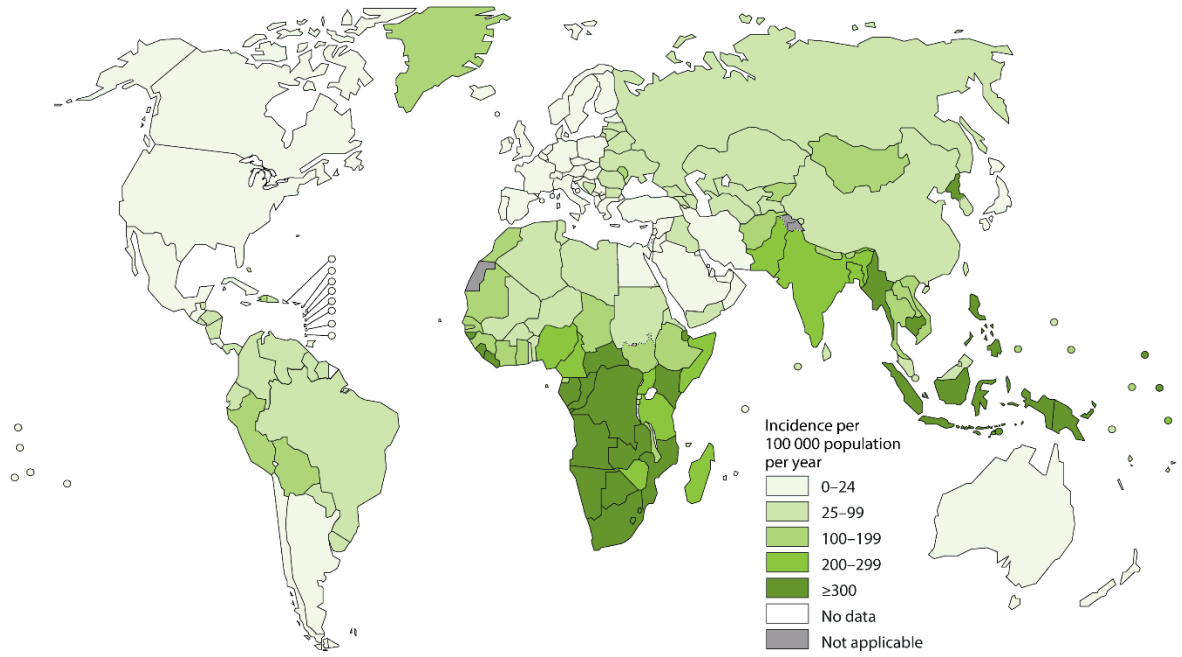

Figure 1. Estimated incidence rates for TB in 2016

(Figure sourced from WHO, Global Tuberculosis report, 2017[1])

1.1.2 *Mycobacterium tuberculosis (Mtb)*

Mtb has been evolving alongside its human host for thousands of years and is a highly adapted pathogen. A recent genetic study indicates that *Mtb* emerged roughly 70,000 years ago and followed humans on their "Out of Africa" migration.[3] The bacterium is a small intracellular bacillus with a doubling time of 12-24 hours. A defining feature of *Mtb* is its complex cell wall structure, which renders it highly impermeable to pharmacological compounds and thereby contributes to its virulence and persistence. The high-lipid content of this cell wall also makes it impermeable to most dyes, meaning *Mtb* is classified as an acid-fast rather than gram-positive or -negative bacterium (once stained, it cannot be decolourised by acid detergents).

The cell wall (Figure 2) is made up of three covalently linked layers: peptidoglycans (grey) and arabinogalactans (blue) form the inner layers, and mycolic acids (green) the outer layer[4]. The extremely low fluidity of the outer, hydrophobic mycomembrane results from covalent bonds between the large hydroxylated branched-chain mycolic acids. Intercalated between these are free lipids specific to mycobacteria, such as phenolic glycolipids, phthiocerol dimycocerosates, cord factor or dimycolyltrehalose, sulpholipids, and phosphatidylinositol mannosides. The outer capsule contains the polysaccharides glucan and arabinomannan.

Protein secretion systems are essential to mycobacterial survival and virulence, and five different type VII secretion systems were identified in *Mtb* (ESX1 – 5). ESX1 secretes the antigens ESAT-6 and CFP-10, and allows *Mtb* to persist in the macrophage. ESX1 is crucial for virulence and loss of this system contributes to the lack of pathogenicity of *Mycobacterium bovis*, which is used in the Bacille Calmette-Guérin (BCG) vaccine.[4]

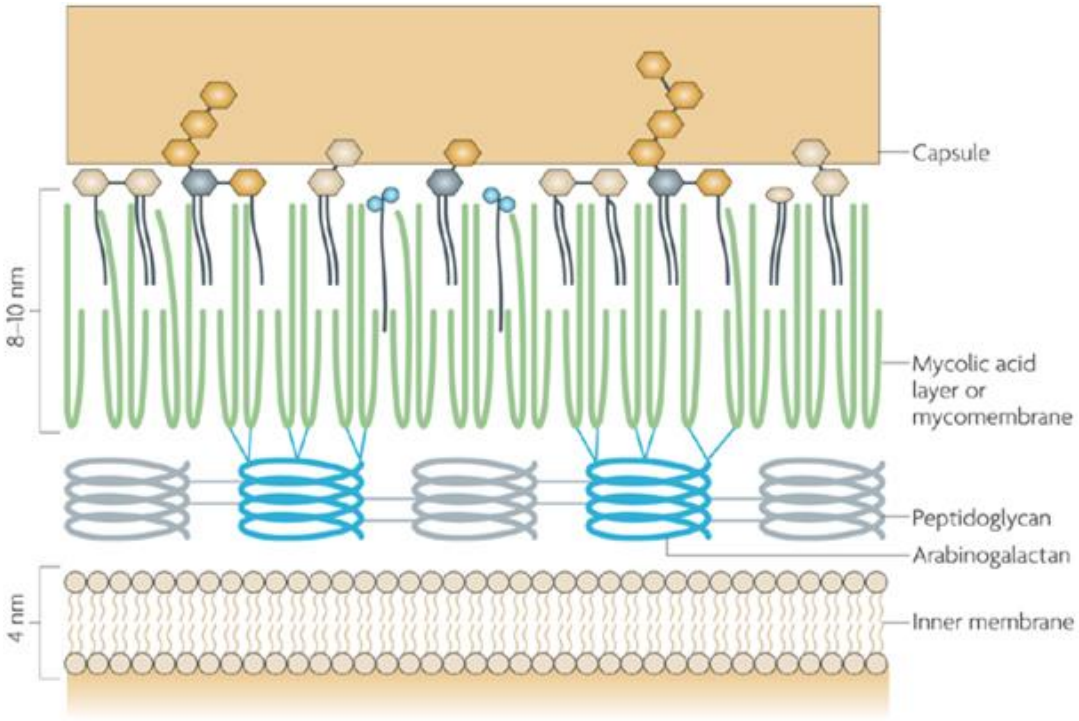

Figure 2. Schematic diagram of the cell wall structure of *Mycobacterium tuberculosis*

This representation shows a cross section of the cell envelope of *Mtb* including the three covalently linked layers: the peptidoglycan and arabinogalactan layer (grey and blue), the mycolic acid layer (green), as well as the outer polysaccharide layer. (Figure sourced from Abdallah *et al.,* 2007)[4]

1.1.3 Pathogenesis of tuberculosis

Immune response

TB is highly infectious and communicable by aerosolized droplets. In active pulmonary TB, patients will cough and produce droplets containing exhaled bacilli that can enter the body by inhalation. A study conducted on rabbits[5] showed that smaller droplets are more likely to result in infection, and these findings were later confirmed in human studies.[6] Small droplets containing one to three bacilli are able to reach the lung alveoli whereas larger droplets would get stuck in the upper airways, where the bacteria could be eliminated by commensal-primed mucosal barrier immunity. Mucosa-lined airways contain microbicidal macrophages that are activated by commensal bacteria via toll-like receptor (TLR) pathways, and are continually recruited to remove potential pathogens from the trachea and nasal passages. By reaching deeper into the lower lung which contains few commensal organisms, *Mtb* is able to evade these host immune strategies.[7]

The cellular components of the innate immune system, the alveolar resident macrophages, are the first to encounter *Mtb*. Phagocytosis is facilitated via opsonic and non-opsonic recognition through various receptors, including scavenger receptors, mannose receptors, and complement receptors. Phagocytosed bacteria can then be eliminated by production of reactive oxygen/nitrogen species (ROS/RNS), acidification of the phagosome, and phagosome/lysosome fusion. However, macrophages often fail to destroy the engulfed bacteria in this way due to *Mtb*'s ability to survive inside phagocytic cells. To achieve this, *Mtb* arrests maturation of the phagosome/lysosome complex,[8] restricts acidification, and prevents fusion with the lysosome, as was first shown by Armstrong and Hart.[9] Furthermore, *Mtb* produces two enzymes that allow it to resist oxidative killing by toxic peroxide species: mycobacterial catalase-peroxidase (KatG), and alkyl hydroperoxide reductase (AhpC).[10] *Mtb* is also able to stop infected macrophages from undergoing apoptosis, causing them to rather go into a necrotic state. Necrosis is a type of cell death that involves cell lysis, and which the pathogen can use to exit the macrophage, spread, and infect new macrophages.[11] Lastly, the bacterium causes changes in cytokine production and thereby affects the shape of the immune response. This allows it to avoid detection, and to induce inflammation that will result in liquefaction of the granuloma, thus producing an infectious cough that will lead to transmission.[12]

Bacilli that have not been eliminated by macrophages will replicate and exit the infected cell after phagocytosis. Bacteria are then recognised and taken up by professional antigen-presenting cells (APC), such as dendritic cells (DC), through C-type lectin receptor (CLR-) and TLR-mediated recognition. After processing the engulfed pathogen, DCs present *Mtb* antigens to naïve T cells in lymph nodes. CD4+ T cells are then activated by extracellular antigens presented on major histocompatibility complex-II (MHC-II), and CD8+ T cells are activated by intracellular antigens presented on MHC-I. After activation, T cells undergo clonal expansion and migrate to the site of infection. Interferon-gamma (IFN-γ) is then released by T cells to activate macrophages and induce production of nitric oxide synthase (NOS) as an intracellular killing mechanism. CD4+ T cells also release tumor necrosis factor-alpha (TNFα), thereby further activating other monocytes, macrophages, and DCs, while CD8+ T cells eliminate *Mtb* directly by releasing the cytolytic toxins perforin and granulysin (both form pores in target cell membrane) and granzymes (induce apoptosis via Fas-Fas-L pathway).[12]

The type 1 CD4+ helper T cell (Th1) response is geared toward the elimination of intracellular pathogens, and is therefore very important in fighting off *Mtb* infection. DCs release interleukin 12 (IL-12), which shapes the immune system towards a Th1-dominant response. The importance of IFN-γ

release by Th1 CD4+ T cells in TB was shown in patients with IFN-γ receptor 1 gene deletions, causing depletion of IFN-γ.[13] Type 17 helper T cells (Th17) are also important in controlling TB, as release of IL-17 by Th17 cells facilitates the recruitment and activation of neutrophils and Th1 CD4+ T cells.[12] However, recent studies have shown that excessive Th17 stimulation leads to tissue damage by inflammation due to increased migration of neutrophils and inflammatory monocytes to the site of infection.[14] Counter-balancing the Th1 response is the Th2 response, which inhibits the former by production of IL-4, IL-5, and IL-10. Similarly, regulatory T cells (T_{reg}) have a suppressive effect on Th1 and Th17, also mediated by their ability to release IL-10 and transforming growth factor-beta (TGF-β). In active disease, Treg cells accumulate at the site of infection and are associated with poor containment. In addition to these, "unconventional" T cells, such as γδ T cells, are thought to be involved in the control of TB by recognising non-peptide components of *Mtb* and initiating inflammation responses and cytotoxicity.[15] Mucosal-invariant T cells (MAIT) are another population of specialized T cells which can identify bacterial metabolites via the major histocompatibility complex-like molecule MR1, and play an important role in the detection of intracellular *Mtb* infection.[16]

Granuloma formation

In the great majority of people infected with TB, the bacteria is effectively contained in granulomas, the formation of which is the hallmark in the progression of TB disease (Figure 3). Infected macrophages release IFN-γ, TNF-α, and other inflammatory cytokines to recruit immune cells (neutrophils, natural killer T cells (NKT), CD4+, and CD8+ T cells) from nearby blood vessels to the site of infection. Amplification of recruitment signals is mediated by the production of other inflammatory cytokines by each of these immune cells. The granuloma structure then begins to form around a central core of infected macrophages, surrounded by foamy macrophages (macrophages loaded with lipid droplets). Other mononuclear cells, as well as giant cells (large multinucleated cells, which form as a result of several monocytes/macrophages fusing together), continue to build on to the granuloma. A fibrous cuff of collagen surrounds and delineates the structure. During granuloma maturation, the fibrous sheath increases while the blood vessels which perfuse the structure disappear. If a change in the immune status of the host occurs, such as malnutrition or HIV infection, the granuloma may become caseous and decay into a mass of cellular debris, leading to the rupture of the entire structure. Live bacilli are then released into the airways and transmitted by means of a productive cough.[17]

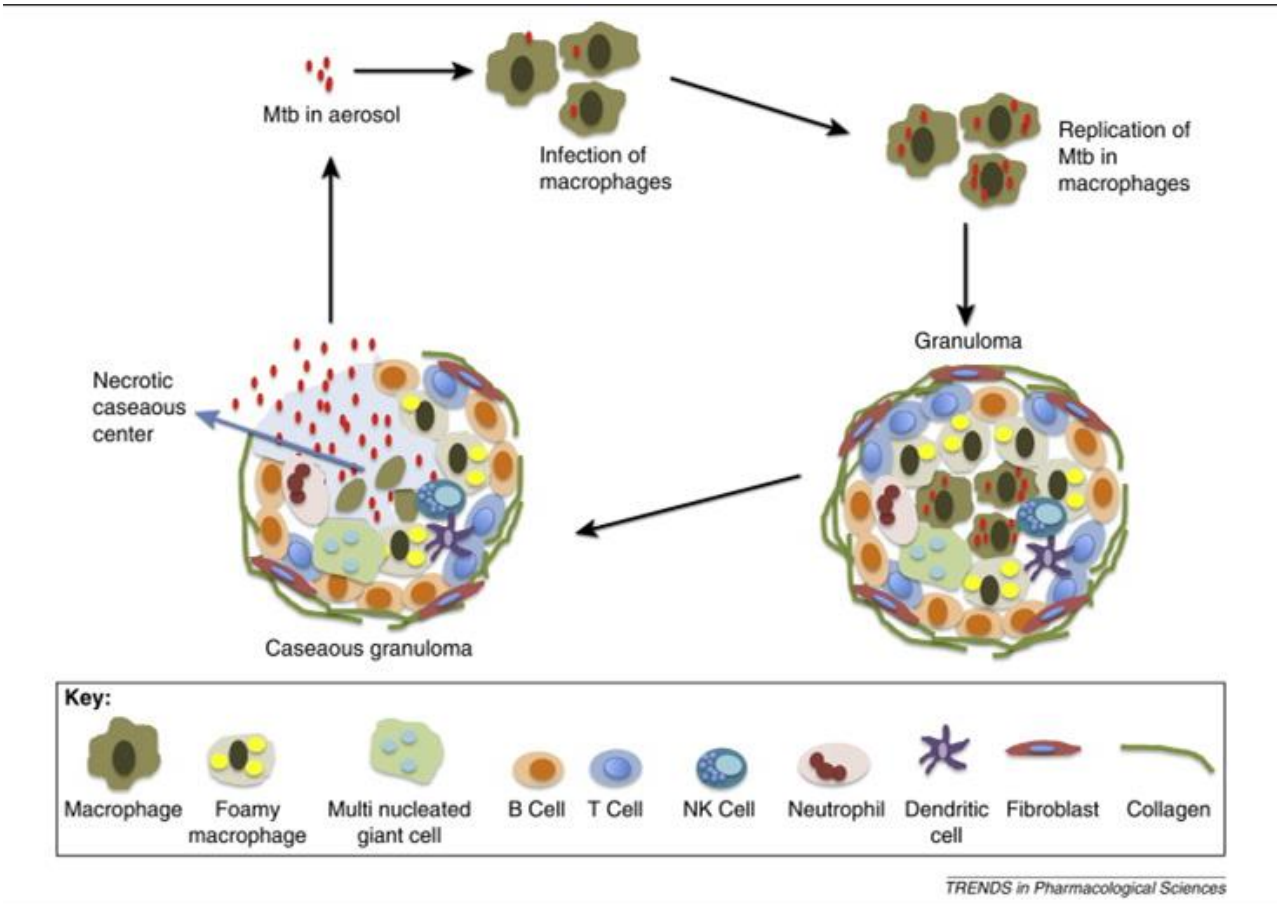

Figure 3. Schematic representation of the formation and structure of the granuloma

Phagocytosed bacilli replicate inside macrophages and promote the recruitment of immune cells to the site of infection. The granuloma forms around a central core of infected macrophages, foamy macrophages, giant cells, and other mononuclear cells. A fibrous and collagen cuff forms around the granuloma in the mature stage, and the structure breaks open during caseation, releasing bacilli into the airways. (Figure sourced from Rayasam *et al*., 2015)[18]

1.1.4 Diagnosis

Rapid and accurate diagnosis of TB is essential for the effective treatment and control of the disease. Although several detection methods for *Mtb* are available, early detection is still hampered by low-resource settings at point-of-care (POC) as well as a high number of false negative test outcomes due to the low sensitivity of many tests, especially in immuno-compromised patients. In addition to this, no test is able to give a differential diagnosis for active TB and latent TB (LTBI). As only 5-15% of people infected with TB will progress to active disease,[19] it is important to differentiate between these two states.

Microbiological culture and microscopy

Detection of the causative agent *Mtb* through microscopy is one of the direct diagnostic methods. The 'gold standard' for TB diagnosis remains the culture of bacilli from clinical samples and subsequent detection through microscopy. However, growth of *Mtb* is slow, taking two or more weeks on average before detection, and requires trained staff as well as a well-equipped laboratory.[19]

Sputum smear microscopy, developed more than 100 years ago, is often the preferred method[20] as it is cheaper and requires minimal biosafety standards, although the presence of *Mtb* bacilli is only identified in 44% of new cases, and 15-20% of children sputum samples.[21] Sputum smear microscopy lacks sensitivity in children and HIV-infected patients, who may have very low bacillary loads, and cannot distinguish between *Mtb* and other non-tuberculous mycobacteria.[19]

Tuberculin skin test (TST)

Today the tuberculin skin test (TST) remains the most wide-spread TB diagnostic test, even with recent advances in other more sensitive molecular tests.[20] The TST uses the immune response to TB antigens as a proxy for diagnosis of the disease. A standard preparation of purified protein derivative (PPD) is injected intradermally, and the patient is re-examined 48 to 72 hours later. The resulting skin reaction is exaggerated in persons who have previously mounted an inflammatory response to TB antigens. If the diameter of the reaction area is greater than or equal to 10 mm, the reaction is considered positive. However, false positives occur if the individual has been vaccinated with the BCG vaccine, and false negatives are common in immunocompromised patients, such as HIV- infected individuals, who do not mount a normal immune response.[21]

Interferon-gamma release assays (IGRAs)

Interferon-gamma release assays (IGRAs) are *ex vivo* blood tests that measure the presence of mycobacteria-specific T cell responses to the antigens ESAT-6 (6kDa early secreted antigenic target), CFP-10 (culture filtrate antigen), and TB7.7, using ELISA (QFT-G test) or ELISPOT (T-SPOT.TB test).[20] However, IGRAs may result in false negatives in high TB/HIV-burden settings as they rely on the indirect measurement of the individual's immunological response, and the WHO has therefore advised against the use of IGRAs (and the TST) in low-income countries with high rates of HIV and TB infections.[22]

Nucleic acid amplification tests (NAATs)

Nucleic acid amplification tests (NAATs) use PCR to amplify and detect mycobacterial RNA or DNA from any clinical sample. However, they show poor sensitivity and specificity in smear-negative TB and the cost associated with these tests means they are not widely used. The most advanced NAAT is the Xpert MTB/RIF assay which can confirm the presence of *Mtb* and identify resistance mutations within two hours. Unfortunately, high costs and the sophisticated equipment required to perform these tests will delay the implementation of Xpert in low-resource settings.[21]

1.1.5 Treatment

First-line treatment

TB is treated with combination drug therapy in order to limit the risk of developing drug resistance. Each drug has a different mechanism and by combining these, chances of treatment success are increased. The recommended oral first-line drugs are isoniazid (H), rifampicin (R), ethambutol (E), and pyrazinamide (Z).[23] The standard regimen for adults and children over 30 kg is 2HRZE (intensive phase consisting of two months' treatment with H, R, Z, and E), followed by 4HR (continuation phase with H and R for four months).

Table 1. First-line drugs for treatment of TB, single-letter abbreviations and mechanism of action

Drug name	Single-letter abbreviation	Mechanism of action
Isoniazid	H	Bactericidal/bacteriostatic; target InhA and inhibits synthesis of mycolic acids[24]
Rifampicin	R	Bactericidal; inhibits bacterial DNA-dependent RNA polymerase[25]
Ethambutol	E	Bacteriostatic; inhibits arabinosyl transferase
Pyrazinamide	Z	Bactericidal; disrupts membrane energetics and inhibits membrane transport systems[26]

According to the South African National Tuberculosis Management Guidelines,[27] the patient's infection status must be re-assessed one week before the end of the intensive phase (week 7) via sputum smear microscopy. If the result is negative, the patient progresses onto the continuation phase at the end of week 8, and is considered to respond well to treatment. If the sputum smear is still positive at week 7, the patient's compliance to treatment is assessed, and the intensive phase is

prolonged for one month. These patients are then checked again at week 11 and if the sputum smear remains positive, further testing is done to establish drug susceptibility and resistance. If drug-resistant (DR) TB is confirmed, DR-TB treatment is initiated (see DR-TB treatmentDR-TB treatment). Finally, patients having progressed to the continuation phase are assessed at week 23 and treatment is stopped at the end of week 24 if results from sputum smear microscopy are negative. If still positive, line probe assays (LPA) or drug susceptibility testing (DST) are performed to check for resistance to Z and/or E. If patient's infection is drug-susceptible, treatment is re-started from the beginning and the patient is counselled on the importance of compliance.

DR-TB treatment

According to the WHO TB country profile, there were 20,040 cases of DR-TB in South Africa in 2016.[19] There are several factors contributing to the emergence of these drug-resistant TB cases, including poor treatment adherence, as well as poor management of drug supply and access to health care and treatment in low-resource settings. DR-TB is classified as rifampicin-resistant only (RR-TB), multi-drug resistant (MDR-TB; resistant to at least both H and R), extensively drug-resistant (XDR-TB; resistant to at least H, R, one of the fluoroquinolones and one of the second-line injectables).

According to the WHO treatment guidelines,[23] all MDR-TB patients should receive a four-drug regimen with one drug from Group 2 (kanamycin and amikacin are first choice), one from Group 3, with ethionamide (Group 4) often added due to its low cost. Group 5 drugs are only recommended in cases where it is impossible to design an adequate regimen using drugs from groups 2 to 4, and in cases of XDR-TB. Some of the second-line drugs used to treat DR-TB are listed in Table 2 below (non-exhaustive list). MDR-TB patients are monitored monthly for sputum conversion, and treatment is continued for at least four months after conversion. Treatment may be as long as 24 months in chronic cases with advanced lung damage.

Table 2. Some of the second-line drugs used to treat DR-TB

Group	Type	Drug name
Group 2	Second-line injectables	Kanamycin Amikacin Streptomycin
Group 3	Fluoroquinolones	Levofloxacin Moxifloxacin
Group 4	Oral bacteriostatic	Ethionamide
Group 5	Agents with unclear role in MDR-TB treatment	Linezolid Amoxicillin/clavulanate

1.2 HIV and AIDS

1.2.1 Significance of disease

HIV is a global leading cause of morbidity and mortality with 36.7 million people infected in 2016, 1.8 million new infections and 1 million deaths.[28] Sub-Saharan Africa (SSA) is particularly affected by the epidemic, and carries 70% of the global HIV burden. South Africa alone has the highest number of HIV-positive people in the world (estimated 7.1 million in 2016) and one of the highest rates of prevalence (estimated 18.9% in adults aged 15 to 49 years).[29] The prevalence of HIV across the world is shown in Figure 4 below.

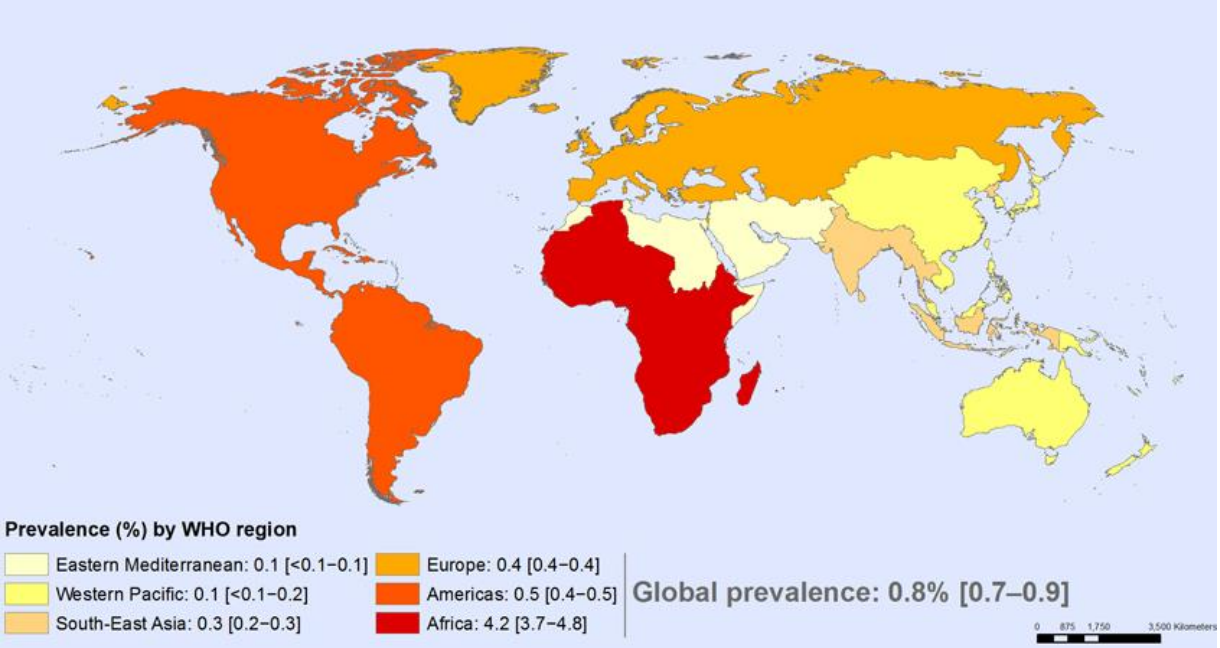

Figure 4. HIV prevalence amongst adults 15-49 years by WHO region in 2016

(Figure sourced from the WHO, Global Health Observatory, 2017)[30]

The global large-scale deployment of anti-retroviral therapy (ART) has been one of the most successful recent public health interventions, giving access to treatment for 3.4 million people in South Africa alone – more than any other country. This increase in treatment is largely responsible for the 26% decrease in AIDS-related mortality since 2010.[31]

1.2.2 The virus

The HI virus is part of the Lentivirus genus and Retroviridae family. Lentiviruses ('lenti' meaning 'slow' in Latin) have long incubation periods and cause long-term illness to their host. Two types of HI viruses have been characterized: HIV-1 shows higher virulence and infectivity and is responsible for most HIV infections globally, while HIV-2 is less genetically diverse and largely confined to West Africa.[32]

Structure

The HI virion consists of a spherical viral envelope containing a conical capsid, which houses several enzymes and two strands of positive ssRNA. The viral envelope is formed from the lipid bilayer of the host cell when the virus capsid buds off and is released. It includes the glycoproteins gp120 and gp41 which are crucial for the virus to bind and enter the host cell.

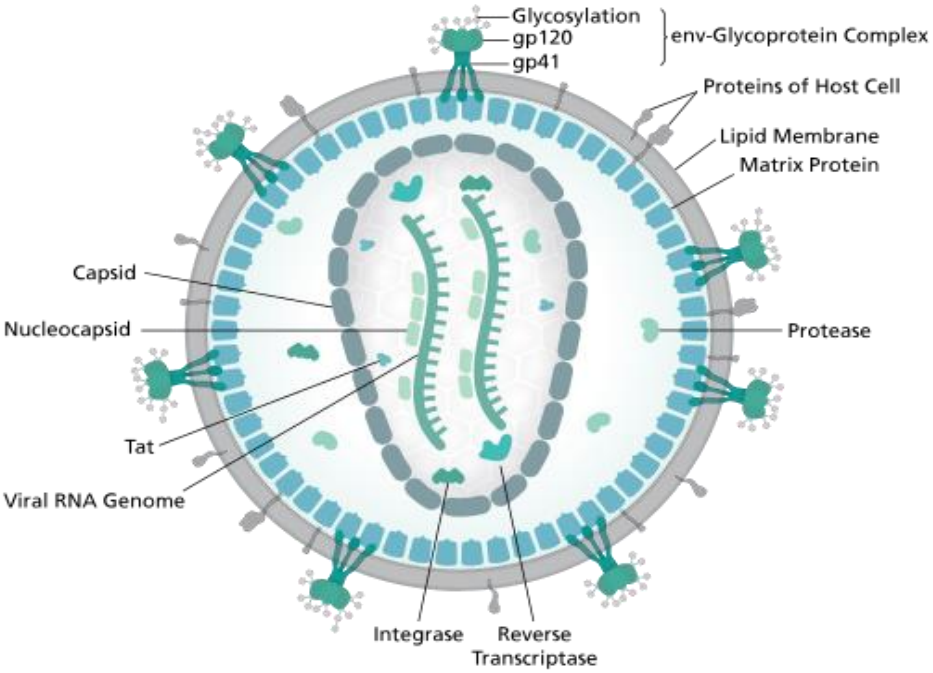

Figure 5. Diagrammatic representation of the structure of the HI virion

(Figure sourced from Wikimedia Commons)[33]

1.2.3 Life cycle

Binding and entry

HIV uses its surface glycoproteins gp120 and gp41 to bind and anchor itself to CD4 glycoproteins on the surface of host immune cells, such as helper T cells, monocytes, macrophages, and dendritic cells. C-C chemokine receptor type 5 (CCR5) and C-X-C chemokine receptor type 4 (CXCR4) are engaged in interaction and gp120 and gp41 undergo conformational changes to allow fusion of the host cell plasma membrane with the viral membrane.[34]

Viral transcription and replication

Shortly after entry into the target cell, the two ssRNA strands are released from the viral capsid by the enzyme reverse transcriptase (RT) and copied to complimentary DNA (cDNA). Viral RT also has ribonuclease activity to degrade RNA, as well as DNA-dependent DNA polymerase activity to create a sense DNA strand from the antisense cDNA. These two complimentary DNA strands are transported to the host cell nucleus and integrated into the host genome by the viral enzyme integrase. The integrated viral DNA may then lie dormant (latent infection phase) until certain cellular transcription

factors, such as NF-κB, are activated. These factors are normally present during activation of the immune system in response to infection, therefore the more the immune system tries to fight off infection, the more HIV is transcribed.

Viral recombination, assembly, and budding

Two copies of viral RNA are encapsulated in the virion thus allowing for recombination between the two different genomes during replication by RT. It is estimated that two to 20 recombination events occur per genome and per replicative cycle. The shuffling of polymorphisms between viruses increases viral genetic diversity and therefore pathogenesis and virulence, giving the virus a better chance at escaping the pressures exerted by its host.[35]

1.2.4 Pathogenesis and disease

Transmission and diagnosis

Heterosexual transmission is responsible for approximately 85% of all HIV infections.[36] Prevalence of HIV is correlated with other sexually transmitted diseases, as well as certain sexual practices, such as concomitant relationships, and alcohol and drug use. HIV diagnosis relies on the detection of antibodies or antigens specific to the virus from various patient samples including plasma, serum, whole blood, or saliva. However, serological tests are ineffective during primary infection (before the body has produced antibodies) and in infants younger than 18 months born to HIV-positive mothers, who might carry maternal HIV antibodies.[36]

Disease progression

The early stages of HIV infection are frequently asymptomatic, although viral replication takes place at a constant rate throughout infection. Viral replication leads to the gradual decimation of the CD4+ T cell population eventually leading to AIDS during the later stages. To monitor disease progression, viraemia is measured via quantification of viral RNA. CD4+ cell counts are also monitored using flow cytometry, and clinical symptoms such as opportunistic infections are indicators of immune deficiency. In the early stages, viral load is quickly reduced following HIV-specific CD8+ responses, but the chronic phase of the disease starts at the formation of latent viral reservoirs in resting HIV-infected immune cells such as long-lived memory T cells.

1.2.5 Treatment

ART leads to long-term viral suppression and reduced mortality and morbidity, but does not achieve full clearance of HIV from the system and treatment must be continued throughout the patient's life. Due to the high rate of viral replication and potential for recombination and mutation, a three-drug combination regimen (highly active ART, HAART) is needed to limit drug resistance and improve effectiveness. The main classes of drugs used to treat HIV include viral non-nucleoside and nucleoside/nucleotide reverse transcriptase inhibitors (NNRTIs and NRTIs, respectively), and protease inhibitors (PIs). ART usually includes two NRTIs, in addition to an NNRTI or PI. UNAIDS guidelines stipulate that ART should be started ideally in all individuals living with HIV, and that it should be initiated in priority in patients with a CD4+ count below 350 cells/mm^3, as well as in pregnant and breast-feeding women and children under the age of two regardless of CD4+ cell counts.[37]

1.3 TB-IRIS

1.3.1 HIV and TB

HIV co-infection is present in approximately 60% of TB cases in South Africa.[2] HIV and TB are synergistic pathogens and TB is a leading cause of death in HIV-infected patients. HIV reduces the frequency and function of CD4+ T-cells, thereby exacerbating the progression of existing TB, while the host immune response to TB, which includes the activation of mononuclear cells, also promotes replication of HIV and progression to AIDS.[38] An estimated 25% of HIV-infected individuals are also infected with latent TB, and are 26 times more likely to progress to active TB than their HIV-negative counterparts.[39] As previously stated, diagnosis of TB in HIV+ individuals is complicated by concurrent HIV infection and immune suppression. Sputum smear microscopy is more likely to be negative in such patients, with active TB successfully identified in 22-43% of cases only.[40] In addition to this, the TST is also more likely to be negative, and disease is more frequently disseminated to extra-pulmonary sites thereby complicating diagnosis through standard methods. Anti-TB treatment and its timing must be considered carefully in HIV+ patients as the potential for drug-drug interactions is high, as is the development of TB-associated immune reconstitution inflammatory syndrome (IRIS).

In a subset of HIV and TB co-infected patients, treatment is complicated by TB-IRIS, a disorder characterized by a post-ART worsening of existing TB after previous response to anti-TB therapy (paradoxical TB-IRIS) or the emergence of new or previously subclinical TB disease (unmasking TB-IRIS). For the purposes of this project, only paradoxical TB-IRIS will be investigated. Although several

pathogens can cause IRIS, mycobacterial infections such as TB are responsible for approximately 40% of cases.[41] The reported incidence of TB-mediated IRIS varies from 10 to 54%,[42,43] with an estimated mortality rate of 3.2%,[44] and it is especially prevalent in South Africa, where the rate of TB and HIV co-infection is high and ART is readily available.

1.3.2 Pathogenesis

The dysregulated restoration of immune responses in ART-treated patients was first reported in 1992[45] and the syndrome is well-known today. Although the immunopathogenesis of TB-IRIS is incompletely understood, it is thought to be multifactorial, and is believed to result from an inappropriately regulated host response to antigenic stimuli upon immune recovery.

TB-IRIS was shown to be associated with increasing peripheral frequency of antigen-specific IFNγ+ Th1, as well as a 24% increase in T cell activation markers at IRIS onset.[46] Bourgarit and colleagues additionally demonstrated an increase in the Th1 cytokines/chemokines IL-2, IL-12, IP10, and MIG/CXCL9, as well as other pro-inflammatory cytokines/chemokines (TNF-α, IL-6, IL-1β, IL-10, RANTES, and MCP-1). However, no Th2 cytokine peak occurred. Similarly, Vignesh and colleagues[47] found that TB-IRIS was associated with CD3+CD4- and CD4+ T cell responses against *Mtb* antigens, and presence of these cells at baseline may therefore suggest a predisposition to IRIS in certain patients. A dysregulated Th1 cell expansion has also been noted in association with TB-IRIS in other studies,[48,49] although expansion of the *Mtb*-specific Th1 population was also observed in patients who do not go on to develop TB-IRIS, calling into question the importance of this population expansion in the pathogenesis of TB-IRIS.[48]

Although findings by Meintjes and colleagues[48] suggest that the central role of Th1 in TB-IRIS pathogenesis be reconsidered, these responses are undoubtedly of crucial importance during the immune response to TB, and are likely involved in generating the TB-IRIS phenotype. Clinical studies investigating differential cytokine levels in TB-IRIS patient samples have been conducted,[46,50,51] and several different cytokines (e.g., IL-6, IFNγ, TNFα, etc.) were found in these studies to be relatively increased in circulation during TB-IRIS thus implicating hypercytokinemia in the pathogenesis of TB-IRIS.

1.3.3 Risk factors, diagnosis, and treatment

Diagnosis of TB-IRIS is challenging due to the lack of reliable diagnostic markers, the variable presentations, and the need to exclude differential diagnoses, such as TB drug resistance.[52] Risk factors for paradoxical TB-IRIS have been identified, including low CD4+ cell count at baseline,[53] rapid CD4+ count recovery post-ART,[53] disseminated TB, a short time interval between initiation of anti-TB therapy and ART,[53,54] as well as potential genetic variations.[55]

Given the temporal association between the initiation of ART treatment and the development of TB-IRIS, delaying the start of ART may reduce the risk of TB-IRIS.[54] However, even short delays in ART initiation in TB patients are associated with a high risk of mortality in severely immunocompromised patients (CD4 count <50). Recommendations regarding co-treatment with anti-TB drugs and ART state that ART should be initiated within 2 weeks of anti-TB treatment in patients with a CD4+ count <50 cells/mm^3, and may be delayed for up to 8 weeks if immunodeficiency is less severe.[56]

A randomised placebo-controlled trial, conducted in a South African TB-IRIS cohort, has shown the use of prednisone, a broad-spectrum corticosteroid, to be effective in "reducing the need for hospitalisation and therapeutic procedures, and hastening improvements in symptoms, performance and quality of life".[57] The prescription of corticosteroids in HIV patients does carry several risks, including the development and progression of herpes zoster[58] and Kaposi's sarcoma.[59] Additionally, re-emergence of TB-IRIS in a subset of patients after cessation of prednisone suggests that corticosteroids do not necessarily correct the pathogenic mechanisms underlying TB-IRIS. More specific prophylactic and therapeutic treatment options for TB-IRIS are therefore required.

1.4 N-3 polyunsaturated fatty acids (PUFA)

1.4.1 Mechanism of action

N-3 polyunsaturated fatty acids (PUFA) are potent immune-modulatory agents that can inhibit certain aspects of inflammation, such as recruitment of leucocytes, cellular adhesion, production of eicosanoids (leukotrienes and prostaglandins) from n-6 arachidonic acid, cytokine release, and Th1 activity.[60] The most potent n-3 PUFA are the long-chain PUFA derived from marine oils in the diet, namely eicosapentaenoic acid (EPA) and docosahexaenoic acid (DHA, Figure 6). EPA, and to a certain extent DHA, is able to compete with n-6 arachidonic acid as an enzymatic substrate in the production of eicosanoids and thereby reduce inflammation.[61] Furthermore, both EPA and DHA give rise to pro-

resolving mediators such as resolvins, protectins, and maresins. N-3 PUFA are also able to modulate T cell-mediated processes specifically, such as altering lipid raft formation at the immunological synapse where T cells and APCs interact for antigen-initiated T cell signalling, and upregulating the Th2 cells sub-population.[62]

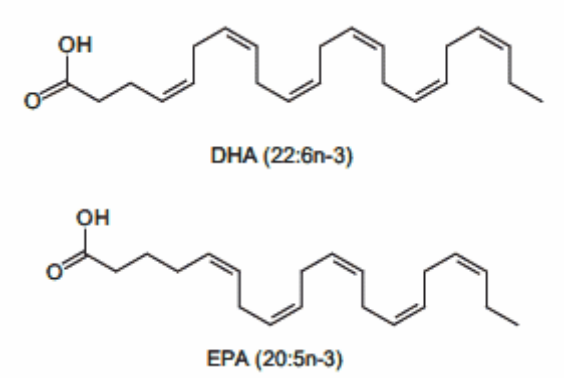

Figure 6. Structures of eicosapentaenoic acid (EPA) and docosahexaenoic acid (DHA)[63]

Since humans do not have the enzymes necessary to inter-convert n-3 and n-6 PUFA, dietary differences in the ratio of the fatty acids are reflected at the physiological level. Arachidonic acid (AA) arises from the essential acid linoleic acid (LA), which is obtained from dietary sources such as safflower and sunflower oils. AA is an important part of the plasma membrane phospholipids and can produce potent pro-inflammatory eicosanoids, such as leukotrienes and prostaglandins, when acted on by cyclooxygenase (COX) and lipoxygenase (LOX). On the other hand, EPA and DHA are derived from α-linolenic acid (ALA), an essential fatty acid obtained from certain nuts/seeds (walnuts, chia, and linseed). When acted on by COX and LOX, these fatty acids give rise to the inflammatory-resolving mediators resolvins, protectins, and maresins. [64] The metabolism of n-3 and n-6 fatty acids is depicted in Figure 7.

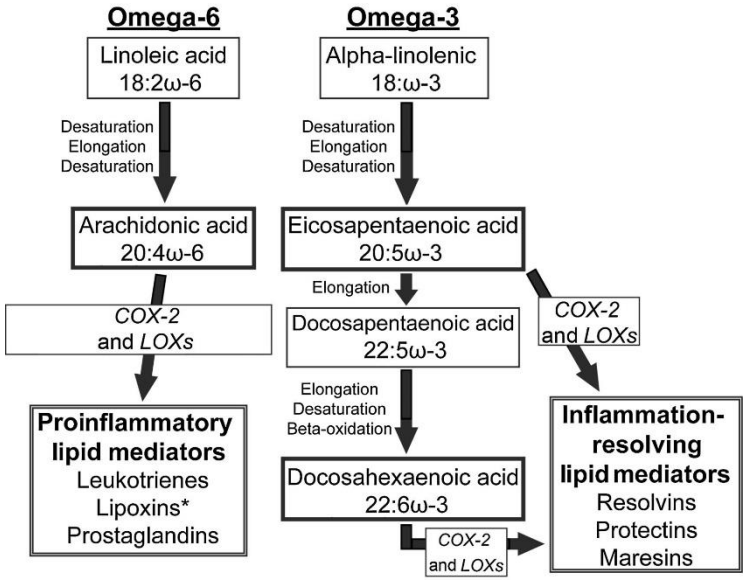

Figure 7. Metabolism of n-3 and n-6 PUFA

Arachidonic acid (AA) arises from the essential acid linoleic acid (LA), and produces pro-inflammatory eicosanoids, such as leukotrienes and prostaglandins (lipoxins are usually pro-resolving), when acted on by cyclooxygenase (COX) and lipoxygenase (LOX). Eicosapentaenoic acid (EPA) and docosahexaenoic acid (DHA) are derived from α-linolenic acid (ALA), and compete with AA for as enzymatic substrates to give rise to pro-resolving resolvins, protectins, and maresins. (Figure sourced from Hidaka et al., 2015)[64]

1.4.2 Clinical use

N-3 PUFA have an excellent tolerability and safety profile, and are thus attractive as potential therapeutic agents for a range of inflammatory and auto-immune diseases.[65] Several clinical trials support the beneficial effects of dietary n-3 PUFA supplementation in chronic inflammatory diseases such as rheumatoid arthritis,[66] inflammatory bowel diseases,[67] asthma,[68] and psoriasis,[69] among others. Particularly, n-3 PUFA appear able to protect against inflammatory fibrosis, even after the inflammatory insult has occurred.[70,71] We therefore hypothesized that similar beneficial effects may be derived in the settings of TB and TB-IRIS, through incorporation of n-3 PUFA into, and the effects of their derivatives on immune cells. In order to test this hypothesis, we investigated a patient-specific *in vitro* model of TB-IRIS using a mass spectrometry-based proteomic approach.

1.5 Proteomics

Proteomics is the study of the structure, function, localisation, and abundance of all the proteins in a system at a given time. Recently, rapid progress has been made due to technical advances in mass spectrometry (MS), facilitating the simultaneous detection, identification, and quantitation of thousands of proteins, rather than focusing on a single protein or handful of proteomic markers generally investigated by other immunological methods.[72] Because proteins perform the end-functions of the cell, the proteome more directly reflects observable phenotypes than the genome or even the transcriptome.[73,74] Proteomic complexity derives from differential mRNA processing, splicing, degradation, post-translational modifications (PTMs), and targeting to different sub-cellular and extracellular compartments. The proteome is hugely varied and dynamic, responding in real time to inherent characteristics (such as age and gender) and external factors (such as diet, exercise, and exposure to toxins). Clinical proteomics aims to provide clinicians with risk stratification, diagnostic, and prognostic tools to facilitate more personalized treatment.[72] Research has focused largely on the discovery of peripheral biofluid markers for the early diagnosis of chronic diseases such as cancer, but also on the discovery of new drug targets. Discovery proteomic analysis must be followed by targeted work, to accurately measure the expression of certain key proteins and validate potential biomarkers. The work presented here covers only the initial and primary investigation in the proteomic pipeline. Here we outline the basic workflow and machinery used in MS-based proteomic approaches (Figure 8).

1.5.1 Mass spectrometry

A mass spectrometer is able to measure ion mass-to-charge ratios (m/z), from which the identity and quantity of any ion can, in principle, be deduced. The instrument comprises three main components: the ion source, which ionizes analytes into the gas phase; the mass analyzer, which measures m/z; and the detector, which counts the number of ions corresponding to each m/z value. Each is these is discussed in further detail.

The typical sample processing workflow for bottom-up, MS-based proteomics involves lysis of the relevant sample (such as tissue, cells, cell culture supernatant, or biofluid) to extract the proteome. Fractions, such as the cell membrane, may be enriched through the use of specific techniques. Proteins are then digested enzymatically, usually with trypsin, to yield peptides. The specificity of trypsin cleavage allows for prediction of peptide products, which ionize more readily than full proteins.

Peptides are injected into the instrument and are further separated by high-pressure liquid chromatography (HPLC). This is achieved via reversed-phase chromatography, which uses the peptides' hydrophobicity as a basis for separation, using a C18 octadecyl bonded silica solid phase column. This decreases complexity and ensures detection of a greater number of peptides as elution of peptides from the HPLC column into the MS is fractionated.

Ionization

Next, peptides undergo ionization for improved MS detection. The two ionization methods most commonly used for proteomics are electrospray ionization (ESI) and matrix-assisted laser desorption ionization (MALDI). In ESI, high voltage (2-6 kV) is applied to the peptide solution that is sprayed as it elutes from the liquid chromatography column.[75] ESI is particularly suited to use in conjunction with liquid-based chromatographic methods such as HPLC, and is therefore more commonly used for the analysis of complex protein samples. MALDI involves spotting a sample onto a light-absorbing matrix, which is then probed with a laser pulse. The matrix absorbs energy from the laser and transfers it to the analyte in the sample, which is then ionized into the gas phase.[75] MALDI is better suited to low-complexity samples, but is particularly useful in analyzing tissue or organ sections as the entire section can be analyzed at once whilst maintaining spatial distribution of the analytes.[76]

Mass analyzers

According to Aebersold *et al*.,[77] the key aspects of the mass analyzer are "sensitivity, resolution, mass accuracy and the ability to generate information-rich ion mass spectra from peptide fragments (tandem mass or MS/MS spectra)". There are several kinds of mass analyzers but the three most commonly used in proteomics are the ion trap, time-of-flight (TOF), and quadrupole. These can also be used in combination. Ion trap mass analyzers 'trap' ions for specified time or until a specific threshold is reached before releasing them for MS analysis. Although ion traps are sensitive and relatively inexpensive, the mass accuracy achieved may be relatively low.[77] However, they remain the source of most proteomics data in the literature, and an Orbitrap instrument, which uses rotational motion of ions around a central spindle, was used in the current study. Strictly speaking, an Orbitrap is not considered an ion trap but a mass analyzer, as conventional ion traps do not measure m/z ratios but merely allow accumulation of ions before measurement by an analyzer. TOF analyzers are more often used in combination with MALDI, as they measure the mass of intact peptides. Peptide ions are accelerated through a tube of fixed length and the time taken to reach the detector in subsequent field-free drift is measured. This allows the ion's exact mass to be calculated. Finally, quadrupole mass

analyzers make use of four parallel metal rods in between which ions navigate and are stabilized by electric fields according to their m/z ratios. In triple quadrupole instruments, ions of a desired m/z ratio are selected in the first quadrupole (Q1), before proceeding to a collision cell (Q2). There, high pressure, electrical voltage, and collision with neutral gases cause collision-induced dissociation (CID). Ion fragments finally proceed to Q3 for identification. Quadrupole mass analyzers are often used for the detection/quantification of selected ions of known mass.

MS1 spectra are continually generated as ionized peptides elute into the mass analyzer. If the intensity of a particular ion is above a certain threshold, the ion is selected for fragmentation, after which further MS spectra (MS2, tandem MS/MS) of the ion fragments will be obtained. Usually, a “top 10” approach is employed, where the ten ions with highest intensities in a given time window are selected for further fragmentation. In the instrument used in this study, a Q Exactive hybrid quadrupole-Orbitrap, precursor ion selection is achieved using a quadrupole mass analyzer, with ions accumulating in a C-trap before fragmenting in the HCD cell, and high resolution MS2 is produced by Fourier-transformed data from an Orbitrap mass analyzer.[78]

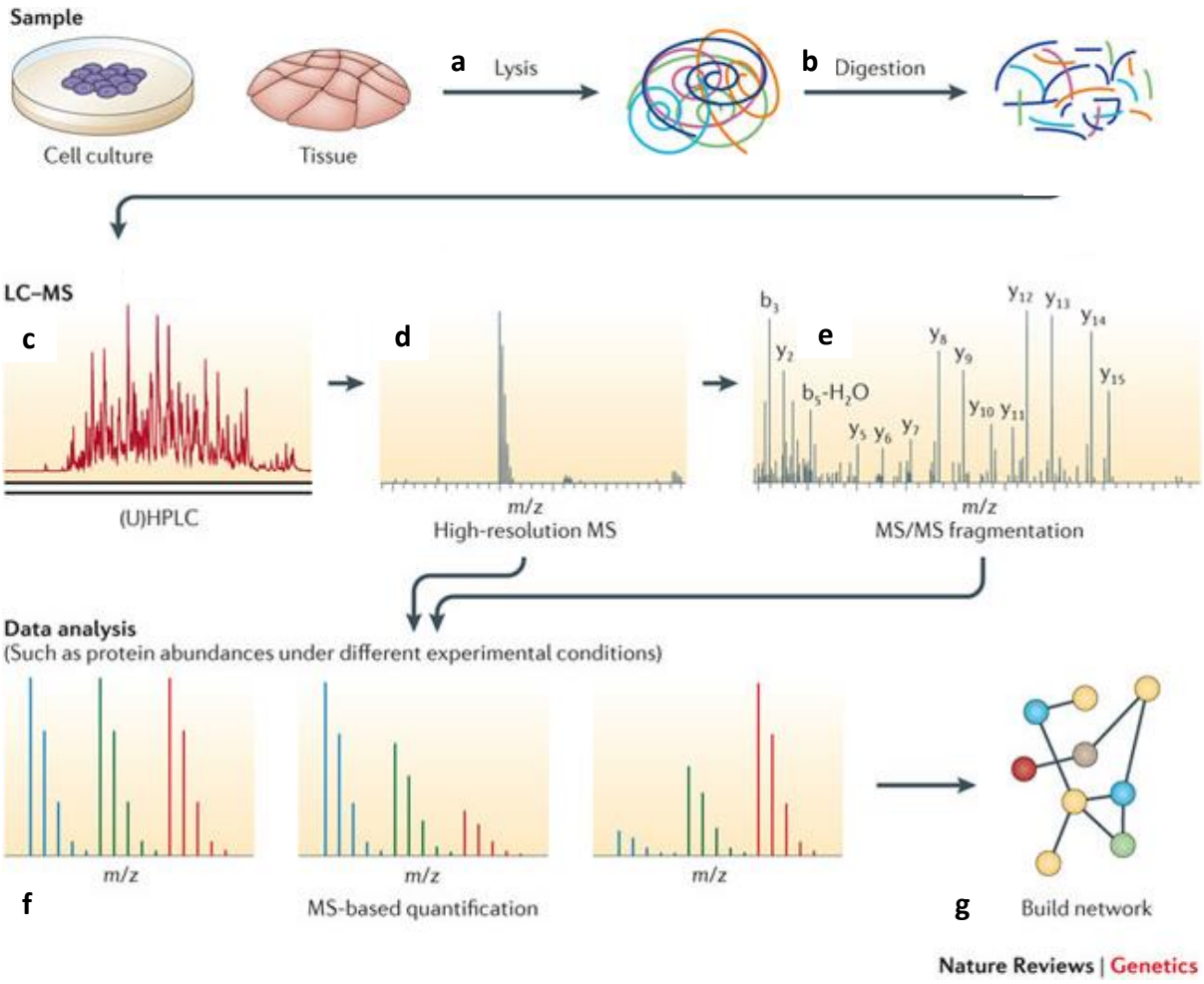

Figure 8. General workflow for mass spectrometry-based proteomics

a) MS-based proteomics involves lysis of the relevant sample (such as tissue, cells, cell culture supernatant, or biofluid) to extract the proteome. b) Proteins are then digested enzymatically, usually with trypsin, to yield peptides. The specificity of trypsin cleavage allows for prediction of peptide products, which ionize more readily than full proteins. c) Peptides are injected into the instrument and are further separated by high-pressure liquid chromatography (HPLC) to decrease complexity and ensure detection of a greater number of peptides. d) Peptide ions are detected as MS1 spectra, and their m/z ration is determined. e) Selected peptides are fragmented, usually by collision-induced dissociation, and fragments are detected at the MS2 level. f) Spectra obtained from precursor and fragment ions are matched to those of a spectral database, produced *in silico*, by software algorithms such as MaxQuant to allow for protein identification. Data are then quantified, by the spectral count or peak intensity methods (label-free quantitation). g) Finally, biological significance is derived from the data through the use of statistical tests, functional classification, and network analyses. (Figure adapted from Altelaar *et al*., 2012)[79]

1.5.2 Computational processing

Identification and quantitation

Identification of proteins from tandem mass spectra is achieved through computational approaches. MaxQuant (www.maxquant.org), the free-ware software used in the present study, uses an internal search engine, Andromeda, to match experimental spectra with a database of theoretical spectra for the *in silico*-generated, trypsin-digested reference proteome specified.[80] This probability-based algorithm is similar to that used in Mascot, another popular search engine. To address the issue of possible false positive matches, Andromeda assigns a posterior error probability (PEP) score to each spectral match, producing a false discovery rate (FDR). This is achieved by comparing peptide-spectrum matches (PSM) made to a decoy database comprising reverse protein sequences, to matches made to a true database.[81]

Although several stable isotope labelling strategies to enable quantitation of proteins are available (such as SILAC[82] or iTRAQ[83]), a label-free quantitation approach was employed in the current study, as it remains the simplest, most cost-effective method that can be applied to clinical samples. Technical variability must be considered in both approaches, but particularly so in label-free studies. To achieve this, technical, as well as biological, replicates must be included in the study design so that this variability may be assessed. Label-free quantitation may be achieved by spectral count, which relies on the assumption that more abundant proteins produce a greater number of peptides that can be identified.[84] Furthermore, protein size is considered, as large proteins produce more peptides and therefore more MS/MS fragments and detection events. The peak intensity method, implemented here via MaxQuant's MaxLFQ, monitors peptide-specific elution profiles and uses the resulting area under the curve to calculate peptide (or pre-cursor ion) abundance.[85] In addition, the "match between runs" feature in MaxQuant allows unidentified or incomplete spectra in certain samples to be matched with identifications in other samples, based on retention times and masses, thereby improving identification and quantitation.[85]

Statistical and biological analyses

To compare protein abundance between different samples and sample groups, tests may be performed to determine statistical significance. Student's t tests can be applied to compare protein expression across two sample groups, while analysis of variance (ANOVA) is used to compare that in three or more conditions. In these tests, the mean expression value (in this case, mean LFQ intensity)

per sample group, as well as the standard deviation from the mean, are considered, and a p-value is calculated. The differences in the mean protein expression between groups are deemed statistically significant is $p < 0.05$ (or other user-defined threshold). Multiple testing correction is applied here using the Benjamini-Hochberg method or permutation-based FDR. In the current study, statistical analyses were performed using the open-source software Perseus (http://www.perseus-framework.org).[86]

Lists of significantly differentially expressed proteins generated here are further analyzed in terms of their biological significance using the STRING (Search Tool for the Retrieval of Interacting Genes/Proteins) database, freely accessible at http://string-db.org/. STRING incorporates data relating to all biologically meaningful protein interactions, both at the direct (physical) and functional levels. Knowledge is gathered from experimental evidence, as well as known pathways and protein complexes extracted from curated databases, co-expression analysis, genomic data, automated text-mining, and gene orthology-based interactions.[87] Other popular functional classification tools include PANTHER (protein annotation through evolutionary relationships), which uses gene ontology, pathways, and statistical analyses to probe large-scale genomic or proteomic data,[88] and Cytoscape, which allows visualizations of biological network pathways using network topological data.[89]

Chapter 2

Project rationale, aims, and objectives

2.1 Rationale

TB-IRIS is an inflammatory disease mediated by the complex and dynamic immune system, and physiologically characterised by an increase in several inflammatory molecules. N-3 PUFA are safe and effective immune-modulatory agents with inflammation-resolving activity, and we hypothesized that they will have beneficial effects on TB-IRIS-associated inflammation. A systems biology approach such as MS-based proteomics is an appropriate strategy for investigation of n-3 PUFA-mediated modulation of TB-IRIS, as it is a systemic disorder involving the complex immune system. The investigation of the proteomic changes induced by n-3 PUFA treatment in TB-IRIS patient-derived PBMCs will provide pre-clinical rationale for the beneficial effects of n-3 PUFA in the TB-IRIS setting.

2.2 Aims

The current work aimed to use MS-based proteomic strategies to:

1) Investigate the effects of re-stimulating healthy donor and IRIS/non-IRIS patient-derived PBMCs with *Mtb* whole cell lysate (WCL)
2) Investigate the effects of n-3 PUFA pre-treatment on *Mtb* WCL-stimulated healthy donor and patient-derived PBMCs
3) Identify any differences in the responses of non-IRIS and IRIS patients-derived PBMCs to *Mtb* WCL stimulation and n-3 PUFA treatment

2.3 Objectives

In order to fulfil the aims, the following objectives were applied:

- Isolate and cryopreserve PBMCs from healthy donors, optimise a cell culture model to culture PBMCs, including re-stimulating with *Mtb* WCL and pre-treating with n-3 PUFA
- Perform MS-based, label-free, discovery proteomic analysis on the cell culture supernatants from healthy donor PBMCs (n = 3) thawed and rested for 18 h, and then re-stimulated with *Mtb* WCL for 24 h

- Repeat the discovery proteomic analysis using cell culture supernatants from healthy donor PBMCs (n = 4) thawed and rested for 18 h, pre-treated with n-3 PUFA for 2 h, and then re-stimulated with *Mtb* WCL for 24 h
- Repeat the discovery proteomic analysis using cell culture supernatants from non-IRIS (n = 5) and IRIS (n = 5) patient-derived PBMCs thawed and rested for 18 h, pre-treated with n-3 PUFA for 2 h, and then re-stimulated with *Mtb* WCL for 24 h
- Analyze the data to identify differentially expressed proteins between control and stimulated or treated conditions, in healthy donor and patient-derived samples.

Chapter 3

Methods

3.1 Cell work

3.1.1 Healthy volunteer sample collection

Eight healthy blood donors were recruited from the Blackburn research group (four males and four females). Each volunteer filled in a questionnaire to collect relevant metadata (Table 3) and two to four vials of blood (18 to 36 mL) were obtained from the cubital vein in heparinised vacutainers.

Table 3. Healthy volunteer characteristics

ID code	Age (years)	Sex	BCG vaccine	Alcohol consumption	Smoker	Medication	Illness
HV01	24	Male	Yes	None	No	No	No
HV02	24	Female	No	Occasionally	No	Oral contraceptive	No
HV03	38	Male	Yes	Occasionally	Yes	No	No
HV04	28	Male	Yes	Rarely	No	No	Allergies
HV05	25	Male	Yes	None	No	No	Asthma
HV06	29	Female	Yes	Regularly	No	No	No
HV07	27	Female	Yes	None	No	No	No
HV08	32	Female	Yes	Regularly	No	Contraceptive implant	No

Volunteers were asked to complete questionnaires to collect the following data: age, sex, whether they had received the BCG vaccine, alcohol consumption and smoking habits, medication taken regularly, and chronic illnesses.

3.1.2 PBMC isolation

Blood samples were processed in a Bio-Safety Level 2 (BSL2) laboratory within 4 h of collection. The standard Ficoll-Paque density gradient centrifugation method was used to isolate PBMCs from whole blood.[90]

Fifteen to 18 mL of blood was diluted with an equal volume of Dulbecco's phosphate buffered saline (PBS; Sigma) at room temperature (approximately 23 °C) in a 50 mL tube. Eighteen millilitres of Ficoll-Paque Plus (GE Healthcare LifeSciences) was placed in a new 50 mL tube, over which an equal volume of the blood/PBS solution was gently layered. The mixture was centrifuged at 700 g for 20 min at room temperature (brake off). As a result of this centrifugation step, the solution separated into four layers (Figure 9): the uppermost layer containing plasma, while the second layer, characteristically milky white, contained PBMCs. The third and fourth layers contained Ficoll-Paque media and granulocytes/erythrocytes, respectively.

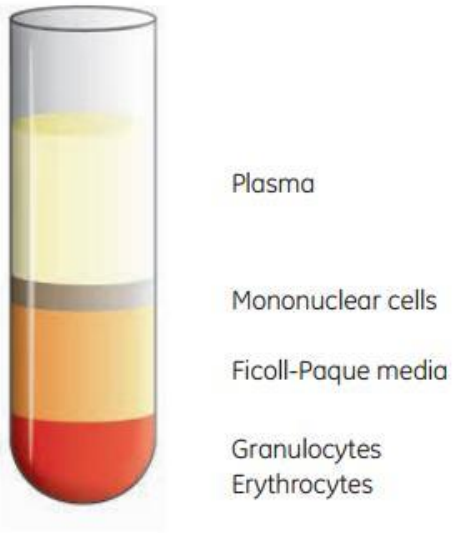

Figure 9. Schematic representation of layers formed after centrifugation

The uppermost layer contains plasma, while the second layer is characteristically milky white and contains PBMCs. The third and fourth layers contain Ficoll-Paque media and granulocytes/erythrocytes, respectively. *Sourced from GE Healthcare BioSciences, 2014.*[91]

Using a Pasteur pipette, the middle phase containing PBMCs was carefully removed, and added to a new 50 mL tube containing 10 mL RPMI-1640 medium (Sigma). The PBMCs were washed by centrifuging at 600 g for 10 min at room temperature (brake on). The supernatant was discarded, and 10 mL RPMI was added to the pellet and triturated to ensure cells were well suspended. A 20-µL aliquot was removed for cell counting (see section 3.1.3 Trypan blue exclusion assay (cell counting)) and cells

were centrifuged once more as previously. The pellet was resuspended in RPMI containing 10% fetal calf serum (FCS, Sigma), and FCS containing 20% dimethyl sulfoxide (DMSO, Sigma) to obtain a concentration of 5-6 million cells/mL in 40% RPMI/FCS, 50% FCS/DMSO, and 10% PBS. The solution was aliquoted into cryovials and placed in a Mr Frosty™ (ThermoScientific) at -80 °C overnight before transferring the following day to a liquid nitrogen tank for long-term storage.

3.1.3 Trypan blue exclusion assay (cell counting)

In a 96-well plate, a 20-µL PBMC cell suspension aliquot was diluted with 20 µL 0.4% trypan blue solution (Sigma). A 10-µL aliquot of the resulting solution was then loaded onto a FastRead 102™ counting chamber microscope slide (Hycor Biomedical) and visualized under the microscope. The cells in the top 16 blocks of the counting chamber were counted (each block contains a volume of 0.1 µL). The total number of cells in the 10 mL PBMC solution was then calculated by multiplying by 2 (as the PBMC solution was diluted with trypan blue at a ratio of 1:1), then by 10 (as the volume in which the cells are suspended is 10 mL), and finally by 10^5 (as the volume of each counting chamber block is 0.1 µL). The formula below (Equation 1. Total number of cells in 10 mL RPMI PBMC solution) was used to calculate the number of PBMCs in solution. In addition, the percentage cell viability was estimated by counting the number of dead cells which had taken up trypan (seen as blue under microscope), dividing by the number of live cells (white), and multiplying by 100.

Equation 1. Total number of cells in 10 mL RPMI PBMC solution

$$\text{Number of PBMCs} = \text{total cells counted in 16 blocks} \times 2 \times 10 \times 10^5$$

3.1.4 Thawing

To thaw, cryovials containing frozen PBMCs were removed from the liquid nitrogen tank and immediately placed on ice after loosening caps. The samples were then thawed in a water bath at 37 °C until a small block of ice remained in the tubes, and were moved to a BSL2 cabinet for further processing. Five hundred microliters of warmed (37 °C) RPMI medium was added dropwise, and the cells were then transferred to a 15 mL tube containing 5 mL warmed medium. One millilitre of medium was used to rinse out the cryovials and added to the rest of the cells. The freezing medium containing 10% DMSO was exchanged for RPMI by pelleting cells at 500 g for 5 min (20-25 °C) and discarding the supernatant. This wash step was repeated. The cells were then resuspended in 2 mL RPMI containing

1% penicillin/streptomycin (pen/strep) solution, and counted (see section 3.1.3 Trypan blue exclusion assay (cell counting)). Another 3 mL of RPMI was added to the cells, which were then rested overnight at 37 °C in a 5% CO_2 atmosphere to ensure lysis of any apoptotic cells.

3.1.5 Cell culture

Following overnight rest, the cells were pelleted at 500 g for 5 min at room temperature, resuspended in 1 mL RPMI supplemented with 1% pen/strep solution, and counted (see section 3.1.3 Trypan blue exclusion assay (cell counting)). Suspension volume was adjusted with RPMI to obtain a concentration of 10^6 cells/mL. Cells were cultured in 24-well, flat-bottomed cell culture plates with lids (Costar, Corning) at a concentration of 5 x 10^5 cells per well. Cells were plated as follows: RPMI was added to all wells first, followed by 1 µL EPA (Sigma) and 1 µL DHA (Sigma), both made up in ethanol to 100 µM stocks, or 2 µL ethanol (Sigma), added to the treatment and vehicle control wells respectively, and finally 500 µL of cell suspension. Cells were then pre-incubated in the presence of EPA and DHA for 2 h, before the addition of 20 µL *Mtb* lysate (whole cell lysate (WCL) from H37Rv, 2 µg/mL) into the relevant wells. Incubation was then continued for a further 24 h. The volumes of all reagents used are shown in Table 4. Volume of each reagent added to cultured PBMCs

Table 4. Volume of each reagent added to cultured PBMCs

Reagents (µL)	Treatment condition			
	Control	*Mtb* control	Vehicle control	PUFA treatment
RPMI	500	480	478	478
EPA/DHA	-	-	-	2
Ethanol	-	-	2	-
Mtb WCL	-	20	20	20
Cell suspension	500	500	500	500
Total volume	1000	1000	1000	1000

3.1.6 MTT viability assay

PBMCs were thawed and rested overnight according to methods described in section 3.1.3 Trypan blue exclusion assay (cell counting). Cells were then plated according to the method described in section 3.1.4 Thawing. For this experiment, three healthy volunteer samples were used and plated in triplicate for each condition.

After overnight incubation, the culture medium was removed from each well and replaced with 500 µL warmed PBS (37 °C) to wash off any cellular debris. The PBS was then removed and 1 mL medium containing MTT reagent (3-(4,5-dimethylthiazol-2-yl)-2,5-diphenyltetrazolium bromide, Sigma) was added to each well (0.5 mg/mL). The plate was briefly shaken on vortex before incubating for 30 min at 37 °C. The plate was visualized under microscope to check for the presence of purple formazan precipitate in the cells. The supernatant was removed, replaced with 300 µL DMSO, and triturated to dissolve formazan crystals. The plate was vortexed briefly before incubating for 10 min. Finally, the contents of each well were transferred to a 96-well plate containing blanks (RPMI processed in parallel using the same method) for analysis on the microplate reader (Bio-Rad). Absorbance was read at 560 nm. Wells containing untreated cells were used as positive controls.

Cell viability was calculated as a percentage by subtracting the mean absorbance of the blank from each sample absorbance, dividing by the mean absorbance of the control minus the mean absorbance of the blank, and multiplying for 100 (see Equation 2. Percentage cell survival).

Equation 2. Percentage cell survival

$$\% \text{ cell survival} = (\text{sample}_{abs} - \text{blank}_{abs})/(\text{control}_{abs} - \text{blank}_{abs}) \times 100$$

3.2 Sample preparation for MS-based proteomic analysis

3.2.1 Collection of cell culture supernatants

After a 24-h incubation period, 1 mL culture supernatant was transferred to 1.5 mL tubes and centrifuged at 500 g for 5 min to pellet any detached cells and cellular debris. The supernatant was then moved to clean 1.5 mL tubes and stored at -80 °C until further processing.

3.2.2 Sample preparation

Bicinchoninic acid (BCA) assay for protein quantitation

Frozen supernatant samples were retrieved from the -80 °C freezer and left to thaw on the bench. The samples were taken through two cycles of boiling (at 95 °C for 3 min) and sonicating (3 min), followed by filtration through 0.2 µm filters to remove any cells or cellular debris. Protein concentration was quantified by micro-BCA protein assay (Thermofisher Pierce BCA protein assay kit) according to the manufacturer's instructions. Briefly, bovine serum albumin (BSA) standards were prepared by serial dilution with RPMI to obtain the following five concentrations: 1, 0.5, 0.25, 0.125, and 0.0625 mg/mL. The working reagent was prepared by adding 392 µL of Solution B to 19 mL of Solution A. Twenty-five microliters of samples and standards was plated in a 96-well plate, and 200 µL of working reagent was added. The plate was covered with parafilm and shaken on vortex, before incubating at 37 °C for 30 min. The plate was cooled to room temperature (20-25 °C) and absorbance was read at 560 nm on microplate reader (Bio-Rad).

Filter-aided sample preparation (FASP)

Reagents used for FASP were made up fresh every time (urea buffer, iodoacetamide, and ammonium bicarbonate). Dithiothreitol (DTT, see Appendix A for preparation) was added to each sample at a ratio of 1:4, and samples were incubated for 30 min at room temperature (20-25 °C). Two different molecular weight cut-off FASP filters (Amicon Ultra 0.5 mL, 10 kDa and 3 kDa size exclusion filters, Merck Millipore) were tested for comparison. All filters were first washed with 500 µL 8M urea buffer (UA, see Appendix for preparation) and centrifuged at 15,000 g for 10 min. FASP filter tubes were placed in the centrifuge with hinges facing towards the rotor, and this orientation was maintained throughout every spin. The flow-through was discarded. Samples was loaded onto each filter, and 200 µL UA added before centrifuging again at 15,000 g for 15 min. The samples were then washed with 200 µL UA and centrifuged for 10 min at the same speed, and the spin was repeated twice until flow-through was no longer bubbly. The flow-through was moved to waste eppendorfs and stored in case protein was lost during processing and needed to be recovered at a later stage. The samples were then alkylated by adding 100 µL 0.5 M iodoacetamide (IAA, see Appendix for preparation), shaking on vortex for 1 min and incubating for 20 min in the dark. The excess IAA was then washed off by centrifugation at 15,000 g for 10 min, before doing three washes with 200 µL UA and 15 min centrifugation steps. The pH of the samples was then increased by adding 100 µL 0.05 M ammonium bicarbonate (ABC, see Appendix for preparation) and centrifuging twice at 15,000 g for 10 min each time. Filters were then moved to new eppendorfs for elution the following day, and flow-through was again stored. For trypsin digestion of samples, 25 µL of 2X Trypsin-Ultra Reaction buffer (see Appendix for contents) was added.

Five microliters of Trypsin-Ultra (see Appendix for preparation) was added to each sample before shaking on vortex for 1 min. The pH was checked using MColourpHast pH indicator strips (Merck Millipore) and adjusted with ABC if necessary to obtain a pH of 8. Samples were placed in a wet chamber and incubated at 37 °C for 18 h.

After incubation, samples were removed from the wet chamber and centrifuged at 15,000 g for 10 min. Eppendorfs were placed in the centrifuge with hinges facing away from the rotor (opposite orientation as the previous day) and were kept in this orientation throughout spins. Forty microliters ABC was added and samples were centrifuged again at 15,000 g for 10 min. To acidify peptides, 50 µL solution A (2% acetonitrile (ACN), 0.1% formic acid (FA) in MS-grade H_2O) was added before centrifuging for 10 min at 15,000 g. This step was repeated twice with 50 µL solution C (60% ACN, 0.1% FA) added each time. The pH was checked using pH strips and adjusted with 0.5 µL formic acid if necessary to obtain a pH of 2-3. In order to confirm that peptides had successfully eluted, each FASP filter was placed upside down in the corresponding waste eppendorf and centrifuged at 15,000 g for 10 min. The flow-through was checked for pellets, as the presence thereof would indicate that the sample protein/peptides had remained on the filter instead of eluting through as desired. If no pellet was seen, samples were taken forward for desalting.

Desalting

Tryptic peptides were desalted using 3M Empore Octadecyl C18 SPE disks (Supelco) following an in-house protocol. Extraction disks were first equilibrated three times by adding with 100 µL solution B (80% ACN, 0.1% FA in water) and centrifuging for 1-2 min at 3000 g. This was followed by two washes with 100 µL solution A, centrifuging 1-2 min at 3000 g as before. Twenty micrograms of peptides was then loaded and washed three times with 50 µL solution A. The flow-through was moved to waste eppendorfs, and desalted peptides were then eluted into tapered glass inserts by washing three times with solution C. Finally, peptides were vacuum-dried until 1-2 µL of solution was left and resuspended to a concentration of 1 µg/µL with 20 µL solution A. This stock solution was further diluted to 200 ng/µL for analysis on a Q Exactive hybrid quadrupole-Orbitrap mass spectrometer (Thermo).

Methanol/chloroform precipitation

Frozen supernatant samples were retrieved from the -80 °C freezer and thawed at room temperature. Samples were transferred to amber vials, and methanol was added to the sample at a ratio of 1:1, and chloroform at a ratio of 3:4. The resulting solution was mixed by swirling and then centrifuged at 4000

g for 5 min. The upper phase containing chloroform was carefully removed by pipetting and stored in eppendorfs at -20 °C for future lipidomic processing. The interphase containing proteins was mixed with the lower phase and further methanol was added at a ratio of 3:4. The solution was again mixed and centrifuged as before. The supernatant was removed and discarded and the resulting pellet was left to air-dry in a fume hood for 1 h. Once dry, the protein pellets were resuspended in 50 µL denaturation buffer (see Appendix A for preparation), transferred to eppendorfs and stored at -20 °C until further processing.

Modified Bradford assay for protein quantitation

Protein was quantitated using the Bio-Rad Protein Assay (Bio-Rad), according to the manufacturer's instructions. This assay is specifically modified to quantitate protein in urea-containing buffer. Briefly, 1 mL of Bio-Rad Bradford reagent was diluted with 4 mL distilled water, and BSA standards were serially diluted with denaturation buffer to obtain five standards at the following concentrations: 1, 0.5, 0.25, 0.125, and 0.0625 mg/mL. The assay was done in a 96-well flat-bottomed plate, with each well containing 90 µL 0.1 M HCl, 150 µL Bradford reagent, and 1 µL sample, added in this order. The absorbance was read at 595 nm on a microplate reader (Bio-Rad).

In-solution protein digestion

One microliter of 1 M DTT reduction buffer (see Appendix A for preparation) was added to the samples at a final concentration of 1 mM before incubating for 1 h at room temperature. IAA alkylation buffer was then added to a final concentration of 5.5 mM, and samples were incubated for 1 h at room temperature in the dark. Samples were then diluted with four volumes of 50 mM ABC. Trypsin-Ultra was added at a ratio of 1 µg Trypsin to 50 µg sample protein, and incubated overnight for 19 h at room temperature. After overnight incubation, the reaction was stopped by adding 1 µL FA and the pH was checked to be between 2 and 3. Samples were then taken forward for desalting, following the method described in 3.2.2 Sample preparation

3.3 LC-MS/MS analysis parameters

Discovery proteomic analysis was performed on a Q Exactive Quadrupole-Orbitrap mass spectrometer (Thermo Scientific), coupled with a Dionex UltiMate 3500 RSLC nano-LC system (Thermo Scientific). A standardised LC gradient, developed in our laboratory for use with mammalian peptide extracts, was used. One microliter of sample (0.5 – 10 µg) was injected onto a trap column packed in-house with

Luna C18 coated silica beads (75 µm x 2 cm fused silica: New Objective; 5 µm Luna C18 resin: Phenomenex). Separation was performed by reversed phase chromatography on a nanoscale analytical column, also packed in-house (5 µm Luna C18 beads, 75 µm x 20 cm). Solvent A comprised 0.1% FA (LC-MS Ultra, Eluent Additive, Sigma) in HPLC grade H_2O (LC-MS Ultra, Sigma), while Solvent B comprised 0.1% FA (LC-MS Ultra, Eluent Additive) in ACN (LC-MS Ultra, Sigma). Samples were eluted using a non-linear gradient at a constant flow rate of 400 nL/min, with solvent B increasing from 6 to 35% over 60 min (12 to 72 min), and from 35 to 80% over 5 min. Twenty-five minutes equilibration and wash (0 to 12 min, and 77 to 90 min) were also included.

Discovery mode data acquisition by the Orbitrap was performed in 'Top 10', data-dependent, positive ion mode. MS_1 settings included resolution at 70 000, automatic gain control (AGC) target of 3e6, and a maximum injection time of 250 ms. At the MS_2 level, resolution was set at 17 500, AGC target of 1e5, ion injection time of 80 ms, isolation window of 2.0 m/z and a normalised collision energy (NCE) of 28. Oxidation (variable) and carbamidomethylation (fixed) were included as modifications.

3.4 Data analysis

3.4.1 Database search

RAW files were submitted to the free-ware software MaxQuant v.1.5.2.8 (http://www.biochem.mpg.de/5111795/maxquant) for protein identification and label-free quantification. The UniProt human and *Mtb* H37RV proteomes (FASTA files) were used for database search (downloaded 2 Feb 2017; human, 71,775 proteins; *Mtb*, 3993 proteins). Carbamidomethylation was set as a fixed modification, and methionine oxidation and N-term acetylation as variable modifications. The following parameters were used: PSM, protein, and site FDR, 1%; MS/MS tolerance, 20 ppm; matching time window, 0.7 min; alignment time window, 20 min. The "match between runs" setting was selected to increase the probability of identifying protein groups in all samples and to aid in the comparison of protein group quantities across samples. MS data quality and summary statistics were assessed in the R environment using scripts developed in-house.

3.4.2 Data processing

Data processing was done via the open-source software Perseus v1.5.5.3 (http://www.biochem.mpg.de/5111810/perseus). The ProteinGroups file produced by the MaxQuant search was loaded onto a new session in Perseus. The protein list was filtered to remove all protein

groups labelled “Contaminants”, “Reverse”, “Only identified by site”, as well as those identified with only one unique peptide (Filter rows -> Based on categorical column, and filter rows -> Based on numerical value -> Unique peptides > 1). The data were then transformed by log2(x). In order to impute missing values, the distribution of the protein intensities was evaluated by looking at the histograms (Visualization -> Histogram) and these were exported to .pdf. Missing values were then imputed from the normal distribution (w = 0.3, downshift = 1.8). Rows were then annotated into the condition groups (Annot. Rows -> Categorical annotation rows). Since the protein list contained both human and *Mtb* proteins, we used the “Find” function to export lists of human-only proteins and *Mtb*-only proteins. Using the human-only list, principal component analyses were carried out (Clustering -> Principal component analysis) and resulting figures were exported to .pdf. Differential expression analysis was performed by hypothesis testing, using paired two-sampled t-tests ($p < 0.05$) for each protein group in order to identify differentially expressed protein groups. Permutation-based FDR multiple testing correction was applied at the 5% level. The resulting protein list was filtered to retain only those with a significant t-test score ($p < 0.05$). The final significant protein lists were visualized as volcano plots (Misc -> Volcano plot). Volcano plots and protein lists were exported to .pdf and .txt files, respectively. Other data visualizations include multi-scatter plots and heat maps. Venn diagrams were produced using the open-source software VennDIS (available at http://kislingerlab.uhnres.utoronto.ca/projects/VennDIS_v1.0.1.zip).

3.4.3 Biological significance analysis

Functional classification and gene annotation were performed using the free online database STRING (http://string-db.org), and the free software FunRich (www.funrich.org).

Chapter 4

Cell culture

4.1 Aim

With the experiments described in this chapter, we aimed to optimise the cell culture platform and ensure that cell isolation, preservation, and culture conditions were appropriate for cell survival. PBMCs were isolated from freshly drawn blood and cryopreserved in liquid nitrogen at ultra-low temperatures. We investigated the recovery rates of cryopreserved (c-)PBMCs after thawing, as well as survival rates after overnight rest and after stimulation with *Mtb* whole cell lysate (WCL) and treatment with PUFA through trypan blue exclusion and MTT assays.

4.2 Introduction

4.2.1 PBMC analysis

The investigation of the immune system is at the heart of understanding the pathogenesis of many immune disorders such as rheumatoid arthritis, multiple sclerosis, and of course, TB-IRIS. Analysis of PBMCs is particularly relevant as it allows for the investigation of the role and phenotype of a heterogeneous population of immune cells, including monocytes and lymphocytes.[92] TB-IRIS is reportedly associated with hypercytokinemia,[50] as well as heightened Th1 cell responses,[48] and we therefore hypothesized that TB-IRIS-specific cell responses would be reflected in the proteome of patient-derived PBMCs.

With access to *ex vivo* PBMCs from HIV-positive and TB-infected patients, some of whom developed TB-IRIS ("IRIS group") and some of whom did not ("non-IRIS group"), we aimed to re-stimulate the cells *in vitro* and treat them with n-3 PUFA before harvesting the culture supernatants to investigate the secretome. Before analyzing clinical samples, the various cell culture methods were optimised using healthy volunteer (HV) PBMCs. The workflow includes collection of PBMCs, re-stimulation and treatment, sample processing for proteomic analysis via LC-MS/MS, followed by statistical and biological analyses. This workflow is depicted in Figure 10 below.

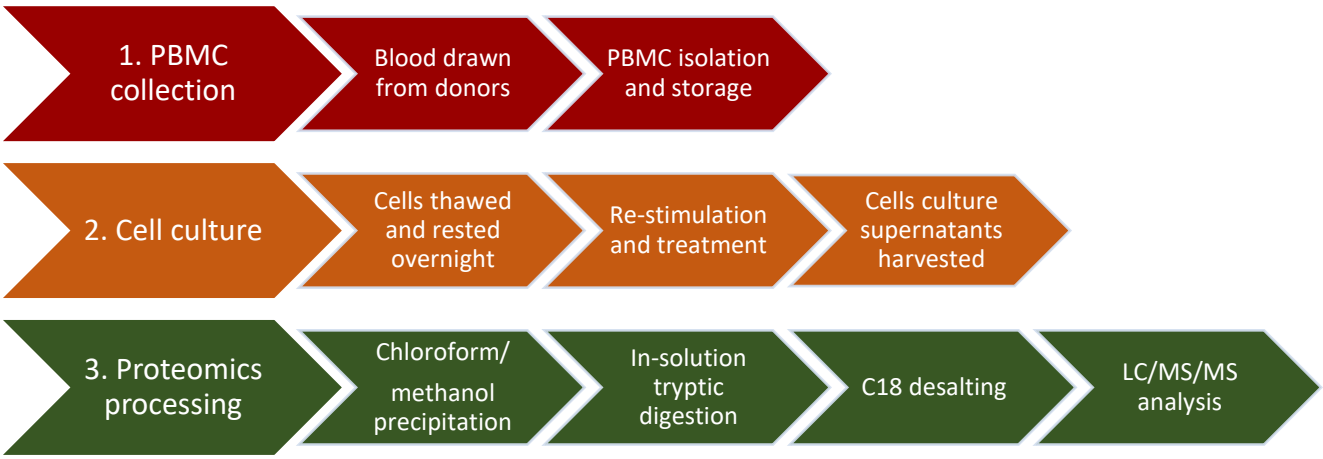

Figure 10. Infographic of the methodology used

1. PBMC collection, 2. cell culture, and 3. sample processing for proteomics.

4.2.2 PBMC re-stimulation with *Mtb* WCL

Isolated *ex vivo* PBMCs can be treated or stimulated with bacterial or viral products to investigate the resulting immune response. In this study, we assessed the proteomic changes induced in the PBMC secretome by re-stimulation with *Mtb* WCL. To this end, healthy donor PBMCs were isolated and cryopreserved. As required, these cells were then thawed, rested, and re-stimulated with H37Rv *Mtb* cells lysed with Triton X-100 for 24 h. Tadokera *et al*.[50] used a similar method, but re-stimulated PBMCs with heat-killed H37Rv *Mtb*. Other methods include re-stimulation with PPD, ESAT-6, and Antigen85B[46], or ESAT-6/CFP10 fusion protein.[49] In this study, we have used WCL from H37Rv bacteria for practical reasons as this was easily available to us. We used a concentration of 2 µg/mL, as did Hoft *et al*.[93] *Mtb* WCL contains cell surface antigens, as well as intracellular products, which are likely to elicit an immune response from PBMCs.

4.2.3 n-3 PUFA treatment

PBMCs were also subjected to n-3 PUFA treatment to investigate the effects of n-3 PUFA on the *Mtb*-activated immune response in PBMCs. In this study, we used a combination of eicosapentaenoic acid (EPA) and docosahexaenoic acid (DHA), the two most potent n-3 PUFA in humans. A dose-response viability assay was performed to assess the effects of three increasing n-3 PUFA concentrations on cell viability, and an appropriate treatment concentration was then chosen for further assays. Both EPA and DHA were dissolved in ethanol, which was used as the vehicle in control experiments.

4.3 Results and discussion

4.3.1 Cell recovery

As part of the cell culture protocol optimisation, healthy volunteer PBMCs were counted at the point of freezing, after thawing, and after overnight rest, in order to evaluate the viability of c-PBMCs in serum-free conditions. PBMCs were cultured in RMPI-1640 medium not supplemented with serum, as the over-abundance of albumin in serum relative to other proteins would have hampered down-stream proteomic analysis.

PBMCs from three healthy volunteers were isolated from whole blood and frozen in liquid nitrogen. Cells were later thawed, and rested overnight in culture conditions. Cells were counted at each of these two stages, and the number of viable cells recovered was calculated relative to the number of cells frozen, and expressed as a percentage. This experiment was repeated several times, and included both biological and technical triplicates. Results are shown in Figure 11. The mean recovery ± SD across all biological and technical replicates was 38.86 ± 6.81% after thawing, and 36.97 ± 4.02% following overnight rest. This indicates that approximately 60% of cells were lost during the freezing period, and that overnight rest in serum-free conditions was well tolerated as only a small number of cells (approximately 1%) were lost over this period. Viability as assessed via trypan blue exclusion assay was > 90% both directly after thawing and after overnight rest.

The recovery rate for our frozen PBMCs was slightly lower than that reported in the literature (50-70% average yield reported[94,95]). This could be due to sub-optimal freezing or thawing conditions and protocols. However, Nazarpour *et al.*[96] compared the effects of several variables on the yield and viability of c-PBMCs, and concluded that the optimal concentrations of DMSO and FCS to be used were 10-15% and 40%, respectively. In this study, PBMC were stored in a solution containing 10% DMSO and 44% FCS. Our thawing process, which includes the addition of warmed medium to the cells to dilute the freeze solution containing DMSO, is also in line with current protocols. Ramachandran *et al*.[97] showed that "warm processing" produced higher yields of viable cells than "cold processing" (adding chilled medium to cells). In our study, the DMSO is washed off immediately when the cells are thawed as prolonged exposure can cause cell toxicity; however, Ramachandran *et al*. showed that c-PBMCs can withstand up to 30 min exposure to DMSO without losing CD4+ or CD8+ T cell functionality.[97] Finally, we followed the recommendation by Ramachandran *et al.* to perform two wash steps to remove or dilute DMSO.[97] Perhaps cell yields could be increased by cooling the freeze

medium to 4 °C before adding to the cell solution, as was recommended by Nazarpour *et al*.,[96] as the medium was added at room temperature in our study.

The cells were rested overnight to allow for lysis of any apoptotic cells. This is supported by Kutscher *et al*.,[98] who showed that c-PBMCs that were not rested overnight contained higher percentages of apoptotic cells than rested PBMCs, which contained more dead cells. Another study found that resting PBMCs presented no advantage when performing ELISPOT assays.[99] In our study, overnight rest did not cause significant cell loss and could possibly be avoided in the future although we would first need to investigate the effects of this on cell viability.

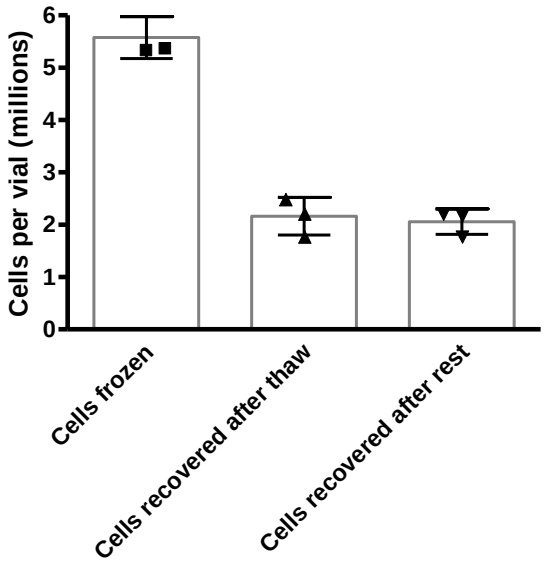

Figure 11. Number of cells recovered after thawing and overnight rest

Results are shown as means ± SD (error bars) from five independent experiments using cells from three healthy donors.

4.3.2 Cell viability

We performed an MTT assay to assess the viability of cells after 24-h incubation with *Mtb* WCL, ethanol (vehicle control), and EPA/DHA treatment. Frozen PBMCs were thawed, rested overnight, and plated at a concentration of 5 x 10^5 cells per well, pre-treated with ethanol or n-3 PUFA, and re-stimulated with *Mtb* WCL. We used concentrations of 100 µM EPA and DHA, and 2 µg/mL *Mtb* WCL. The EPA/DHA concentration used was based on the literature (50 to 100 µM[100,101,102]) as well as previous in-house experiments, and a dose-response MTT assay was performed to assess the effects of three increasing EPA/DHA doses on cell viability. The concentration of *Mtb* WCL used was based

only on the literature: Bourgarit *et al*.[46] re-stimulated PBMCs with 1 µg/mL PPD and ESAT-6, and 2 µg/mL 85B, while Skolimowska *et al*.[103] used 5 µg/mL PPD and other *Mtb* antigens at 10 µg/mL. Finally, heat-killed H37Rv has been used at an MOI = 1 in several studies[50,103] or MOI = 5.[104] Hoft *et al*.[93] used whole *Mtb* WCL at 2 µg/mL to re-stimulate PBMCs, and this is the concentration we also used.

After 24-h incubation, the MTT assay was carried out according to the standard method.[105] Percentage viability was calculated relative to the untreated and unstimulated control. The results are shown in Figure 12 below. There was no significant change in viability in the cells stimulated *with Mtb* WCL, or treated with ethanol and n-3 PUFA. Cell viability was consistently >85% for stimulated and treated cells. The results obtained from this assay were confirmed via trypan exclusion assay, which showed viability >98% in the unstimulated and untreated control. These results show that neither the serum-free culture conditions, nor the re-stimulation/treatment of the PBMCs were causing cell death.

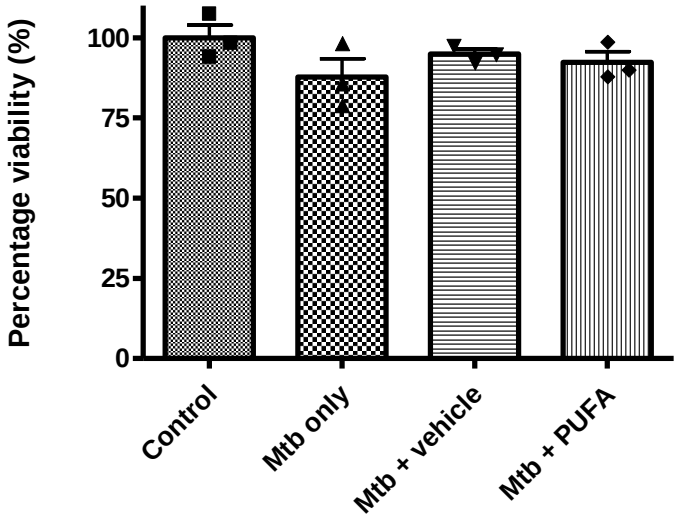

Figure 12. Percentage cell viability for each treatment condition

Results presented are means ± SD (error bars) from two independent experiments with samples plated in biological triplicates. Control: untreated unstimulated cells, *Mtb* only, cells stimulated with 2 µg/mL *Mtb* WCL; *Mtb* + vehicle, cells pre-treated with 0.2% ethanol for 2 h and stimulated with 2 µg/mL *Mtb* WCL; *Mtb* + PUFA, cells pre-treated with 100 µM EPA and DHA for 2 h and stimulated with 2 µg/mL *Mtb* WCL. There were no significant differences in cell viability between any of the treatments ($p > 0.05$).

PUFA dose-response assay

We performed an MTT assay to assess the effects of increasing n-3 PUFA concentrations (50, 100, and 200 µM) on cell viability. Viability was greater than 90% at each concentration (Figure 13). The final n-3 PUFA concentration used for treatment was 100 µM EPA and DHA, and this is in line with the literature (50 to 100 µM[100,101,102]).

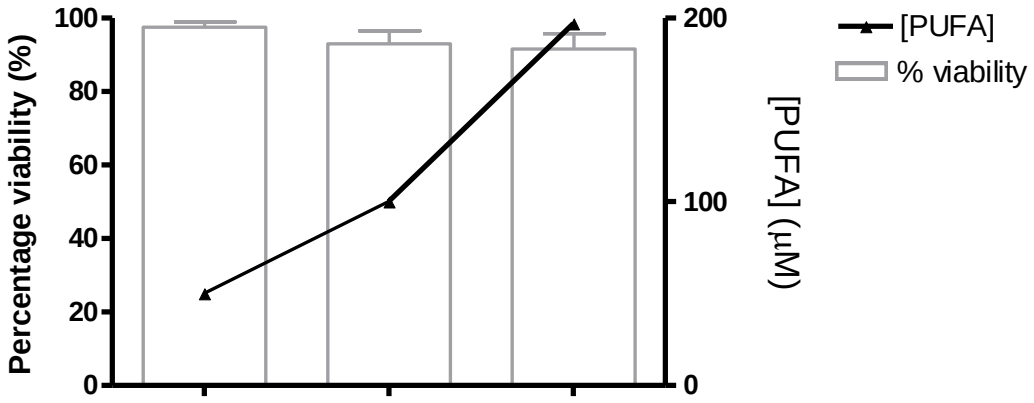

Figure 13. Percentage cell viability after 24-h treatment with increasing PUFA concentrations

Results presented are means ± SD from two independent experiments with samples plated in biological triplicates. Three PUFA doses were tested: 50, 100, and 200 µM. There were no significant differences in cell viability between any of the treatments ($p > 0.05$).

4.4 Conclusion

We developed a cell culture platform to assess the effects of n-3 PUFA treatment and *Mtb* re-stimulation of donor-derived c-PBMCs. The cells can be cultured in serum-free conditions for 48 h and viability was not affected by PUFA or ethanol pre-treatment, or re-stimulation with *Mtb* WCL. This cell culture protocol is compatible with down-stream MS-based proteomic analysis, as no serum is used. With this, the effects of various agents on the PBMC proteome can be assessed in healthy donor cells or patient-derived cells in the context of various diseases. We preferred to use whole PBMC populations rather than separate cells into distinct groups as we believed this is a better *in vitro* representation of the complex immune system, although it would also be possible to separate out cell populations after culture in order to further evaluate specific cellular signals.

Chapter 5

Secretome analysis of *Mtb*-stimulated healthy volunteer PBMCs

5.1 Aim

The experiment described in this chapter was designed to test the sample processing methods, and to evaluate technical and biological variation, as well as reproducibility. To this end, PBMCs isolated from three healthy donors were cultured and re-stimulated with *Mtb* WCL. Unstimulated cells were used as controls. In addition to the three biological replicates, all cells were plated in triplicate (different wells) to produce three technical replicates for each biological replicate and treatment condition. The cell culture supernatants were collected after 24 h and processed for MS-based proteomics analysis by chloroform/methanol precipitation followed by in-solution digestion with trypsin and desalting on C18 stage tips. Samples were analyzed on a Q Exactive hybrid Orbitrap mass spectrometer and peptide and protein identification were performed using MaxQuant. Data were analyzed using Perseus.

5.2 Introduction

5.2.1 Studying the cellular secretome

The "secretome" refers to the set of molecules produced and secreted by cells, although the more modern definition also includes molecules that are shed from the cell's surface[106]. Secreted proteins are of particular interest as they are responsible for intracellular signalling and interactions. In the cancer field, proteins secreted by tumours are often useful as biomarkers. Proteomic profiling of cellular secretomes is notably challenging for several reasons as highlighted by Markakis *et al.*,[106] including (i) the presence and over-abundance of serum proteins such as bovine serum albumin in cell culture media, (ii) contamination by non-secreted cytoplasmic proteins as a result of cell death, and (iii) very low concentrations of secreted proteins in body fluids such as plasma and urine, or cell culture media. Brown et al.[107] have stated that secretomic analyses from mammalian cells generally identify between 100 and 600 proteins, which is in line with our results.

(i) Serum-free culture conditions

The problem of serum protein contamination is generally circumvented by culturing cells under conditions of serum starvation in serum-free culture medium. However, it is important to consider the effect of serum starvation on cellular survival: proliferation rate may be reduced[108] and apoptosis pathways may be switched on by the metabolic stress of serum starvation.[109] On the other hand, survival pathways may be activated, especially in the case of tumour cells.[110] Levels of cytosolic proteins, such as beta-actin and beta-tubulin can be monitored to assess cell autolysis in serum-free conditions.[111] For long-term cell culture (> 24 h), cells can initially be maintained in serum-supplemented medium before washing thoroughly to remove medium and switching to serum-free conditions for the last 12-48 h of the experiment. In this study, PBMCs were maintained in RPMI-1640 medium not supplemented with serum for 24 h.

(ii) Concentrating secreted proteins

Proteins secreted in cell culture medium or body fluids are highly diluted, and usually require concentration before mass spectrometry-based analysis. Classical concentration methods include precipitation using trichloroacetic acid (TCA), chloroform/methanol, or acetone, as well as ultracentrifugation on molecular weight cut-off filters (for example, 10 or 30 kDa). According to Makridakis *et al.,* precipitation with TCA supplemented with 0.01-0.1% sodium deoxycholate or sodium lauroyl sarcosinate significantly increased precipitation yields and allowed for the enrichment of low-abundance proteins such as cytokines from bladder cancer cells.[112] In this study, we assessed concentration on 10 and 30 kDa FASP filters, as well as chloroform/methanol precipitation followed by in-solution digestion.

5.3 Results and discussion

5.3.1 Sample processing optimisation

Two sample-processing methods were tested for the proteomic analysis of cell culture supernatants: FASP and precipitation with chloroform/methanol coupled with in-solution digestion. Both methods were followed by desalting on C18 stage tips.

After protein quantitation via modified Bradford assay, samples were processed using 10 and 30 kDa FASP filters. MS analysis showed that most proteins were lost during FASP and protein identification using a database search was impossible. The starting amount of protein was less than 10 µg, which would explain the poor results obtained via FASP as this method is not suited to use in samples with low protein concentration. We therefore tested the alternative chloroform/methanol precipitation method. Proteins in the supernatants were first precipitated by mixing with chloroform and methanol, concentrated by air-drying, and subsequently resuspending in a small volume. This method was particularly well-suited here as protein concentration in supernatants was so low. Reconstituted proteins were then reduced with DTT, alkylated with IAA, and digested in solution with trypsin overnight. Digested peptides were desalted as previously the following day on C18 stage tips.

5.3.2 Technical reproducibility of protein quantitation

Total protein was quantified via modified Bradford assay[113] (Figure 14). Cell culture supernatants from unstimulated samples contained between 1.85 and 2.15 µg total protein (mean concentration: 0.040 µg/µL), while stimulated samples yielded between 3.75 and 4.20 µg protein (mean concentration: 0.079 µg/µL). Stimulated supernatants contained more protein than their unstimulated counterparts partially because *Mtb* WCL was added to these samples at a concentration of 2 µg/mL (total protein added: 2 µg). In addition, stimulated cells are likely to produce more protein in response to the perturbation experienced. Very similar protein concentrations were obtained from both the technical replicates as illustrated by the small standard deviations (error bars), and the biological replicates. This indicates that technical and biological variability with regards to protein content in cell culture supernatants in our experiment was low.

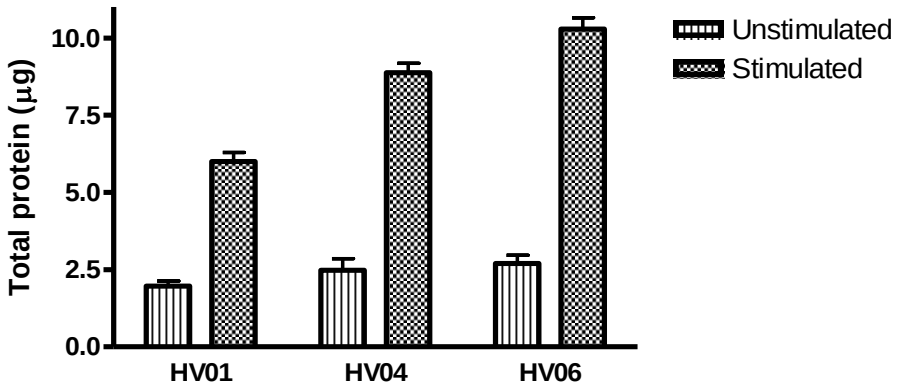

Figure 14. Total protein content in stimulated and unstimulated cell culture supernatants.

Data are presented as means ± SD (error bars) of three technical replicates. HV, healthy volunteer.

5.3.3 Technical reproducibility of MS spectra

Processed samples were initially injected on a Q Exactive LC-MS/MS at 200 ng/µL (1 µL injection volume), and we subsequently re-submitted any sample with a total ion chromatogram (TIC) that was too high or too low (target: 4e9 to 5e9). The injection volumes were then adjusted to ensure consistency of TIC intensities across samples.

The technical replicates for unstimulated samples performed well and were very similar to each other in terms of shape of the TIC and retention time for individual peaks: the peak eluting at 83.96 min in all samples (Figure 15, Figure 16, and **Error! Reference source not found.**) is very consistent, as are sample-specific peaks, such as peaks eluting at approximately 46 min in the control samples from HV01 (Figure 15), or the peak at approximately 57 min in the *Mtb*-stimulated samples from HV06 (Figure 17). Samples from HV04 (Figure 16) performed somewhat differently from the other volunteer samples, and produced 'flat' spectra with a large wide peak at approximately 58 min. This suggests poor protein extraction, digestion, or desalting. The sharp peak at 84 min, although it is also seen in other samples, could be greater in intensity and therefore responsible for suppressing the signal from the rest of the peptides.

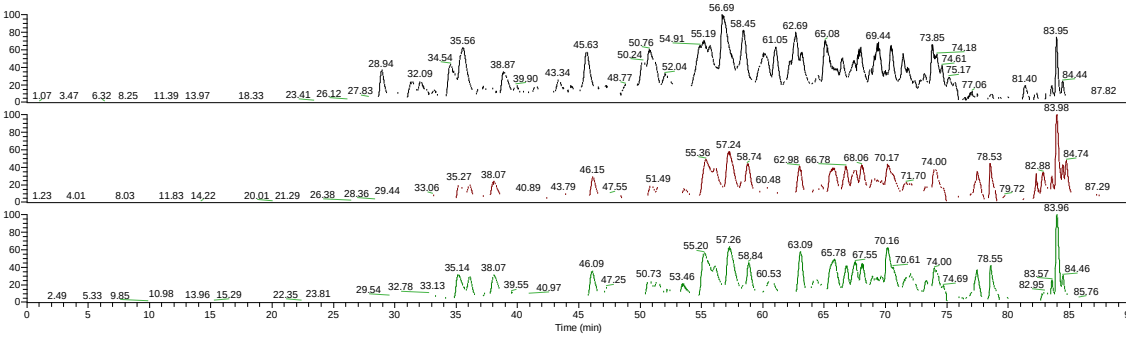

Figure 15. MS chromatogram overlay (TIC) of the unstimulated control samples (HV01, technical replicates)

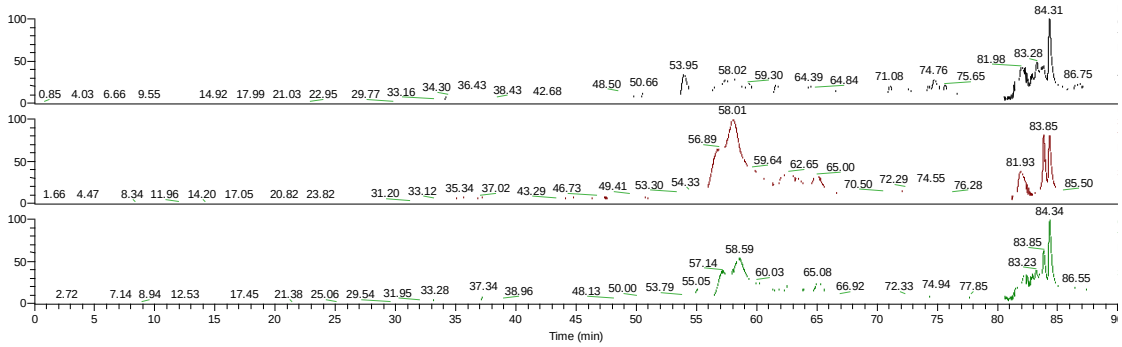

Figure 16. MS chromatogram overlay (TIC) of the unstimulated control samples (HV04, technical replicates)

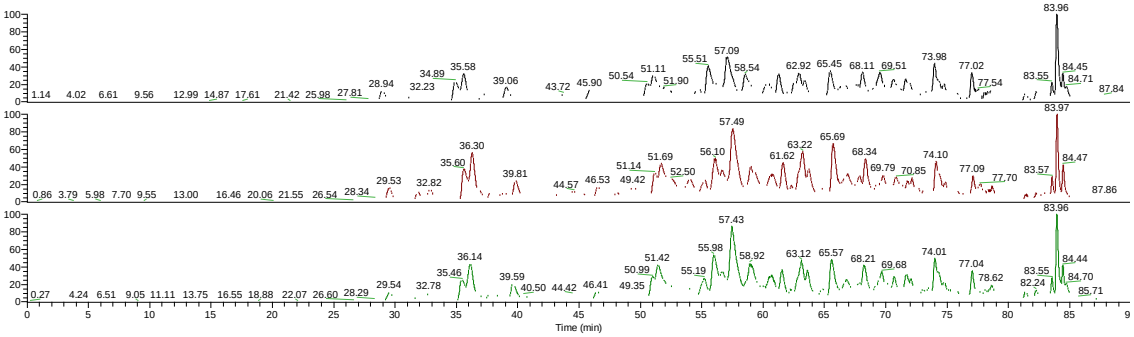

Figure 17. MS chromatogram overlay (TIC) of the unstimulated control samples (HV06, technical replicates)

Technical replicates of stimulated samples (Figure 18, Figure 19, and Figure 20) also performed constistently as shown by the similar retention time of peaks at approximately 53 min in Figure 18 and 54 min in Figure 19, and 57 min in Figure 7. However, the chromatogram in Figure 18 shows poor spray at 70 to 80 min, resulting in jagged peak lines. Unfortunately, due to time constraints we could not re-inject this sample. Overall, we concluded that the variability between biological and technical replicates in terms of TIC shape was low.

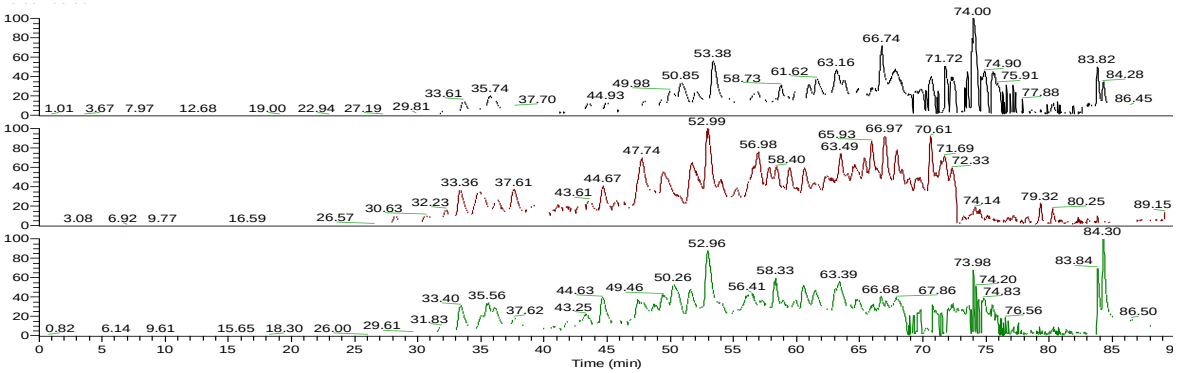

Figure 18. MS chromatogram overlay (TIC) of *Mtb*-stimulated control samples (HV01, technical replicates)

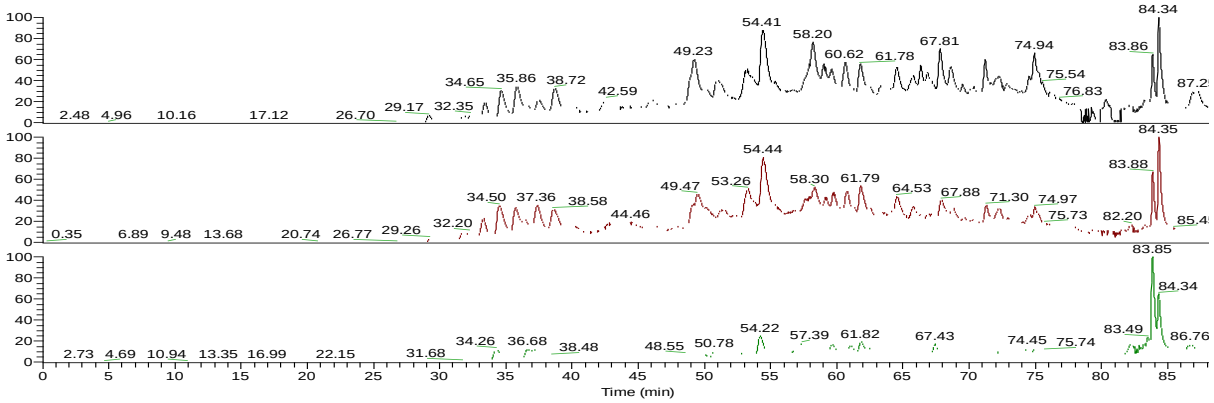

Figure 19. MS chromatogram overlay (TIC) of Mtb-stimulated control samples (HV04, technical replicates)

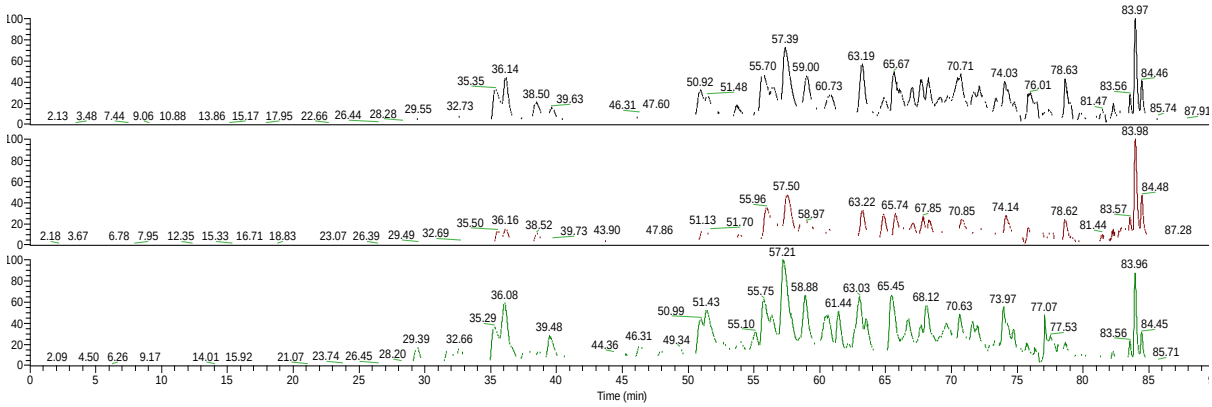

Figure 20. MS chromatogram overlay (TIC) of *Mtb*-stimulated control samples (HV06, technical replicates)

5.3.4 Data quality

Protein identification

The quality of the MS data and MaxQuant peptide identifications were assessed in the R environment using a script developed in-house. A total of 1096 protein groups were identified by MaxQuant using its built-in search algorithm Andromeda and the proteomic libraries for *Homo sapiens* and H37Rv from Uniprot. A total of 571,815 spectra were submitted to MaxQuant for analysis, of which 72,243 (12.63%) were matched to peptides in the database. Although the percentage spectra identified is low, it is similar to other experiments performed within our research group on PBMCs, neutrophils, and monocytes (unpublished). The number of spectra identified did increase in subsequent experiments involving a greater number of samples.

A data quality analysis was performed using MS-GF+ IDPicker. This analysis revealed the number of protein groups identified per sample (summarized in Table 5 below). There were approximately twice as many protein groups identified in the stimulated samples as in the unstimulated samples. This is due both to the *Mtb* proteins added, and to the increase in human secreted protein. The percentage coefficient of variation (CV) shows that the number of protein groups identified and distinct peptides varied more in the unstimulated samples than in the stimulated samples. This could suggest that cells responding to a stimulus tend to behave more similarly than cells that are not responding to a specific perturbation factor, and this hypothesis is also supported by further results.

Table 5. Mean number of protein groups and distinct peptides identified per condition

Condition	Mean ± SD protein groups	% CV	Mean ± SD distinct peptides	% CV
Unstimulated	438 ± 121	27.63	1440 ± 662	45.98
Stimulated	983 ± 37	3.77	3752 ± 342	9.11

Digestion efficiency

The tryptic digestion efficiency was similar to that usually achieved when performing in-solution digestion within our research group, i.e., 56.3% no missed cleavages, 34.4% with one missed cleavage, and 9.3% with two missed cleavages (Figure 21). This was also improved in subsequent experiments by adjusting the concentration of trypsin.

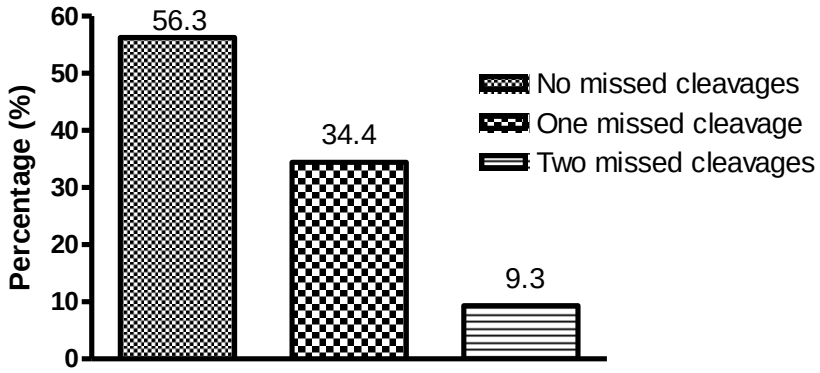

Figure 21. Tryptic digestion efficiency (missed cleavages)

Protein identification correlates

After visual inspection of the spectra, the protein groups identified were loaded to Perseus for further analysis. A total of 1096 protein groups were identified, of which 842 were left after excluding proteins only identified by site, reverse hits, potential contaminants, and proteins identified with fewer than two unique peptides. Of these, 549 were *Mtb* proteins and 293 were human proteins. Total protein intensities were then transformed by log2 and histograms were visualized to assess the distribution of the data (Figure 22). The data are primarily normally distributed, with some positive skewing (skewed to the right).

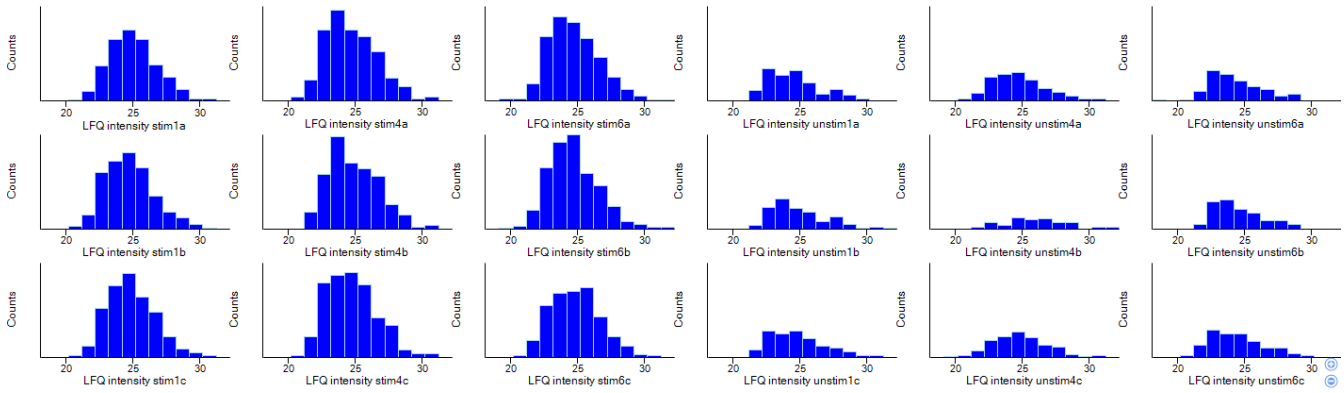

Figure 22. Distribution histograms of log2-transformed protein intensities

log2 protein counts were plotted to assess data distribution. Left to right: stimulated HV01, HV04, and HV06, and unstimulated HV01, HV04, and HV06 samples. Top to bottom: technical replicates for each sample. Protein counts are lower in the unstimulated samples as these did not include any *Mtb* proteins.

Scatter plots and R^2 values were generated for each set of technical replicates. The Pearson correlation coefficients for unstimulated replicates were between 0.756 and 0.953 (

Figure 23). The replicates from HV04 performed the least consistently, as predicted by the poor spectra (Figure 16). Technical replicates from HV06 performed the most consistently with Pearson correlation coefficients of 0.943, 0.951, and 0.953.

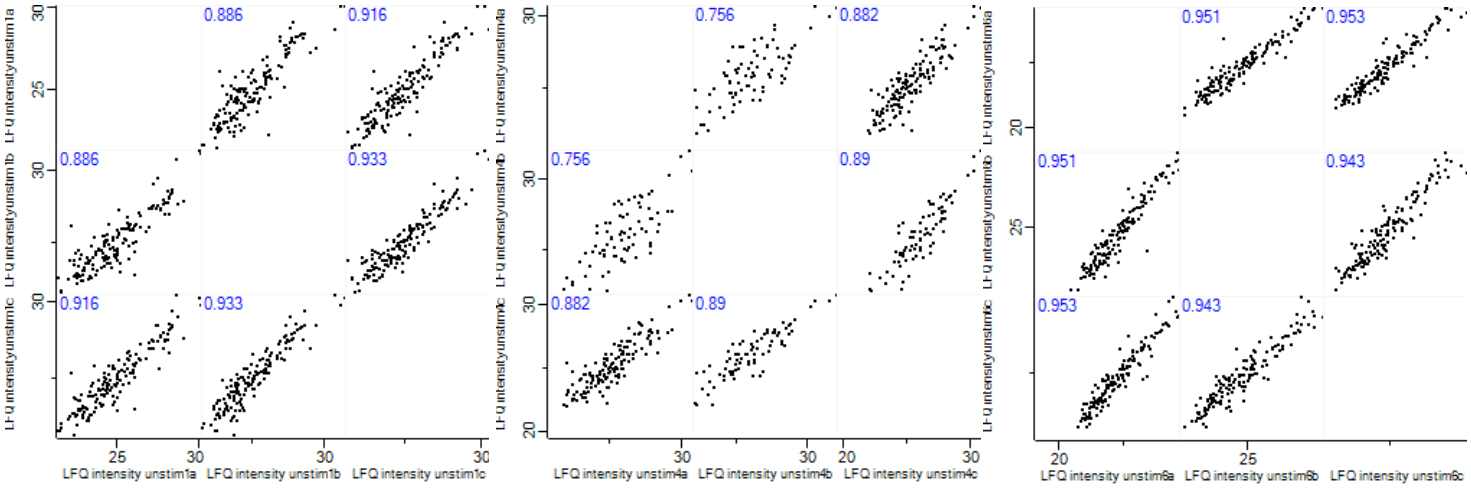

Figure 23. Scatter plots showing correlation between protein groups identified in unstimulated technical replicates

log2 protein expression values from each experimental sample were plotted against those from other experimental samples. Numeric values at the top of each graph indicate the Pearson correlation coefficient for each comparison. Left to right: HV01, HV04, and HV06.

Technical replicates from stimulated samples performed slightly more consistently than their unstimulated counterparts, with correlation coefficients between 0.809 and 0.951 (Figure 24). Again, this may indicate that cells exposed to a specific stimulus are pushed towards a more similar phenotype than unstimulated cells. Overall, agreement between technical replicates was good, although not perfect, and this can be explained by the use of patient-derived samples which display more inherent variability than cell lines. Furthermore, PBMCs are a heterogeneous cell population, comprising B and T lymphocytes, as well as monocytes/macrophages, and a small number of other immune cells such as dendritic cells. A substantial level of variation is therefore to be expected between patient samples. Finally, these technical replicates were PBMCs from the same individual plated in separate wells and incubated for a total of 48 h. Although these samples are considered technical replicates, more variation is generated than if cells from a single well were precipitated and processed in triplicate (however, this would also produce technical replicates).

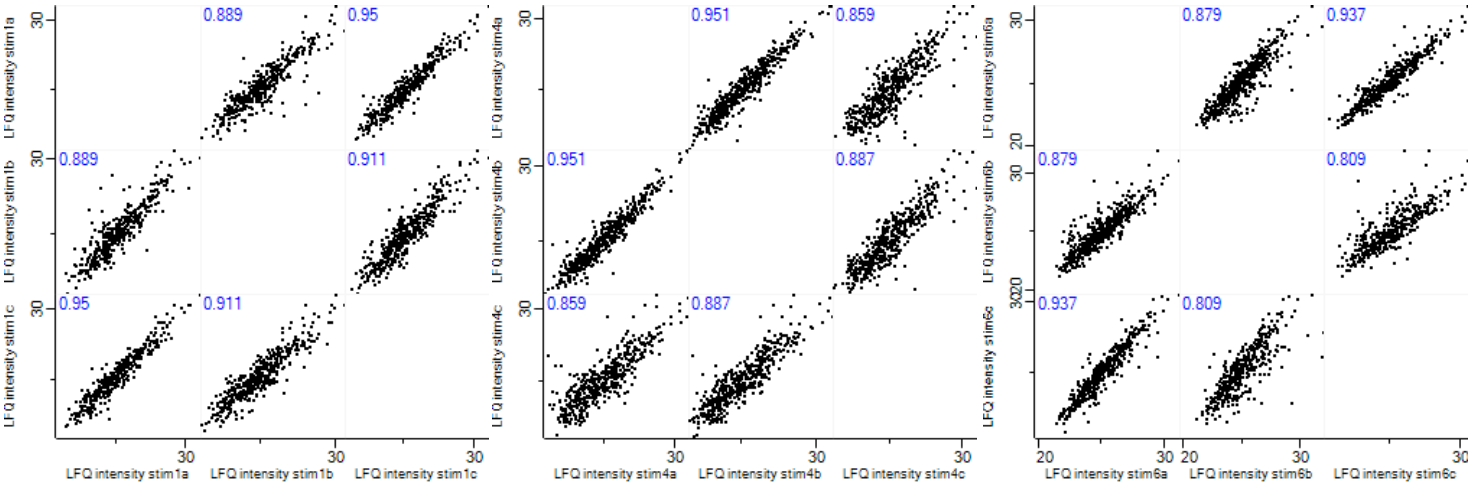

Figure 24. Scatter plots showing correlation between protein groups identified in stimulated technical replicates

log2 protein expression values from each experimental sample were plotted against those from other experimental samples. Numeric values at the top of each graph indicate the Pearson correlation coefficient for each comparison. Left to right: HV01, HV04, and HV06.

Cellular component gene ontology (GO) analysis

To confirm that the majority of proteins identified were in fact secreted proteins, we performed protein network and interaction analyses using the online database STRING. The 293 human proteins identified were added to STRING and mapped to the STRING database. The resulting network comprised 293 nodes and 3515 edges. The top four cellular component GO terms are shown in Table 6. Top four cellular component GO terms and indicate that most proteins in the dataset were secreted or extracellular proteins, including vesicle-bound and exosomal proteins. This was confirmed using the GO enrichment tool FUNRICH, which mapped 76.9% of genes in the dataset to the GO term "exosomes" (p value = 7.08e-128).

Table 6. Top four cellular component GO terms

GO term ID	GO term description	Count in gene set	False discovery rate
GO:0070062	Extracellular exosome	221	2.70e-130
GO:0031988	Membrane-bound vesicle	228	1.01e-119
GO:0044421	Extracellular region part	225	7.49e-110
GO:0005576	Extracellular region	226	4.68e-95

Shared and unique protein groups identified

We performed a presence/absence analysis on the data to investigate shared and unique protein groups identified. This analysis was done using data without imputed values, and a protein was considered 'absent' from a specific treatment condition if it had an LFQ intensity value of zero in all samples for that particular condition. Of the 293 human proteins identified, 233 were shared between control and *Mtb*-stimulated samples, while 40 were unique to control samples, and 20 were unique to *Mtb*-stimulated samples (Figure 25. Shared and unique proteins identified in control and *Mtb-stimulated* samples. This indicates that 79.52% of the cells' secretome remained qualitatively unchanged after re-stimulation with *Mtb* WCL.

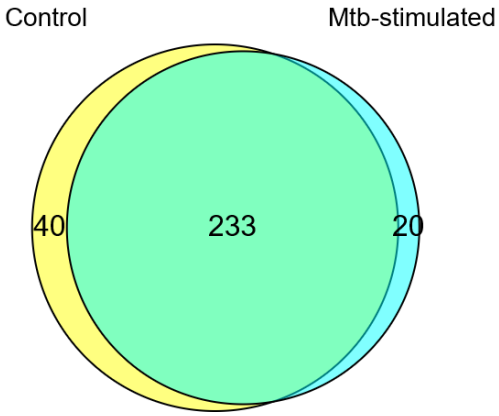

Figure 25. Shared and unique proteins identified in control and *Mtb*-stimulated samples

We also compared shared and unique proteins identified in each biological replicate, per condition. In control samples, there were 161 proteins identified in all three biological replicates, and in *Mtb*-stimulated samples, there were 166 proteins identified across biological replicates (Figure 26. Shared and unique proteins identified per biological replicate in control and *Mtb-stimulated* samples.). Therefore, 60.08% of proteins in control samples were identified in all replicates, compared to 67.76% in *Mtb*-stimulated samples.

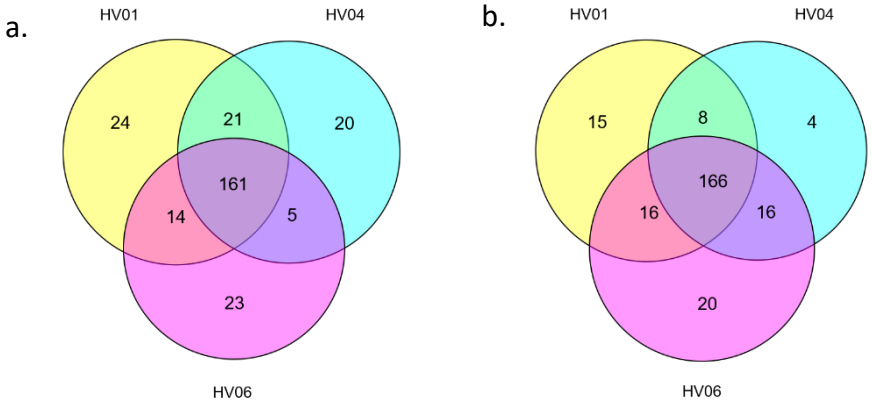

Figure 26. Shared and unique proteins identified per biological replicate in control and *Mtb*-stimulated samples.

a. Control samples. b. *Mtb*-stimulated samples.

Hierarchical clustering and principal component analysis

We performed a hierarchical cluster analysis using a Euclidean model of absolute distance to determine whether samples in each group clustered together based on their protein expression profiles. These were visualized as heat maps, in which light blue bands indicate lower expression of the particular protein and darker bands indicate greater expression. Hierarchical clustering of the total proteome (Figure 27a) revealed strong clustering in each condition. However, since this analysis included both human and *Mtb* proteins, clustering was primarily driven by the presence and absence of *Mtb* proteins. The two orange boxes in Figure 27a highlight proteins whose expression is much greater in *Mtb*-stimulated samples and are therefore most likely *Mtb* proteins. Clustering analysis using only human proteins showed weak clustering, with one of the unstimulated sample from HV04 ("unstim4b") as a clear outlier (Figure 27b).

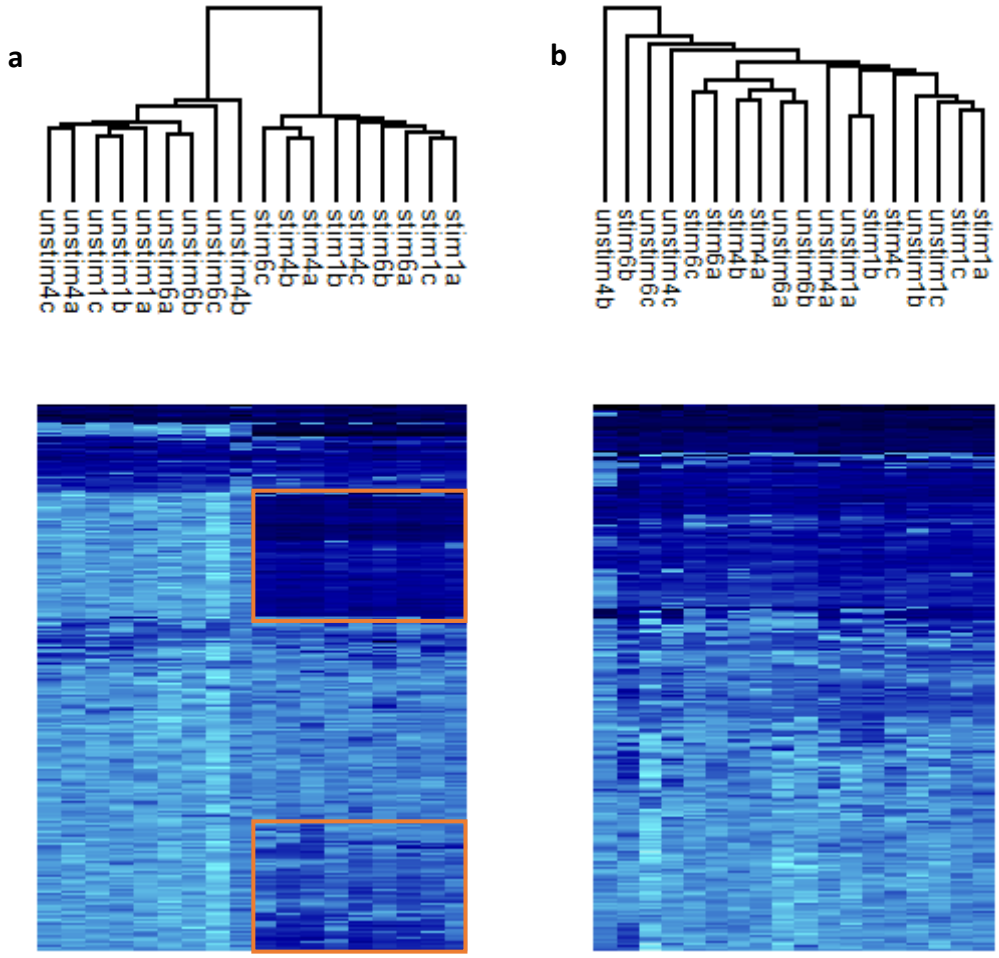

Figure 27. Hierarchical clustering analysis of protein expression profiles using log_2 LFQ values

a Human and *Mtb* protein expression. b human proteins only.

A principal component analysis (PCA) was performed to further investigate clustering. When both human and *Mtb* proteins were included in the analysis, principal components 1 and 2, accounting for 70.9 and 4.5% of the variation respectively, created distinct clusters, as shown in Figure 28. The presence and absence of *Mtb* proteins most likely accounts for much of this clustering, so PCA was repeated using human proteins only (Figure 28). Principal component 3 distinguished between control and *Mtb*-stimulated samples, and accounted for 9.5% of the variance.

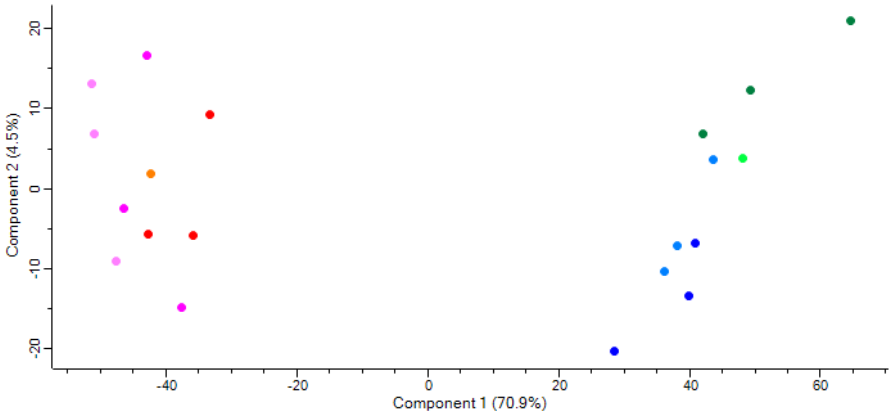

Figure 28. Principal component analysis of protein expression profiles (human and *Mtb* proteins)

Red and pink dots represent control samples; blue and green dots represent *Mtb*-stimulated samples. Principal components 1 and 2 are represented on the x- and y-axis, respectively, and account for 70.9 and 4.5% of the total variance, respectively.

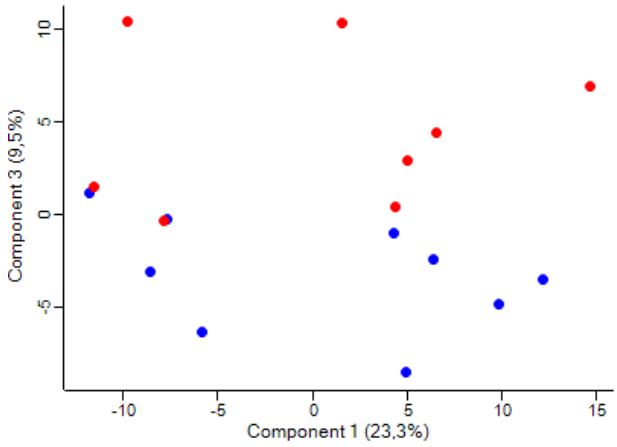

Figure 29. Principal component analysis of protein expression profiles (human proteins only)

Blue dots represent control samples; red dots represent *Mtb*-stimulated samples. Principal components 1 and 3 are represented on the x- and y-axis, respectively, and account for 23.3 and 9.5% of the total variance, respectively.

5.3.5 Preliminary biological analysis

Differential expression analysis

We performed paired Student's t-tests to identify protein groups expressed differentially in the *Mtb*-stimulated and control samples. Multiple testing correction (MTC) was applied following both the permutation-based and the Benjamini-Hochberg methods (FDR < 0.05). When the Benjamini-

Hochberg MTC method was applied, the differences in proteins expressions between the *Mtb*-stimulated and control samples were not considered statistically significant. However, use of the permutation-based method revealed differential expression of seven proteins shown in Figure 30 and listed in Table 7.

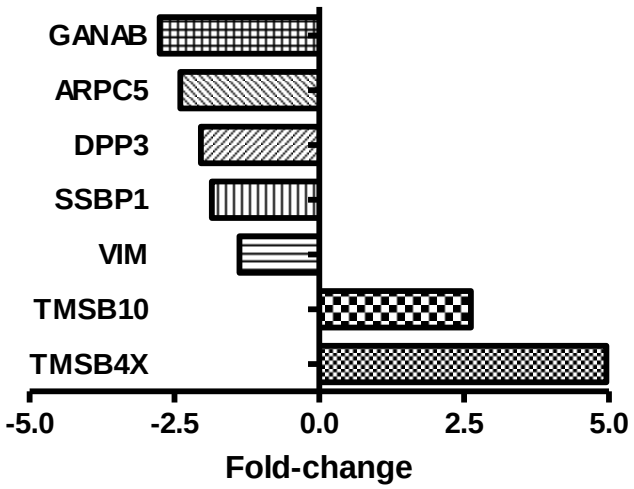

Figure 30. Differentially expressed proteins in *Mtb*-stimulated samples

Blue, up-regulated in *Mtb*-stimulated samples (FC > 2); orange, down-regulated in *Mtb*-stimulated samples (FC > 2); green, down-regulated in *Mtb*-stimulated samples (FC < 2).

Table 7. Differentially expressed proteins

Protein ID	Gene ID	Protein name	Role	P value	Fold-change	q value
Q14697	GANAB	Glucosidase II, alpha subunit	Glycan metabolism, carbohydrate binding	5.75e-4	-2.75	0.0067
O15511	ARPC5	Actin-related protein 2/3 complex subunit 5	Cytoskeleton organization, Fc-γ receptor-mediated phagocytosis pathway, neutrophil degranulation	0.003	-2.39	0.0400
Q9NY33	DPP3	Dipeptidyl peptidase 3	Peptide cleavage, zinc binding	0.002	-2.04	0.0300
Q04837	SSBP1	Single-stranded DNA-binding protein, mitochondrial	Mitochondrial DNA replication	0.003	-1.85	0.0460
P08670	VIM	Vimentin	Maintains cytoskeletal integrity, involved in disassembly (apoptotic process)	1.74e-4	-1.38	0.0080
P63313	TMSB10	Thymosin β-10	Cytoskeleton organization	7.08e-4	+2.62	0.0150

P62328	TMSB4X	Thymosin β-4	Cytoskeleton organization, inhibits TNFα -induced NF-κB activation and IL-8 expression[114]	0.002	+4.96	0.0288

Thymosin β-4 (Tβ4) and β-10 (Tβ10) are both up-regulated in *Mtb*-stimulated samples (2.3-fold and 1.4-fold, respectively). Beta thymosins are small peptides expressed in multiple tissues, and show versatile intra- and extra-cellular activities. Tβ4 is implicated in motility and phagocytosis in macrophages, via sequestration of G-actin and regulation of actin polymerization.[115] Furthermore, Tβ4 has wound-healing, anti-inflammatory, and anti-microbial properties, and was shown to inhibit TNFα-induced NF-κB activation and IL-8 expression.[114] It is therefore an important immuno-regulatory protein. Tβ10 also sequesters actin monomers, and predisposes cells to undergo apoptosis.[116] Gutierrez-Pabello *et al*.[116] showed that infection of bovine macrophages with *Mycobacterium bovis* induced over-expression of Tβ10 associated with macrophage apoptosis. It is therefore plausible that re-stimulation of human PBMCs with *Mtb* WCL would elicit a similar response and lead to over-expression of Tβ10.

Glucosidase II, also known as neutral alpha-glucosidase AB or alpha-glucosidase 2, is a key protein located in the endoplasmic reticulum (ER), and is involved in the quality control of glycoprotein folding. It was shown to increase in response to UV radiation, but is down-regulated in response to ER stress.[117] Lim *et al*. showed that *Mtb* infection caused an increase in ER stress, and demonstrated the association of ER stress-induced apoptosis with *Mtb*-induced cell death in murine macrophages.[118] Apoptosis is an important host defence mechanism against intracellular pathogens such as *Mtb*, as it prevents the release of intracellular bacteria and components. Here, the down-regulation of glucosidase II, which is known to occur in response to ER stress, may be indicative of *Mtb*-induced ER stress in PBMCs. Although glucosidase II is an endoplasmic protein, it has previously been identified in the extracellular region (extracellular matrices and extracellular exosomes) as a secreted protein.[119,120]

Actin-related protein 2/3 complex (Apr2/3) subunit 5 regulates actin polymerization and more specifically, the formation of the phagocytic cup (source: Reactome, R-HSA-2029482). ARPC5 has also been linked to Fcγ receptor-mediated phagocytosis and neutrophil degranulation (Reactome, R-HSA-6798695). Neutrophil degranulation is a mechanism used to kill engulfed bacteria although there is controversy as to whether neutrophils are in fact able to kill *Mtb* once engulfed.[121] ARPC5 is reportedly associated with cell migration and invasion in cancer,[122] and finally, in the KEGG pathway database, it is associated with bacterial invasion pathways involving *Escherichia coli*, shigellosis, and salmonella (hsa05130-hsa05132).

ARPC5 interacts with ARPC4, another Arp2/3 complex subunit, which itself binds to *Mtb* protein Rv1626, an essential secretory mycobacterial protein.[123] According to Ghosh *et al*., this could be related to *Mtb*'s ability to alter the host cell cytoskeleton and use actin-based motility to infect new cells through direct cell-to-cell contact, by inducing actin polymerization through the recruitment of host cytoskeletal factors such as the Arp2/3 complex.[123]

Dipeptidyl-peptidase III (DPP3) is an metallo-aminopeptidase which cleaves and degrades bioactive peptides and is involved in several physiological processes. Singh *et al*. investigated the negative correlation between DPP3 and IL-6 and showed that this cytokine is responsible for transcriptional down-regulation of DPP3, via the transcription factor CCAAT/enhancer binding protein beta (C/EBP-b).[124] Although IL-6 plays a complex role in *Mtb* infection, there is consensus about its up-regulation in response to macrophage infection by *Mtb*.[125] It is therefore likely that re-stimulation with *Mtb* WCL induced increased IL-6 expression, which in turn caused down-regulation of DPP3.

The last two proteins, vimentin and single-stranded DNA-binding protein (SSBP1), although significantly dysregulated, had changes in expression between one- and two-fold. It is common to exclude proteins with FC < 2 from further analysis, but I have included these here at there were only seven dysregulated proteins in total.

Although single-stranded DNA-binding protein (SSBP1) is primarily a mitochondrial protein, it has previously been identified in B-cell derived extracellular exosomes.[126] It is involved in mitochondrial DNA replication and repair, mitochondrial organization, and morphogenesis, and binds to ssDNA. It is unclear why this protein is significantly down-regulated in *Mtb*-stimulated PBMCs, but it may be related to *Mtb*-induced, reactive oxygen species (ROS)-mediated mitochondrial stress.[127]

Vimentin is a type III intermediate filament that is responsible for maintaining cell integrity and shape. It is also associated with macrophage differentiation, phagocytosis, and production of ROS, is expressed on activated macrophages, and is secreted in response to pro-inflammatory signals.[128] Mahesh *et al*. showed that *Mtb* was able to down-regulate vimentin expression in macrophages. The authors suggest that expression of vimentin may be part of the inflammatory response of macrophages in an effort to contain the pathogens, and its down-regulation may be a result of *Mtb*'s

negative modulation of the inflammatory response of macrophages, possibly in a ROS-dependent manner.[128]

5.4 Conclusion

The aim of this experiment was to assess technical and biological variability, as well as confirm that we were able to isolate proteins from the PBMC secretome. The modified Bradford assay revealed very similar protein contents between biological and technical replicates. TIC chromatograms from technical replicated were also similar, with the exception of a few outliers. We investigated protein expression correlation through multi-scatter plots and assessed changes to the proteome in response to stimulation with *Mtb* WCL using Venn diagrams, heat maps, and PCA. Finally, we confirmed that proteins identified were primarily extracellular, thereby indicating that we had successfully isolated the cellular secretome. Preliminary biological analyses revealed that a small number of proteins were dysregulated in response to *Mtb* stimulation, consistent with the fact the PBMCs investigated here were derived from healthy volunteers and so were presumed to be naïve to *Mtb* antigens.

This experiment confirmed that the sample processing methods used were appropriate and allowed for proteomic analysis of the cellular secretome. Biological and technical variability was low, and we therefore proceeded with further experiments using the methods optimised here.

Chapter 6

Secretome analysis of PUFA-treated, healthy volunteer PBMCs

6.1 Aim

The aim of this experiment was to investigate the PBMC secretome and any changes associated with the re-stimulation of PBMCs with *Mtb* whole cell lysate (WCL). In addition, cells were pre-treated with n-3 PUFA (DHA and EPA, 100 nM each) or the vehicle control (2% ethanol) prior to re-stimulation with *Mtb* WCL to assess the effects of n-3 PUFA pre-treatment on cellular response to *Mtb* re-stimulation. PBMCs from four healthy volunteers were used. Cells were cultured as described in Chapter 4, and incubated for 24 h with *Mtb* WCL, in addition to 2-h pre-treatment with the vehicle control or n-3 PUFA for the relevant treatment groups.

6.2 Results and discussion

6.2.1 Protein quantitation

Total protein content in cell culture supernatants was quantified via modified Bradford assay. Mean total protein recovered from control samples was 1.90 µg, 4.37 µg for *Mtb* WCL only samples, 5.70 µg for *Mtb* WCL + vehicle samples, and 10.96 µg for *Mtb* WCL + PUFA samples (Figure 31). The differences in protein content between *Mtb* + PUFA samples and *Mtb* only samples were significant ($p < 0.01$), as were differences between Mtb + PUFA and Mtb + vehicle samples ($p < 0.05$). Differences in protein content between *Mtb* only and control samples ($p < 0.05$) may be partially accounted for by the addition of *Mtb* WCL proteins. Biological variability was low, as shown by the small error bars.

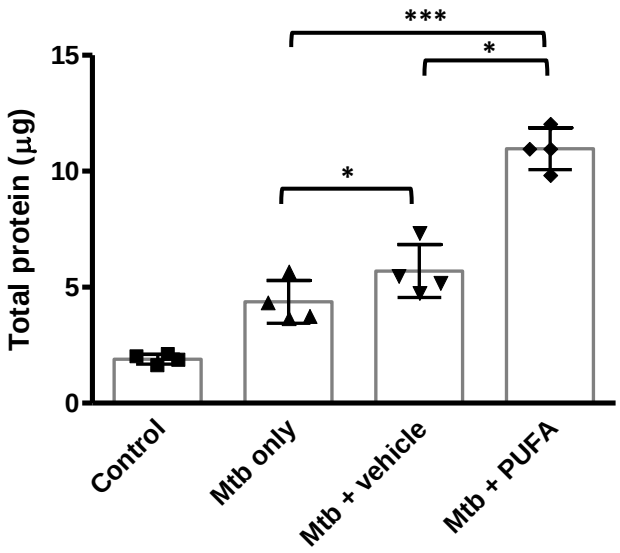

Figure 31. Total protein content in control, *Mtb* only, *Mtb* + vehicle and *Mtb* + PUFA samples

Data are presented as means ± SD (error bars) of four biological replicates. *p < 0.05, ***p < 0.01.

6.2.2 MS spectra, data quality, and protein identification

MS spectra

The supernatant samples were processed for MS-based proteomics (as per the method described I Chapter 3), and trypsin-digested peptides were subjected to discovery MS analysis on a Q Exactive instrument. The spectra obtained are shown in Figure 32, Figure 33, Figure 34, and Figure 35 below. These chromatograms display TICs from the four biological replicates (HV01, 02, 03, and 06) for each treatment condition. The four biological replicates performed consistently in most runs, as can be seen in the shape of the TIC. TIC variability is also shown in Figure 36, which reveals that TIC across *Mtb* only samples were much lower than that of other samples. Since TIC from the *Mtb* only samples were about half of that in the control samples (approximately 5e9 compared to approximately 10e9), comparison between the two treatment conditions would be hampered. *Mtb* + vehicle samples displayed the greatest scatter in TIC intensities and controls showed the least variability between samples.

Peak retention times were very consistent across samples: for example, in Figure 32 (control), the same peak eluted at 53.16, 53.07, and 53.75 minutes for HV02, 03, and 06, respectively. Notable exceptions include the control sample for HV01 (Figure 32), which had a different TIC shape and lower peak intensity, and the Mtb + vehicle sample for HV02 (Figure 34), which also had a different TIC shape

and much higher intensity. The maximum intensity for this sample was also higher than desired (2.26e10). Unfortunately, due to time constraints and the high demand for machine time, we were not able to rerun these samples to improve signal intensity. This sample was therefore excluded from further analyses. Chromatograms from three of the four *Mtb* only samples (Figure 33) revealed poor spray from approximately 68 to 80 min but again, due to time constraints, we were not able to repeat these runs.

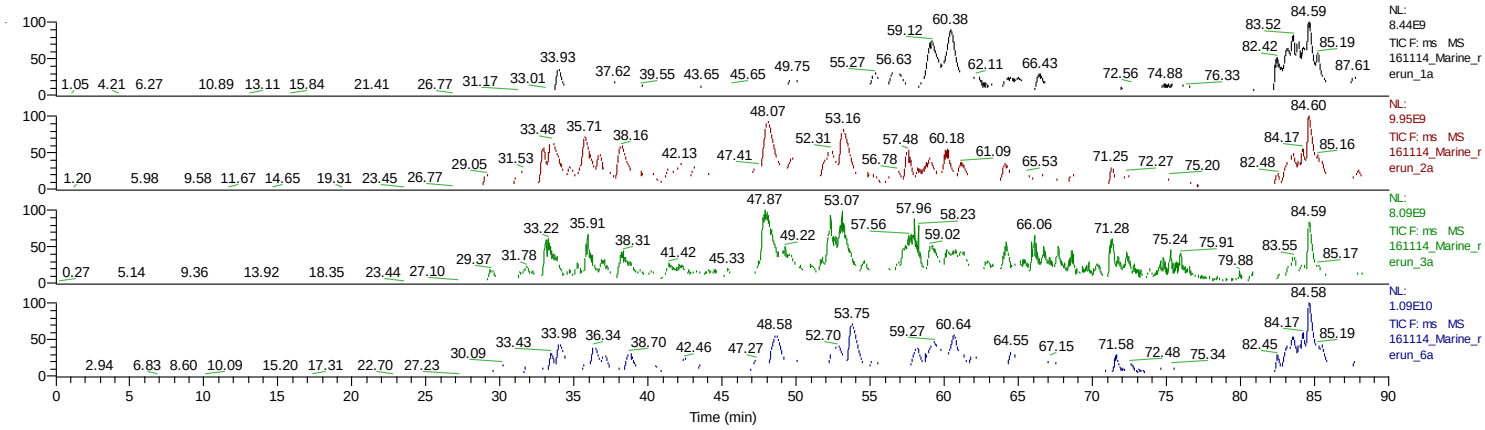

Figure 32. MS chromatogram (TIC) of control samples

From top to bottom: black, HV01; red, HV02; green, HV03; blue, HV06.

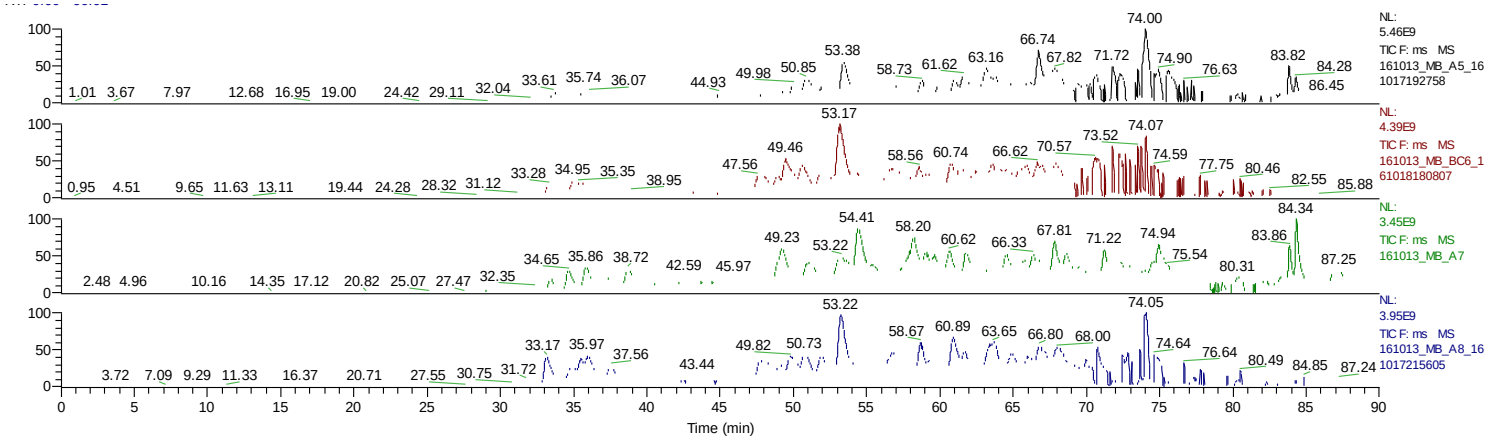

Figure 33. MS chromatogram (TIC) of *Mtb* only control samples

From top to bottom: black, HV01; red, HV02; green, HV03; blue, HV06.

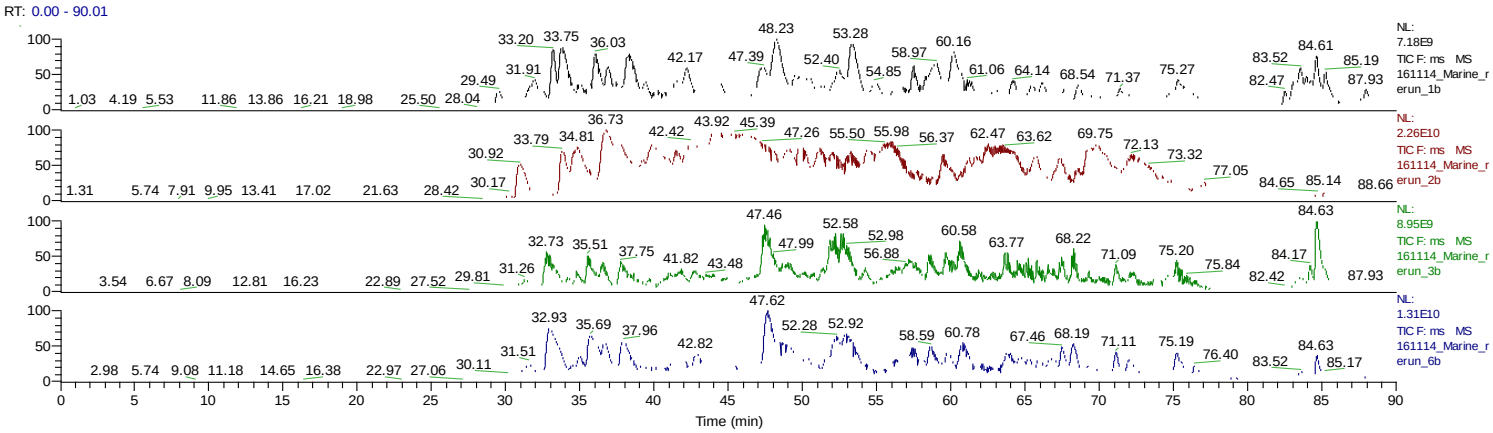

Figure 34. MS chromatogram (TIC) of *Mtb* + vehicle samples

From top to bottom: black, HV01; red, HV02; green, HV03; blue, HV06.

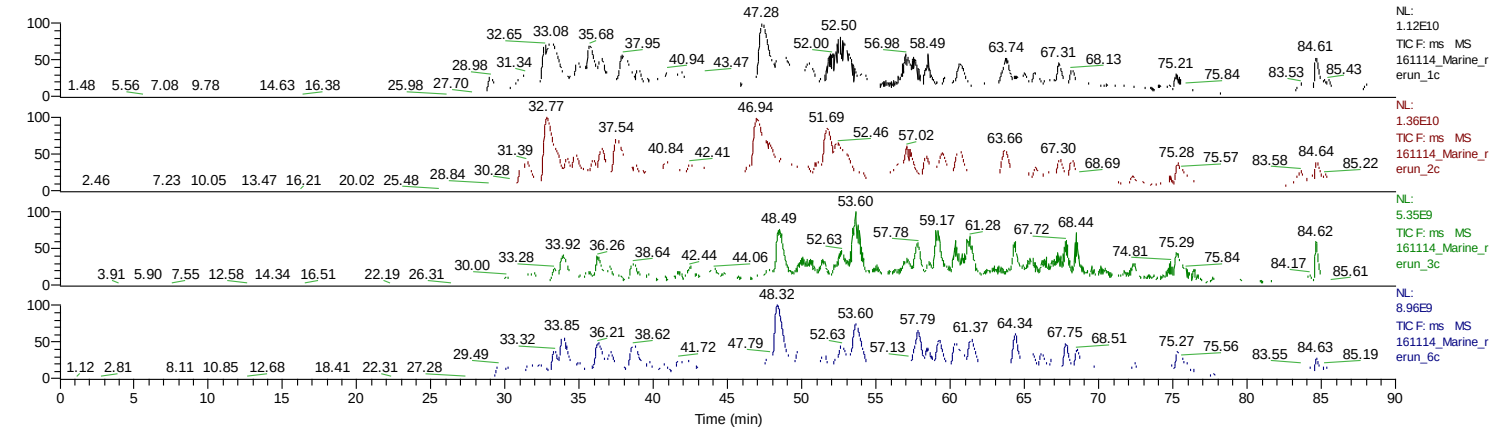

Figure 35. MS chromatogram (TIC) of *Mtb* + PUFA samples

From top to bottom: black, HV01; red, HV02; green, HV03; blue, HV06.

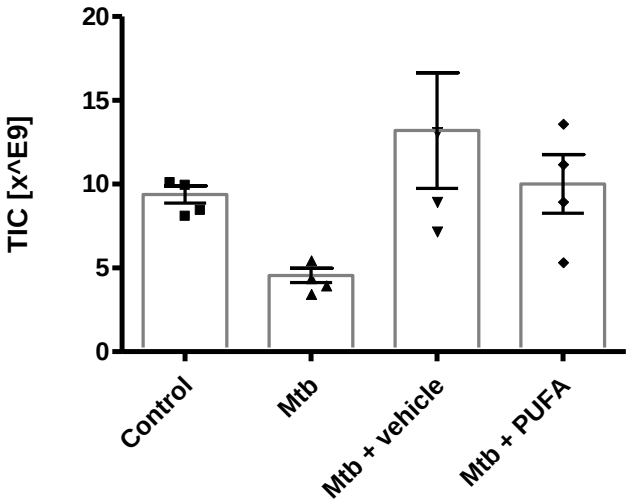

Figure 36. TIC variability across biological samples and treatment conditions

Protein identification

The spectra generated via discovery MS analysis were submitted to MaxQuant for protein identification and quantitation. The number of spectra submitted was 607,484, of which 101,237 (16.66 %) were identified. There were 13,323 peptides identified, mapping to 2083 protein groups. In order to improve the rate of spectra identified, we performed two alternative MaxQuant searches: 1) tryptic digestion was set to "semi-specific", and 2) PSM FDR was set to 0.05. All other settings were kept the same (see Chapter 5). The results of these two alternative searches are shown in Table 8. Although more peptides and spectra were identified in the search with increased FDR, the number of protein groups identified was fractionally lower. Since increasing FDR to 0.05 may increase false positives and did not result in increased identifications, these settings were rejected. Similarly, the semi-tryptic search resulted in fewer peptides, protein groups, and spectra identified. Therefore, protein groups identified using the original search and standard settings were used for further analysis. The percentage spectra identified did increase compared to the initial optimization experiment described in Chapter 5, where only 12.63% spectra submitted were identified. This may be due to higher TIC intensities or better spray in the current experiment.

Table 8. Summary of results obtained using standard and alternative MaxQuant search settings

Settings	Standard settings	Semi-tryptic	PSM FDR* = 0,05
Protein groups identified	2083	1652	2074
Reverse hits	24	17	28
% contaminants	4,66	4,60	4,29
Peptides identified	13323	9548	13806
Spectra submitted	607,484	606,287	607,345
% spectra identified	16,66	13,52	20,53
Modified peptides	845	623	831
% no missed cleavages	61,8	61,4	62,4

*Peptide-spectrum match false discovery rate

Digestion efficiency

Tryptic digestion efficiency was improved compared to that in the optimization experiment described in Chapter 5 by increasing the trypsin-to-sample ration to 1:10 (Figure 37). The percentage "no missed cleavages" was 61.8% compared to 56.3% in the previous experiment.

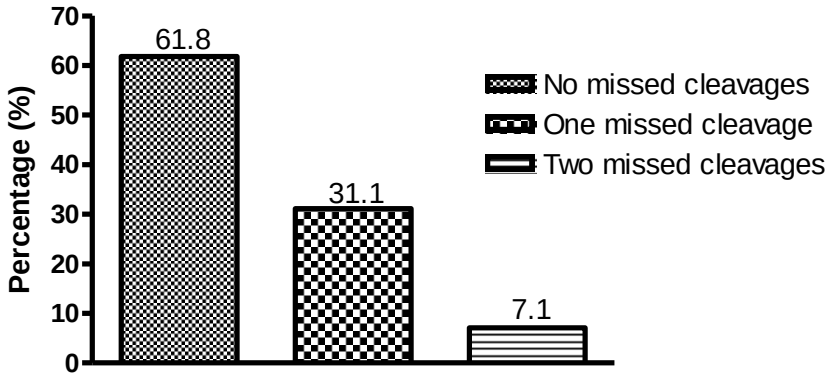

Figure 37. Tryptic digestion efficiency (missed cleavages)

Distribution of LFQ intensities and correlation between biological replicates

Protein groups were further analysed using the software Perseus. A total of 2083 protein groups were identified, of which 1559 were left after excluding proteins only identified by site, reverse hits, potential contaminants, and proteins identified with fewer than two unique peptides. Of these, 832 were *Mtb* proteins and 727 were human proteins. Total protein LFQ intensities were then transformed by log2 and histograms were visualized to assess the distribution of the data (Figure 38). The data are primarily normally distributed, with some positive skewing (skewed to the right). LFQ intensity was much lower for HV02 Mtb + vehicle sample, as was predicted by the poor spectra.

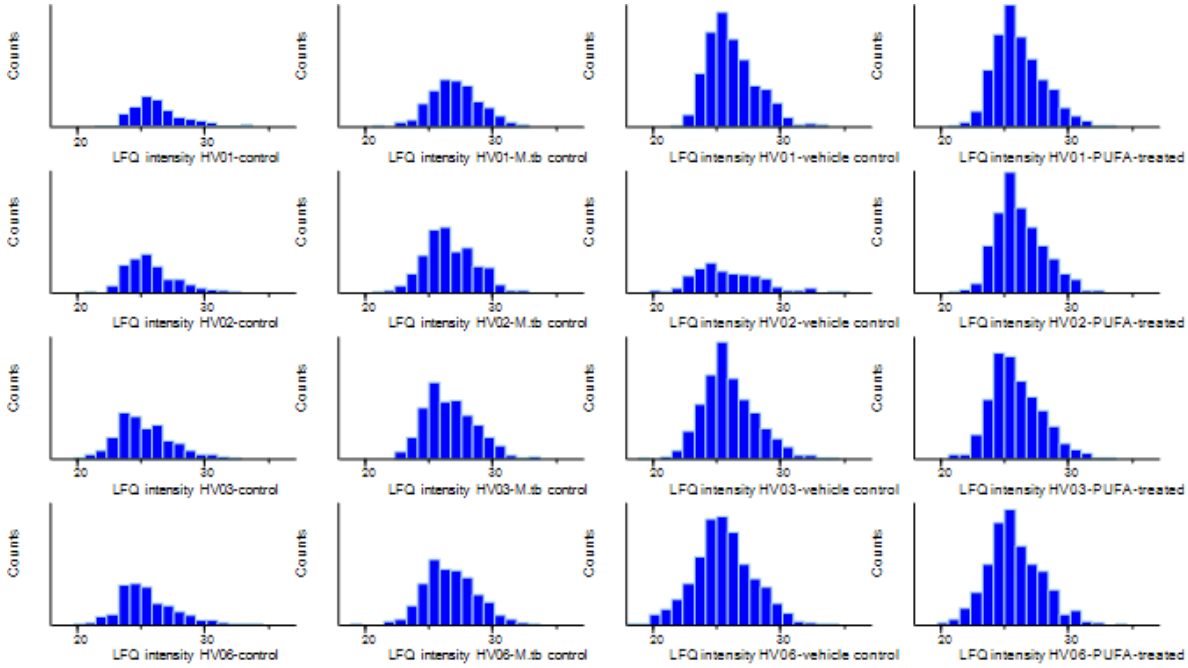

Figure 38. Distribution histograms of log2-transformed protein LFQ intensities

log2 protein LFQ were plotted to assess data distribution. Left to right: control, *Mtb* only, *Mtb* + vehicle, and *Mtb* + PUFA samples. Top to bottom: HV01, HV02, HV03, and HV06. Protein counts are lower in the control samples as these did not include any *Mtb* proteins.

Scatter plots and Pearson's correlation coefficients were generated for each set of biological replicates per condition. Overall, biological replicates performed similarly to one another, with Pearson's correlation coefficients between 0.741 and 0.919. PUFA-treated samples were most strongly correlated, with Pearson's correlation coefficients between 0.888 and 0.919 (Figure 39).

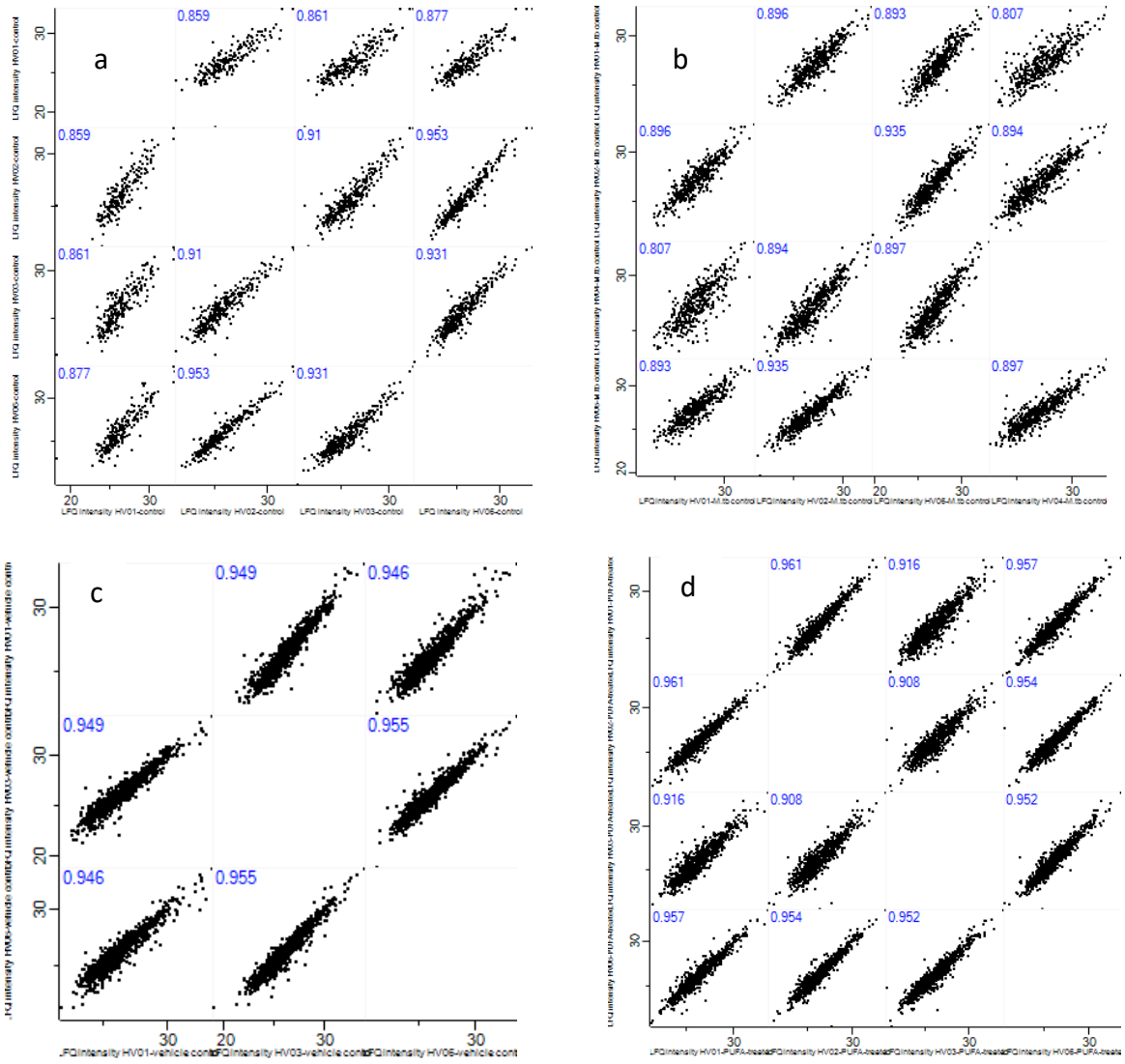

Figure 39. Scatter plots showing correlation between protein groups identified in control, *Mtb* only, *Mtb* + vehicle, and *Mtb* + PUFA biological replicates

log2 protein LFQ values from each experimental sample were plotted against those from other experimental samples. Numeric values at the top of each graph indicate the Pearson's correlation coefficient for each comparison. a, controls; b, *Mtb* only samples; c, *Mtb* + vehicle; and d, *Mtb* + PUFA samples. The HV02 *Mtb* + vehicle sample was excluded from analysis due to poor LC-MS/MS performance.

Hierarchical clustering

Hierarchical clustering revealed strong clustering of samples per condition according to expression of both human and *Mtb* proteins, and expression of human proteins only (Figure 40). In Figure 40 (a), we see that the expression of certain proteins is down-regulated in *Mtb* only samples in comparison with the other three conditions (orange box 1). These proteins must be human proteins as they are strongly expressed in control samples. The same trend is seen in Figure 40 (b), which shows clustering based

on human protein expression only (orange box 2). This indicates that re-stimulation with *Mtb* WCL causes decreased expression of certain proteins that are strongly expressed in control samples.

"Control1" (HV01 control) is a clear outlier in Figure 40 (b) (human proteins) and appears to cluster more strongly with the *Mtb* only samples. This is supported by the slightly different TIC shape of this sample compared to that of the other three control samples (Figure 32). This difference may have arisen at the *in vitro* level (i.e., different cellular response to culture conditions) or *in vivo* (different immune status and response in the volunteer when blood was drawn). The fact that this sample seems to cluster closer to *Mtb* only samples could also indicate that this healthy volunteer, although asymptomatic at the time of blood collection, was mounting an immune response (perhaps to a cold or mild infection), or had experienced differential exposure to the *Mtb* pathogen (perhaps working in close contact with infected carriers). Finally, HV01 does not consume any alcohol whereas the other three volunteers reported regular alcohol consumption (see Chapter 3). This may be relevant as alcohol is a known immuno-modulatory agent.[129]

Finally, there appears to be increased expression of certain proteins in the *Mtb* + PUFA samples, as shown by darker blue bands highlighted in orange box 3 in Figure 40 (b). These may be proteins whose expression is up-regulated in response to treatment with n-3 PUFA, as this increased expression is not seen in other conditions. N-3 PUFA-treated samples cluster separately from *Mtb* only samples on the one side, and control/vehicle control samples on the other, both of which are closely clustered, suggesting PUFA-specific modulation of protein expression.

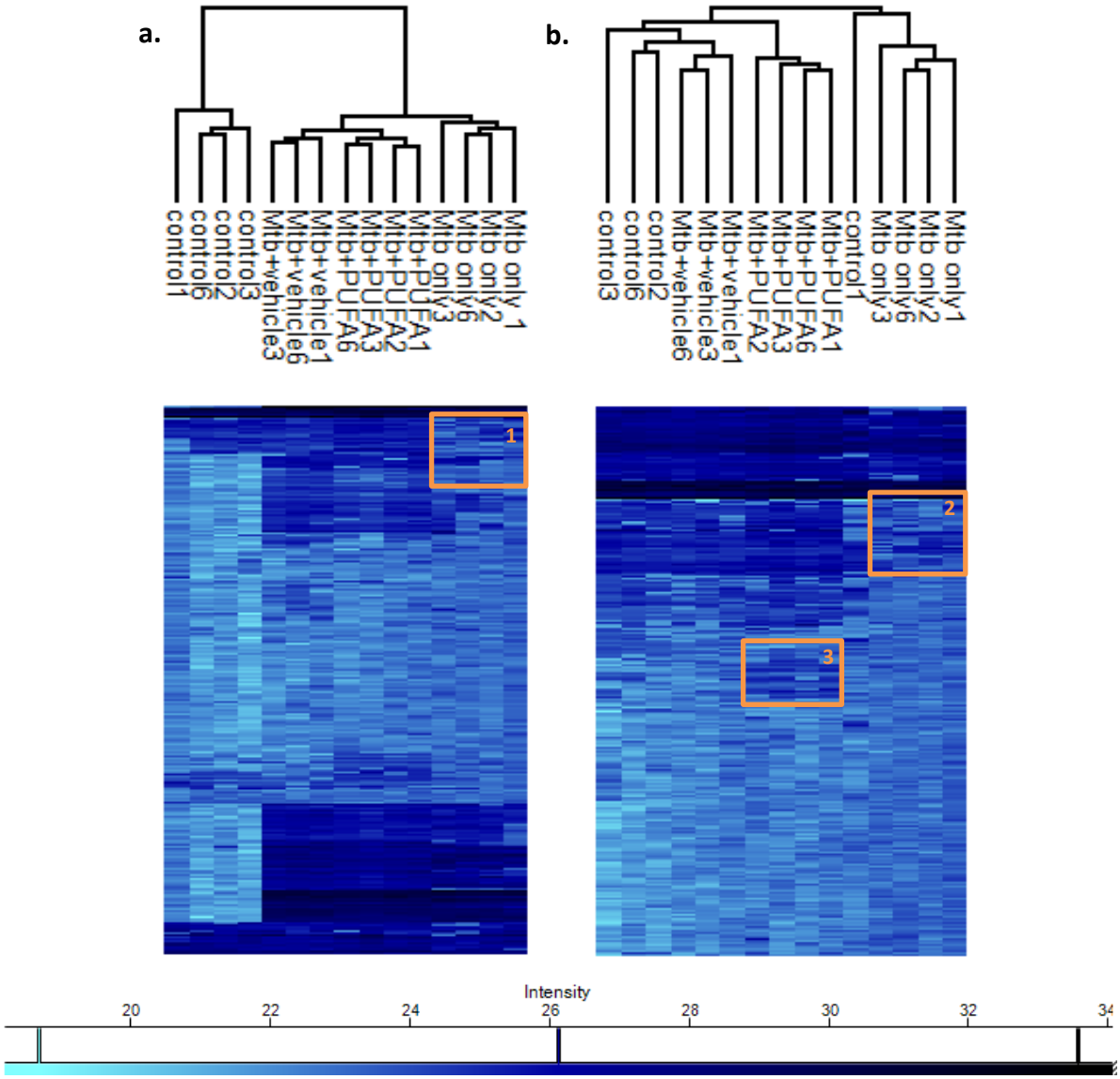

Figure 40. Hierarchical clustering analysis of protein expression profiles using log_2 LFQ values

a Human and *Mtb* protein expression. b human proteins only.

Principal component analysis

A principal component analysis (PCA) was performed to further investigate clustering. The first PCA plot generated includes both human and *Mtb* proteins (Figure 41) while the second includes only human proteins (Figure 42. Principal component analysis of protein expression profiles (human proteins only). In Figure 41, principal component 1 clearly distinguished samples containing *Mtb* WCL from those that did not. In Figure 42, both components 1 and 2 created distinct clusters for each condition, with control samples (yellow) showing the most spread and variance (HV01 was already identified as an outlier previously), and *Mtb* + PUFA samples (green) forming the most distinct grouping.

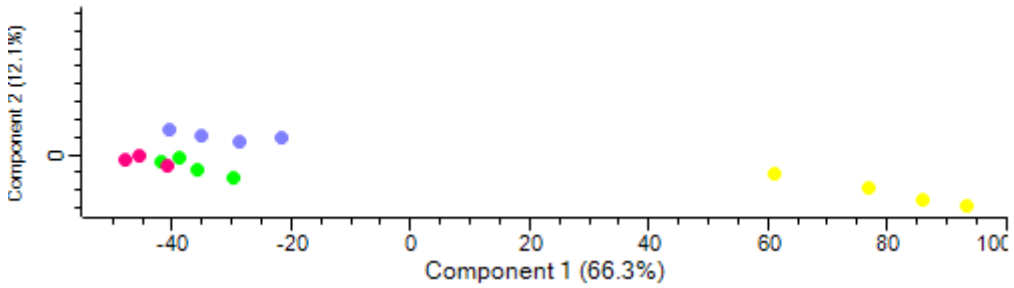

Figure 41. Principal component analysis of protein expression profiles (human and *Mtb* proteins)

Yellow, control samples; blue, *Mtb* only samples; magenta, *Mtb* + vehicle samples; and green, *Mtb* + PUFA samples. Principal components 1 and 2 are represented on the x- and y-axis, respectively, and account for 66.3 and 12.1% of the total variance, respectively.

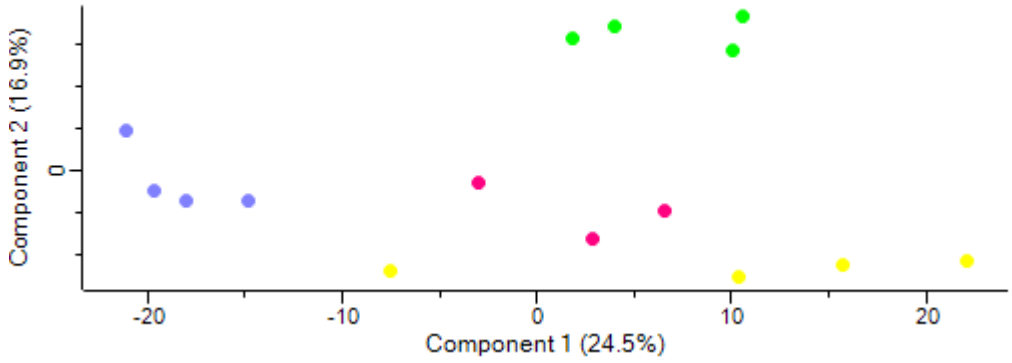

Figure 42. Principal component analysis of protein expression profiles (human proteins only)

Yellow, control samples; blue, *Mtb* only samples; magenta, *Mtb* + vehicle samples; and green, *Mtb* + PUFA samples. Principal components 1 and 2 are represented on the x- and y-axis, respectively, and account for 24.5 and 16.9% of the total variance, respectively.

Cellular component GO analysis

To confirm that we had successfully isolated the PBMC secretome, the 727 human proteins identified across all samples and conditions were added to STRING, thus creating a network of 713 nodes and 12,464 edges. The top four enriched GO terms for cellular component revealed that approximately 70% of proteins identified were extracellular (Table 9), with very small false discovery rates.

Table 9.Top four enriched cellular component GO terms

GO term ID	GO term description	Count in gene set	False discovery rate
GO:0070062	Extracellular exosome	480	2.17e-260
GO:0031988	Membrane-bound vesicle	494	1.57e-232
GO:0044421	Extracellular region part	500	2.33e-194
GO:0005576	Extracellular region	505	1.4e-83

6.2.3 Biological analysis

Shared and unique protein groups identified

We performed a presence/absence analysis to investigate shared and unique protein groups amongst the identified protein groups. This analysis was done using data without imputed values, and a protein was considered 'absent' from a specific treatment condition if it had an LFQ intensity value of zero in all samples for that particular condition. It is important to note that this may not mean the protein is totally absent from the sample, but rather that it may be present but at a concentration that is below the level of quantification/detection of the mass spectrometer. Of the 585 quantifiable proteins identified, 240 (41.03%) were common to all four conditions (Figure 43). There were 56 proteins unique to the control samples, 5 to the *Mtb* only samples, 19 to the *Mtb* + vehicle samples, and 84 to the *Mtb* + PUFA samples. We performed GO enrichment analyses on the unique proteins identified in each treatment condition using STRING.

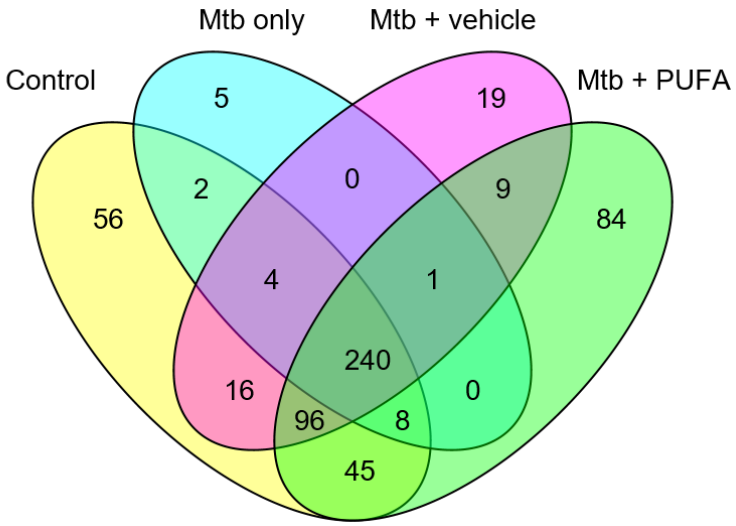

Figure 43. Shared and unique proteins identified in control, *Mtb* only, *Mtb* + vehicle, and *Mtb* + PUFA samples

The 56 proteins unique to control samples were uploaded to STRING and produced a network comprising 54 nodes and 115 edges (enrichment p-value: 1.25e-06, Figure 44). The top four enriched GO terms for biological process and molecular function are shown in Table 10 below. These terms are associated with 'house-keeping' and form part of the cell's normal maintenance and function. Although there are several ribosomal proteins identified, all of these have previously been identified as exosomal proteins.[126,130] Therefore, although they may be present in the cell culture supernatant as a result of cell death, it is also possible that they were secreted as extracellular exosomes.

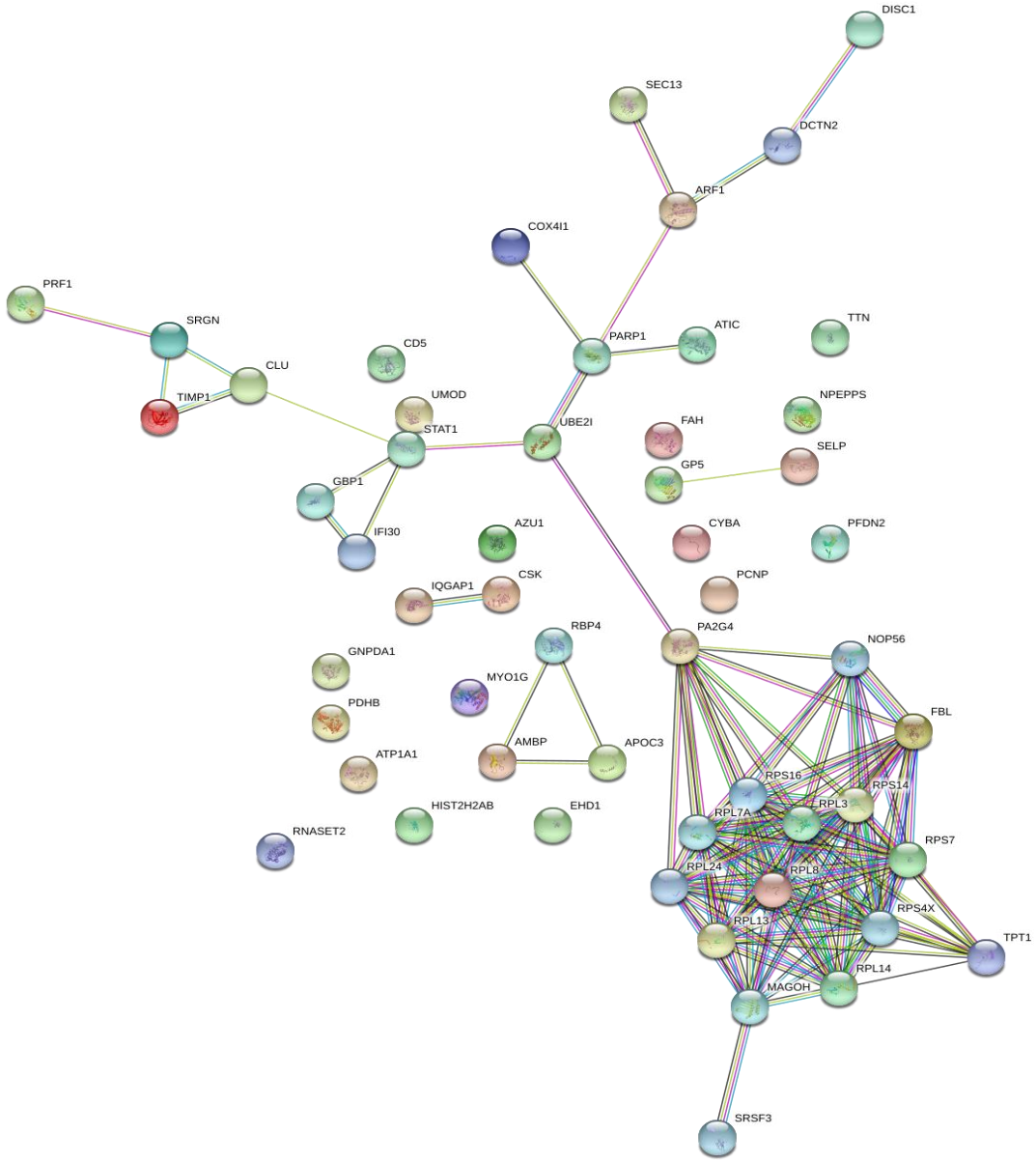

Figure 44. STRING network of 56 proteins quantifiable only in control samples

Table 10. Top four enriched GO terms for biological process and molecular function in proteins only quantifiable in control samples

GO pathway ID	Description	Gene count	False discovery rate
	Biological process		
GO:0000184	nuclear-transcribed mRNA catabolic process, nonsense-mediated decay	11	1.29e-10
GO:0006401	RNA catabolic process	12	7.21e-10
GO:0006614	SRP-dependent co-translational protein targeting to membrane	10	7.21e-10
GO:0019083	viral transcription	10	7.22e-10
	Molecular function		
GO:0003735	structural constituent of ribosome	8	4.35e-06
GO:0044822	poly(A) RNA binding	17	4.35e-06
GO:0003723	RNA binding	18	2.58e-05
GO:0005198	structural molecule activity	9	1.26e-02

The five proteins quantifiable only in *Mtb* only samples were also investigated in STRING. However, these proteins did not form a significantly enriched network. These are listed in Table 11 and include three notable proteins. Lipoprotein lipase, in addition to its role in lipoprotein hydrolysis, is known to positively regulate the inflammatory response and secretion of chemokines.[131] Angiotensin-converting enzyme (ACE) also plays a role in immunity through antigen processing and presentation via MHC class I and promoting mononuclear cell proliferation.[132,133] Finally, apolipoprotein A-IV plays an anti-inflammatory role in the innate response[134]. These three proteins are therefore likely related to the immune response generated by re-stimulation of PBMCs with *Mtb* WCL. However, it is important to note that each of these five proteins was quantified in only one of four biological samples. Furthermore, these were not part of the proteins identified only in *Mtb*-stimulated samples in the previous experiment (Chapter 5). This disconnect between the two experiments may be related to the low TIC in this experiment's *Mtb* only samples, as well as to biological variation.

Table 11. Proteins quantified only in *Mtb* only samples

Protein ID	Gene	Protein name	Role
P06858	LPL	Lipoprotein lipase	Hydrolysis of chylomicrons and very low-density lipoproteins (VLDL). Positive regulator of the inflammatory response and chemokine secretion[131]
P12821	ACE	Angiotensin-converting enzyme	Converts angiotensin I to II, inactivates bradykinin. Involved in antigen processing and presentation via MHC class I,[133] mononuclear cell proliferation,[132] and neutrophil-mediated immunity (inferred from homology)
P06727	APOA4	Apolipoprotein A-IV	Secretion and catabolism of chylomicrons and VLDL. Also involved in the innate immune response (anti-inflammatory)[134] and removal of superoxide radicals[135]
P35268	RPL22	60S ribosomal protein L22	Heparin and RNA binding, structural constituent of the ribosome, translation
O43488	AKR7A2	Aflatoxin B1 aldehyde reductase member 2	Catalyzes NADPH-dependent carbohydrate metabolic reduction reactions

The 19 proteins uniquely quantified in vehicle control samples also did not form an enriched network in STRING. Notable proteins that play a role in the immune response are shown in Table 12. Notable proteins quantified only in *Mtb* + vehicle samples below. These include C-X-C motif chemokine 5, which plays a notable role in neutrophil activation and chemotaxis,[136] thioredoxin domain-containing protein 17 and protein phosphatase 1A, both of which modulate TNF-α signaling and NF-κB activation,[137,138] and finally complement C4-A, a complement component involved in propagation of the classical complement pathway.[139] It is likely that these proteins were also present in other samples but may have been just below the level of quantification/detection. Furthermore, each of these proteins was only quantified in one of the four biological replicates.

Table 12. Notable proteins quantified only in *Mtb* + vehicle samples

Protein ID	Gene	Protein name	Role
P42830	CXCL5	C-X-C motif chemokine 5	Neutrophil activation,[140] positive regulation of cell proliferation and neutrophil chemotaxis,[136] inflammatory response
Q9BRA2	TXNDC17	Thioredoxin domain-containing protein 17	Disulfide reductase, modulates TNF-α signaling and NF-κB activation. Has peroxidase activity and may contribute to the elimination of cellular hydrogen peroxide[137,141]
P35813	PPM1A	Protein phosphatase 1A	Plays an important role in the termination of TNF-α-mediated NF-κB activation through dephosphorylating and inactivating IKBKB/IKKB,[138] negatively regulates TGF-β-mediated signalling[142]
P0C0L4	C4A	Complement C4-A	Non-enzymatic component of C3 and C5 convertases, essential for the propagation of the classical complement pathway. Covalently binds to immunoglobulins and immune complexes and enhances the solubilization of immune aggregates[139]

The 84 proteins quantified only in *Mtb* + PUFA samples formed a STRING network comprising 80 nodes and 127 edges (enrichment p-value: 1.77e-07, Figure 45). These terms are associated with molecule assembly, metabolism, and RNA splicing/binding. Again, most of these proteins were quantified only in one of four biological samples, therefore it is unlikely that their presence in only treatment condition holds strong biological significance.

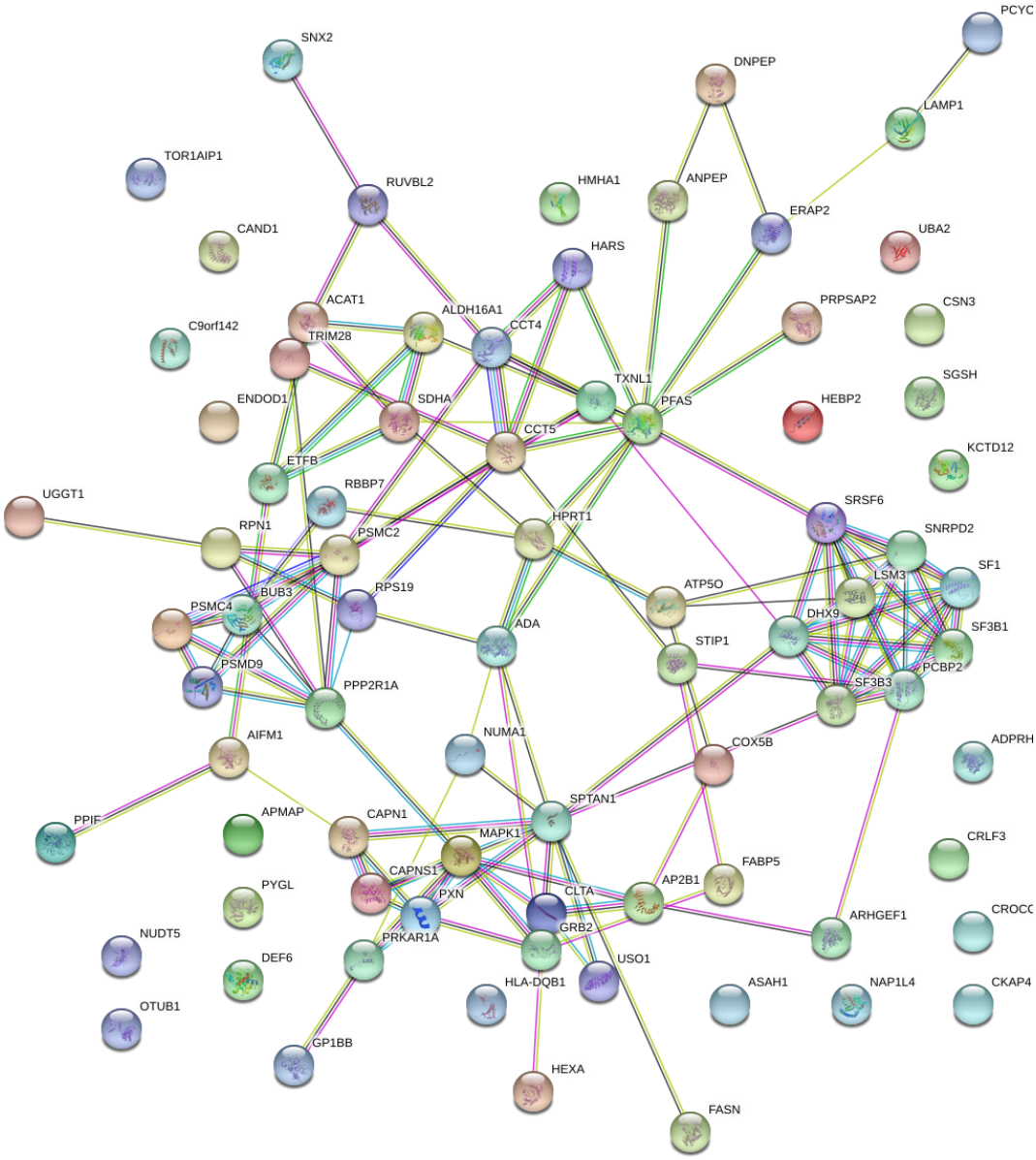

Figure 45. STRING network of 84 proteins quantifiable only in *Mtb* + PUFA samples

Table 13. Enriched GO terms for biological process and molecular function in proteins only quantifiable in *Mtb* + PUFA samples

GO pathway ID	Description	Gene count	False discovery rate
	Biological process		
GO:0065003	macromolecular complex assembly	18	1.87e-03
GO:0000398	mRNA splicing, via spliceosome	8	3.39e-03
GO:0006461	protein complex assembly	15	3.39e-03
GO:0044281	small molecule metabolic process	23	3.39e-03
	Molecular function		
GO:0003723	RNA binding	21	4.79e-04
GO:0044822	poly(A) RNA binding	18	4.79e-04

Comparison of control vs *Mtb* only samples

We compared proteins quantified in control and *Mtb* only samples and visualized the intersection using a Venn diagram (Figure 46. Proteins quantified in control and *Mtb* only samples). This revealed that 254 out of 473 quantifiable proteins were common to both conditions (53.7%). However, there were 213 proteins quantifiable only in control samples, and six proteins uniquely quantifiable in *Mtb* only samples. This surprising result contradicts expectations that re-stimulation with *Mtb* WCL would induce increased protein expression in PBMCs, and instead suggests that re-stimulation may be down-regulating protein expression. This is discussed further later on.

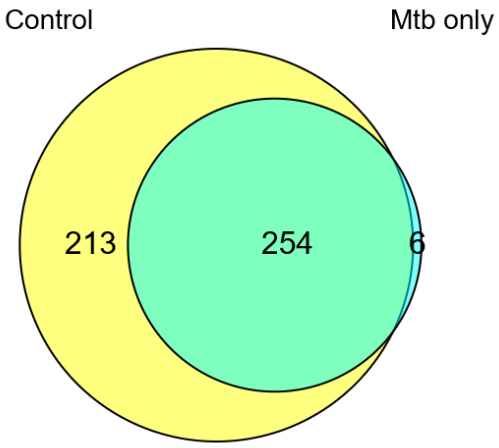

Figure 46. Proteins quantified in control and *Mtb* only samples

We performed paired Student's t-tests to identify protein groups expressed differentially in the four treatment conditions. Multiple testing correction (MTC) was applied following both the permutation-based (PB) and the Benjamini-Hochberg (BH) methods (FDR < 0.05). When comparing control and *Mtb* only samples, only one protein was significantly dysregulated when applying PB MTC (Table 14). When applying BH MTC, no proteins were considered significantly differentially expressed, although 68 proteins showed significantly different expression before any MTC was applied.

Table 14. Differentially regulated protein in *Mtb* only samples (comparing to control)

Protein ID	Gene ID	Protein name	Role	P-value	Fold change
Q9NUV9	GIMAP4	GTPase IMAP family member 4	Regulates lymphocyte survival and homeostasis through apoptosis[143]	4.17e4	-2.07

GTPase of immunity-associated proteins 4 (GIMAP4) is part of a family of septin-related guanine nucleotide-binding proteins that are abundantly expressed in immune cells. Knockout studies have shown the essential role of this protein family in the survival of lymphocytes, and interaction of GIMAP3, -4, and -7 with Bcl-2 proteins has suggested a role in the regulation of apoptosis.[143]

It was anticipated that re-stimulation with *Mtb* WCL would produce a significant response in PBMCs, and it is therefore surprising that the expression of only one protein was significantly different when comparing the control with *Mtb* only group. The much lower TIC obtained in Mtb only samples compared to control samples may have masked more pronounced differences between these two treatment groups. Since a label-free quantitation approach is employed here, it is important for TIC to be matched across samples for accurate quantitation and comparison.

We suggest that there may be several other reasons for which strong immune responses were not observed here. *Ex vivo* stimulation of immune cells with *Mtb* WCL has previously been shown to induce an immune response, such as an increase in IFN-γ production by NK cells,[144] and production of nitric oxide in monocytes.[145] The PBMCs re-stimulated in this experiment were derived from healthy donors who, to the best of our knowledge, were not infected with *Mtb*. Since the immune response is more pronounced after previous exposure to pathogens, this may explain why '*Mtb*-naïve' cells from healthy donors responded less vigorously to challenge by *Mtb* WCL. Indeed, a much greater reaction was observed when this experiment was repeated in TB-infected patient-derived PBMCs (Chapter 7).

It must also be noted that various concentrations of *Mtb* WCL have been used to re-stimulate immune cells *in vivo*. Here we have used 2 µg/mL, as in the work by Hoft *et al*.[93] and von Reyn *et al*.,[146] although higher concentrations of 10 µg/mL[144,145,147] and 50 µg/mL[148] have also been used. It is possible that a higher concentration of *Mtb* WCL would have elicited a greater response, but as a more prominent response was observed in patient-derived samples also stimulated with 2 µg/mL *Mtb* WCL, it is unlikely that the concentration used was too low. Another factor which may contribute here is the incubation time. Although most of the literature states 18-24 h incubation with the immunogenic stimulus, certain groups performed longer incubations such as 48 h (detection of NO production)[145] or 72 h (detection of IFN-γ).[147] Again, a slightly longer incubation period may have resulted in greater immune response. In our experiment, this had to be balanced by the risk of cell death increasing with prolonged culture in serum-free medium, which is why incubation could not be extended.

Further to this immunological reasoning, the data presented here may be skewed by mass spectrometry-related aspects, such as the "semirandom nature of data-dependent acquisition".[149] As previously mentioned, proteins not quantifiable in certain samples may be present at concentrations below the level of detection of the instrument in other samples. It is well-known that peptides experience different ionization efficiency, leading to observed enrichment of certain peptides over others in a manner that does not reflect biological significance.

Mtb + vehicle samples vs *Mtb* only samples

There were no significantly differentially regulated proteins identified when comparing vehicle controls with *Mtb*-stimulated samples. Although ethanol is known to have immune-modulatory effects, the concentration used in this experiment (0.2%) was too low to cause significant changes to the PBMC secretome.

Mtb + PUFA samples vs Mtb + vehicle samples

We compared proteins quantified in Mtb + vehicle and *Mtb* + PUFA samples to investigate the effects of n-3 PUFA treatment compared to that of the vehicle alone (Figure 46. Proteins quantified in control and *Mtb* only samples). This revealed that 353 of 666 quantifiable proteins were common to both conditions (53%). However, there were 183 proteins quantifiable only in *Mtb* + vehicle samples, and 130 proteins uniquely quantifiable in *Mtb* + PUFA samples. This may indicate that treatment of PBMCs with n-3 PUFA prior to re-stimulation with *Mtb* WCL leads to expression of certain proteins (proteins uniquely quantified in *Mtb* + PUFA samples).

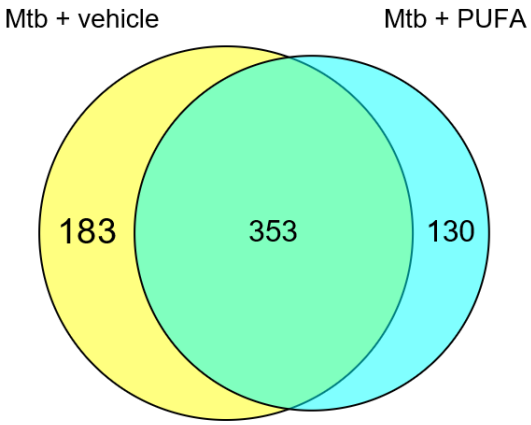

Figure 47. Proteins quantified in *Mtb* + vehicle and *Mtb* + PUFA samples

Mtb + vehicle

We investigated interactions between the 183 proteins quantified in *Mtb* + vehicle samples but not in *Mtb* + PUFA samples via STRING. The resulting network formed comprised 170 nodes and 567 edges with enriched GO terms for biological process, molecular function, and KEGG pathways listed in Table 15. We hypothesize that since these proteins were not quantified in *Mtb* + PUFA samples, treatment with PUFA may have caused their down-regulation in *Mtb*-stimulated PBMCs. Since our study did not include a PUFA only control, without *Mtb* WCL, we are unable to conclude about the effects n-3 PUFA in isolation and can only observe the impact of n-3 PUFA treatment on *Mtb*-stimulated cells. Therefore, the 'net effects' include those of *Mtb* WCL re-stimulation and n-3 PUFA treatment.

Table 15. Top four enriched GO terms for biological process, molecular function, and KEGG pathways in proteins quantified in *Mtb* + vehicle samples but not *Mtb* + PUFA samples

GO pathway ID	Description	Gene count	False discovery rate
	Biological process		
GO:0006810	transport	68	2.57e-11
GO:0051179	localization	74	4.62e-10
GO:1903034	regulation of response to wounding	21	5.84e-09
GO:0044765	single-organism transport	56	1.22e-08
	Molecular function		
GO:0005515	protein binding	78	9.67e-10
GO:0004857	enzyme inhibitor activity	17	4.21e-06
GO:0005539	glycosaminoglycan binding	13	7.52e-06
GO:0030234	enzyme regulator activity	26	7.52e-06
	KEGG pathways		
03320	PPAR signalling pathway	8	1.34e-05
04610	Complement and coagulation cascades	7	1.46e-04
01100	Metabolic pathways	24	2.44e-03
04510	Focal adhesion	9	2.87e-03

Interestingly, the enriched GO terms for biological process seem to relate to the cell's response to stimulus or stress. This is further supported by evidence from the enriched KEGG pathway term "complement and coagulation cascades". The complement system mediates innate immunity and triggers the recruitment of inflammatory cells, as well as the opsonization and killing of pathogens. The coagulation cascade leads to the formation of thrombin, as well as a fibrin clot, and is closely related to the kinin-kallikrein system (KKS), which is itself involved in inflammation, coagulation, vascular permeability, and pain, amongst others.[150] The interaction between these two pathways is shown in Figure 48. KEGG pathway for complement and coagulation cascade (04610) with red boxes indicating which proteins were identified in the current dataset.

Several complement proteins were identified here. Complement component 3 (C3, P01024), which plays a central role in the alternative and classical activation of the complement system and acts as a chemoattractant for neutrophils. Over-expression of C3 has been associated with metabolic disorders characterized by low-grade inflammation, such as insulin resistance, diabetes, and metabolic syndrome (MetS).[151] Complement component 4A (C4A, P0C0L4), the product of C4 degradation, mediates local inflammation, and complement factor B (CFB, P00751), which is cleaved into two fragments and produces C3 convertase, is involved in the proliferation and differentiation of activated B lymphocytes. We also identified plasma protease C1 inhibitor (C1INH, P05155), which is involved in regulating complement activation, coagulation, fibrinolysis, and is an inhibitor of kallikrein. As a suppressor of inflammation, dysregulation of C1INH has been implicated in the pathogenesis of TB-IRIS-associated chronic inflammation.[152] Kininogen 1 (KNG1, P01042), a coagulation pathway component, was also identified. Hydrolysis of kininogens lead to formation of bradykinin, an important vasodilator and inflammatory mediator.[150] Alpha-2-macroglobulin (A2M, P01023) is a regulator of complement activation via the lectin pathway, and ligand for IL-1[153] and -8.[154] Finally, antithrombin 3 (AT3, P01008) is an important protease inhibitor which inactivates several coagulation pathway components.

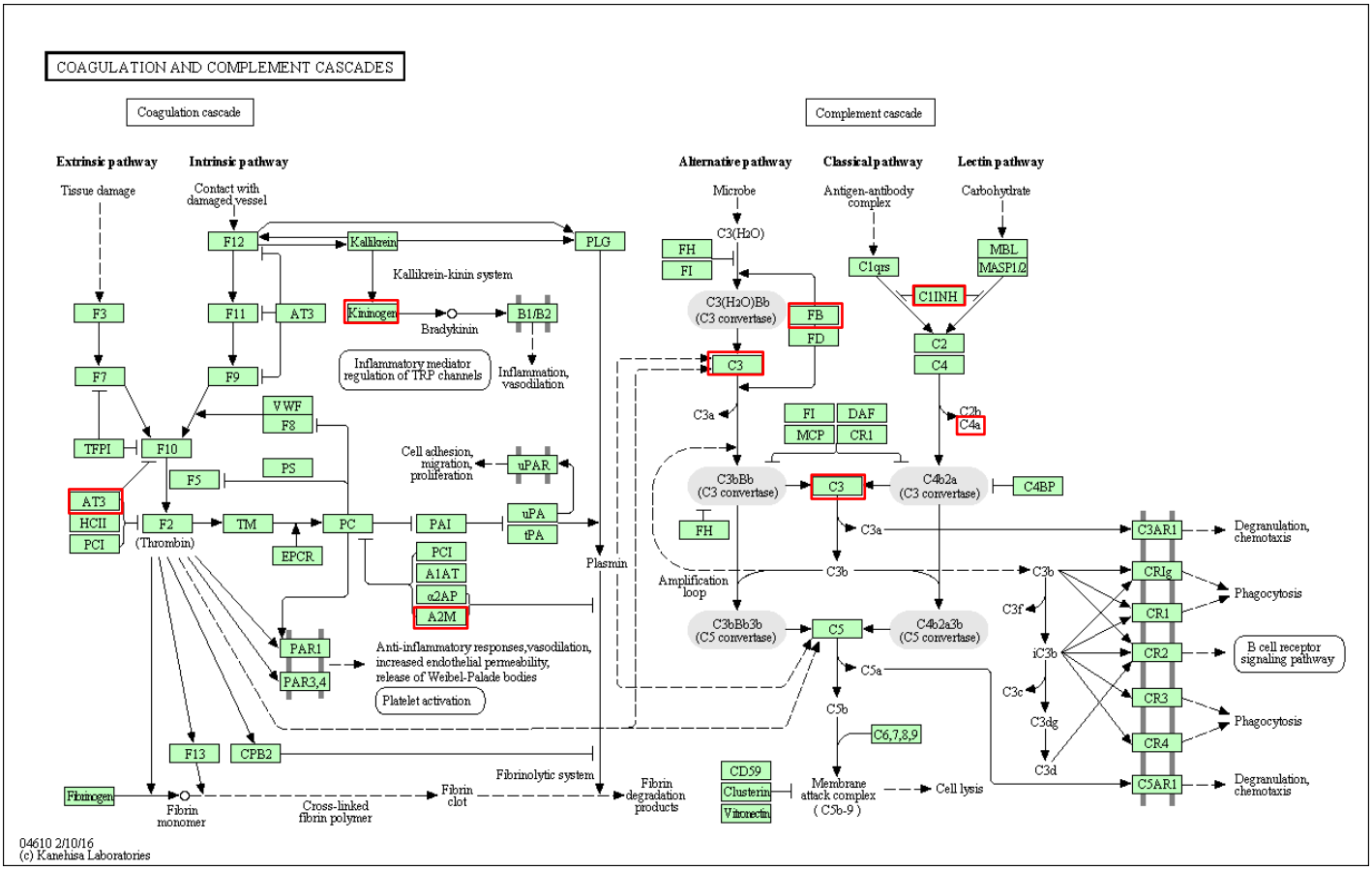

Figure 48. KEGG pathway for complement and coagulation cascade (04610)

Proteins highlighted in red boxes were identified in the current dataset. AT3, antithrombin 3; kininogen, KNG1; A2M, alpha-2-macroglobulin; C3, complement component 3; FB, complement factor B; C1INH, complement 1 inhibitor; C4a, complement component 4a.

Since several key proteins relating to the complement and coagulation pathways were identified and quantified in *Mtb* + vehicle samples but not in samples pre-treated with n-3 PUFA, the data may suggest a decrease in complement and coagulation pathway involvement mediated by n-3 PUFA in *Mtb* WCL-stimulated PBMCs. With regards to literature investigating the effects of PUFA on the complement pathway, a recent study reported over-expression of C4 regulator miRNA after increased PUFA dietary intake, although this included both n-3 and n-6 PUFA.[155] Phillips *et al*.[151] investigated the interaction between PUFA and C3 polymorphisms in the context of MetS. This study revealed that n-3 and n-6 PUFA led to both increased and decreased MetS risk, depending on the individual's *C3* gene variant, highlighting the difference in responses observed in individuals. The effects of n-3 PUFA on complement activation are not well understood, and performing targeted MS analysis on key regulators of the pathways would perhaps shed more light on n-3 PUFA activity in complement and coagulation regulation.

Mtb + PUFA

Interactions between proteins unique to *Mtb* + PUFA samples were further investigated through STRING. An enriched network comprising 125 nodes and 332 edges was produced and is shown in Figure 49. The top four GO terms enriched in biological process were macromolecular complex assembly, protein complex assembly, protein complex biogenesis, and mRNA splicing (Table 16). Since these terms are enriched in proteins expressed in *Mtb* + PUFA samples but not in *Mtb* + vehicle samples, we hypothesize that treatment with n-3 PUFA may cause increased expression of proteins associated with these terms in *Mtb*-stimulated PBMCs.

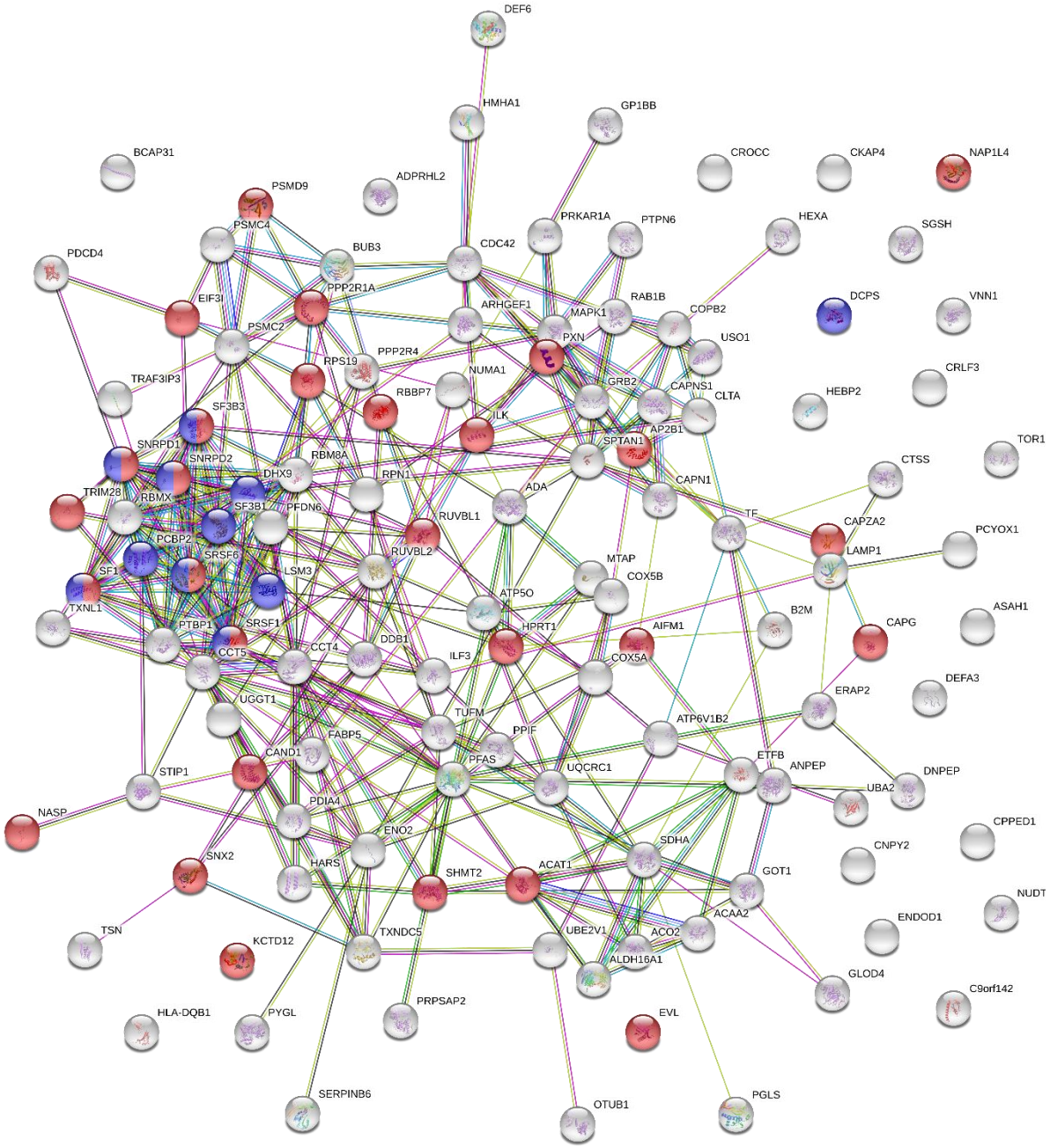

Figure 49. STRING network of 125 proteins quantified in *Mtb* + PUFA samples but not *Mtb* + vehicle samples

Red nodes, proteins associated with the GO term “macromolecular complex assembly” (GO:0065003); blue nodes, proteins associated with the GO term “mRNA splicing, via spliceosome” (GO:0000398).

Table 16. Top four enriched GO terms for biological process and molecular function in proteins quantified in Mtb + PUFA samples but not Mtb + vehicle samples

GO pathway ID	Description	Gene count	False discovery rate
	Biological process		
GO:0065003	macromolecular complex assembly	28	7.4e-07
GO:0006461	protein complex assembly	23	1.76e-05
GO:0070271	protein complex biogenesis	23	1.76e-05
GO:0000398	mRNA splicing, via spliceosome	11	0.000142
	Molecular function		
GO:0003723	RNA binding	31	3.01e-06
GO:0044822	poly(A) RNA binding	26	6.34e-06
GO:0003824	catalytic activity	54	0.00111
GO:0005488	binding	85	0.00111

Macromolecular assembly refers to the formation of structures such as organelles and membranes, comprising peptides, saccharides, and other macromolecules. This includes lipid rafts, which are plasma membrane micro-domains rich in cholesterol and sphingolipids that are not integrated into the membrane, but facilitate interactions between membrane lipids and proteins.[156] N-3 PUFA are known to interact with and act upon cell membrane components such as lipid rafts. Fan *et al*.[157] investigated the effects on EPA and DHA on lipid raft constitution, demonstrating a significant decrease in sphingomyelin content in mouse-derived T cells. These sphingolipids play an important role in lipid raft formation and T cell activation. The stability of lipid rafts is disrupted by altering fatty acid composition and depleting sphingolipids, which may contribute to the decrease in T cell activation that is observed in response to n-3 PUFA treatment. Moreover, secretion of NF-κB and IL-2 is suppressed, as is the proliferation of lymphocytes as a result of n-3 PUFA interaction with lipid rafts. It was further shown that subsets of T cells (Th1 and Th2) respond differentially, and that n-3 PUFA may also inhibit antigen presentation via disruption of the lipid raft-dependent immunological synapse.[156]

It is therefore likely that the terms macromolecular and protein complex assembly may relate to lipid rafts and modulation thereof. There were 11 proteins in this dataset that were previously identified as lipid raft-associated proteins by Chadwick *et al*.[158] who isolated lipid rafts in the detergent-resistant membranes of mouse-derived brain tissue. However, to further investigate the effects of EPA and DHA on the cells of interest in our study, lipid rafts in the cell membrane would need to be enriched during sample processing.

"mRNA splicing" was another enriched GO term, which refers to the process by which introns are removed from mRNA molecules. Dietary changes are known to affect mRNA splicing, particularly that of glucose-6-phosphate dehydrogenase (G6PD). This enzyme catalyzes the first, rate-limiting step of the pentose phosphate pathway, which produces NADPH that is later used to synthesize fatty acids in the liver and adipose tissues.[159] It was shown that an increase in dietary PUFA intake could inhibit splicing of G6DP mRNA and further, that enzymatic efficiency of mRNA processing for all lipogenic genes could be regulated by dietary PUFA.[160] Another important enzyme that is regulated by alternative splicing is fatty acid desaturase 2 (FADS2). It is essential for the biosynthesis of n-3 and n-6 PUFA, and alternative splicing is modulated by polypyrimidine tract binding protein 1 (PTBP1, UniProt ID P26599). Reardon et al.[161] demonstrated that PTBP1 knock-down in HepG cells caused a significant decrease in n-3 PUFA relative to n-6 PUFA, especially with respect to the ratio of EPA to AA (43% decrease). PTPB1 was identified (with five unique peptides) and quantified only in *Mtb* + PUFA samples, suggesting a link between PUFA treatment and regulation of the expression and activity of PTBP1 in these samples.

Identification of interleukins

While we did identify several interesting and relevant proteins, there were no inflammation-specific proteins dysregulated. Of particular interest was the identification and differential quantification of cytokines (interleukins especially). Although no interleukins were significantly differentially regulated, it is worth noting that several were identified in this experiment.

IL-8 (P10145, gene CXCL8) was identified with only one unique peptide, and was therefore excluded from further analysis. Interestingly, IL-8 was quantified in eight of 16 samples in this experiment, and in all conditions other than *Mtb* + PUFA samples. This chemotactic factor attracts other inflammatory mediators such as neutrophils, basophils, and T cells. It is involved in the activation of neutrophils and various other roles in the immune system. EPA and DHA have previously been reported to inhibit production of IL-8 induced by endotoxin in human endothelial cells,[162] as well as in UVB-challenged keratinocytes,[163] and endothelial progenitor cells.[164] Our result therefore correlates well with this, but targeted MS analysis would be necessary to confirm the presence and enable accurate quantitation of IL-8.

Pro-interleukin-16 (Q14005, gene IL-16) was identified with 18 unique peptides, in 15 of 16 samples. Finally, IL-19 (Q9UHD0, gene IL-19) was identified in only one sample (vehicle control) with two unique peptides.

These low-abundance proteins are notoriously difficult to identify through LC-MS/MS-based methods so it is encouraging that we were at least able to identify three. A larger sample size and a targeted approach may reveal more in terms of the quantification and differential expression of such cytokines.

6.4 Conclusion

In this experiment, we aimed to assess the effects of re-stimulation with *Mtb* WCL in PBMCs isolated from four healthy volunteers, as well as investigate the effects of pre-treatment with n-3 PUFA. The secretome from these PBMCs was analyzed via MS-based proteomic methods, and the data were interrogated using statistical tests to reveal significant differences in protein expression between the various treatment groups. We were able to identify over 2000 proteins in total, of which 727 human proteins remained after filtering according to our set criteria.

When comparing *Mtb* only and control samples, we identified one differentially regulated protein, which was not identified in our previous experiment (Chapter 5). This surprising result may be explained by our small sample size (n = 4 in this experiment, and n = 3 in the previous experiment). Furthermore, variation in this dataset is important as these are donor-derived samples. The greater the variation in protein expression, the more difficult it is to distinguish between biological variability and significant, treatment-induced differences in expression. By repeating this experiment and increasing the sample size, more meaningful conclusions may be drawn from the data.

We also compared *Mtb* only samples with those pre-treated with n-3 PUFA. Although none of the proteins identified were considered significantly differentially regulated, qualitative analyses (presence/absence) revealed that several proteins from the complement and coagulation pathways quantified in *Mtb* + vehicle samples were not quantifiable in *Mtb* + PUFA samples. This may suggest down-regulation of these pathways by n-3 PUFA in *Mtb* WCL-stimulated PBMCs. In the current experiment, it may be difficult to tease out causal relationships as the effects of *Mtb* stimulation and n-3 PUFA treatment are compounded. The inclusion of a control treated with n-3 PUFA but not re-

stimulated with Mtb WCL may have been of use to tease out the effects of both these perturbations. This is a limitation of the current study and should be considered in future work.

While we saw a change in the PBMC secretome following pre-treatment with n-3 PUFA, it was not possible to conclude whether PUFAs exerted the anti-inflammatory effects that we expected, as we did not see a decrease in the expression of specific pro-inflammatory proteins. The addition of orthogonal biochemical methods such as ELISA or multiplex Luminex panels may contribute important data relating to the expression of lower abundance proteins, and particularly cytokines, chemokines, and growth factors (such as interleukins, TNF-α, IFN-γ, TGF-β, which are known pro-inflammatory mediators involved in TB immunity). Furthermore, it may be of interest to harvest cell culture supernatants at different time points, as different factors produced reach maximal concentration in cell medium at different times. Therefore, in the future, an experiment such as this one may be improved by i) increasing the sample size, ii) incorporating targeted MS-based proteomics and another, orthogonal method, iii) including different time points, and iv) including a control treated with n-3 PUFA but not re-stimulated with *Mtb* WCL (PUFA only control).

Chapter 7

Secretome analysis of TB-IRIS patient-derived PBMCs: Part I

7.1 Aim

The aim of this experiment was to investigate the PBMC secretome of PBMCs derived from TB- and HIV-infected patients who developed TB-IRIS, and compare it to that of PBMCs from patients co-infected with TB and HIV but who did not go on to develop TB-IRIS. As in Chapter 6, PBMCs were pre-treated with n-3 PUFA and re-stimulated *ex vivo* with *Mtb* WCL, and the same methods for cell culture and sample processing for MS-based proteomics were applied. The current chapter presents and assesses patient characteristics, cell culture data, quality of MS chromatograms and protein identification, and sample clustering.

7.2 Results and discussion

7.2.1 Patient recruitment and characteristics

The sub-study presented here is part of a larger study (TBTD2, HREC REF: 516/2011), and was approved by the University of Cape Town's ethics committee (HREC REF: 136/2013). Patients were recruited from Ubuntu Clinic, Kayelitsha site B. As a densely populated and largely informal settlement, Kayelitsha hosts many previously disadvantaged, low-income communities. The incidence of HIV, TB, as well as DR-TB, is high,[165] and many of the patients presenting at Ubuntu Clinic therefore require co-treatment. For this study, HIV/TB co-infected, ART-naïve but eligible patients were recruited and followed up for 12 weeks post ART initiation. The inclusion criteria were as follows:

- Confirmed TB diagnosis (sputum smear positive, sputum culture positive, or clinical features highly suggestive of TB with diagnostic features on chest x-ray)
- Confirmed HIV diagnosis
- ART-naïve but eligible
- CD4 count < 250 (patients at high risk of developing TB-IRIS)

Exclusion criteria were as follows:

- Patients younger than 18 years
- Unknown or unconfirmed HIV status
- TB infection not confirmed by smear microscopy and culture
- Pregnancy
- Current corticosteroid treatment

As per national guidelines, patients began TB treatment immediately after confirmation of TB diagnosis, and ART was initiated within 2 weeks of TB treatment. Follow-up visits were conducted at 2, 4, and 12 weeks post ART initiation. Extra visits were also scheduled in the event of clinical deterioration and appearance of symptoms suggestive of TB-IRIS. Data were collected from patients at various time-points and include patient history, description of symptoms, weight measurements, phlebotomy (weeks 2 and 4), urine sample collection, and clinical examination.

Two patient groups were investigated in this study: the "non-IRIS" group (patients infected with TB and HIV who did NOT develop TB-IRIS), and the "IRIS" group (patients infected with TB and HIV who DID develop TB-IRIS). Blood samples used in this study are those collected two weeks after patients began ART, which is usually the time at which TB-IRIS symptoms first manifest.[52] We thus expect to see the greatest differences between the proteome of IRIS patients and that of non-IRIS controls at this time point. As in the previous experiment, blood was drawn from patients and PBMCs were isolated within 4 h of blood collection by another student. Cells were then cryopreserved until further analysis. This sub-study comprised samples from 10 patients (n = 5 per group). Patient characteristics are listed in Table 17 below. There were six males and four females, aged 25 to 47 (mean = 34.8 years). Baseline CD4 counts varied quite widely from 4 to 233 cell/mm^3, as did viral load (31,788 to 1,597,770 copies/mL). The mean interval between the beginning of TB treatment and initiation of ART (TB-ART interval) was 18.3 ± 5.6 days. Recommendations have been made to begin ART immediately if CD4+ count < 50 cells/mm^3, and to delay ART initiation until 8 weeks after starting TB treatment is CD4+ count > 50 cells/mm^3 in order to limit toxicity and risk of developing TB-IRIS.[56] Although six of the patients in this study had CD4+ counts < 50 cells/mm^3 at baseline, ART was only initiated a minimum of 14 days after starting TB treatment.

Table 17. Patient characteristics

ID code	Group	Age (years)	Sex	Baseline CD4 count (cells/mm^3)	Baseline viral load (copies/mL)	TB-ART interval (days)	White cell count (10^9/L)	BMI
CL1	non-IRIS	26	F	5	59,224	19	7	39.72
CL2	non-IRIS	41	M	4	401,016	15	4.42	23.15
CL3	IRIS	34	M	15	313,118	14	11.14	20.49
CL4	IRIS	44	M	233	31,788	14	6.53	23.41
CL5	non-IRIS	32	F	89	95,093	18	2.67	23.12
CL6	non-IRIS?*	31	M	143	981,890	16	4.89	19.56
CL7	non-IRIS	47	M	6	515,804	32	4.73	19.94
CL8	IRIS	31	M	7	184,559	18	7.74	18.06
CL9	IRIS?*	37	F	42	739,647	14	6.33	20.16
CL10	IRIS	25	F	170	1,597,770	23	6.99	15.89
Mean		34.80		71.40	491,990.90	18.30	6.24	22.66
SD		7.36		83.46	496,212	5.60	2.30	6.87

*Final classification is not available for patient CL6 and CL9. This is the current presumed classification.

7.2.2 Cell recovery

PBMCs were thawed, rested overnight, and cultured for a further 24 h after pre-treatment with n-3 PUFA and re-stimulation with *Mtb* WCL. Cells were counted at the time of freezing, after the initial thaw, and after overnight rest. These results are presented in Figure 50. Number of cells recovered after thawing and overnight rest. The mean recovery ± SD was 35.72 ± 19.22% after thawing, and 16.84 ± 12.27% following overnight rest. Thus, cell recovery from patient-derived samples was lower than that from healthy volunteer-derived PBMCs (Chapter 4, Figure 11) where percentage recovery after was thawing was 38.86%, and 36.97% after overnight rest. However, the difference in mean recovery after thaw was not significant ($p > 0.05$), and the difference in recovery after overnight rest was just significant ($p = 0.05$, Student's t test, unpaired, two-tailed distribution). This suggests that PBMCs isolated from patients co-infected with *Mtb* and HIV may be less resistant to cryopreservation than their healthy counterparts; however, a larger sample size would be needed to confirm this. We also compared cell recovery rates between the two patient groups (TB-IRIS vs non-IRIS patients) and there were no significant differences in recovery after thaw or after overnight rest. Viability as assessed via Trypan blue exclusion assay was > 90% both directly after thawing and after overnight rest. However, cell recovery after overnight rest was < 10% for sample CL7. This sample was therefore excluded from further analysis, resulting in n = 4 for the non-IRIS group and n = 5 for the IRIS group.

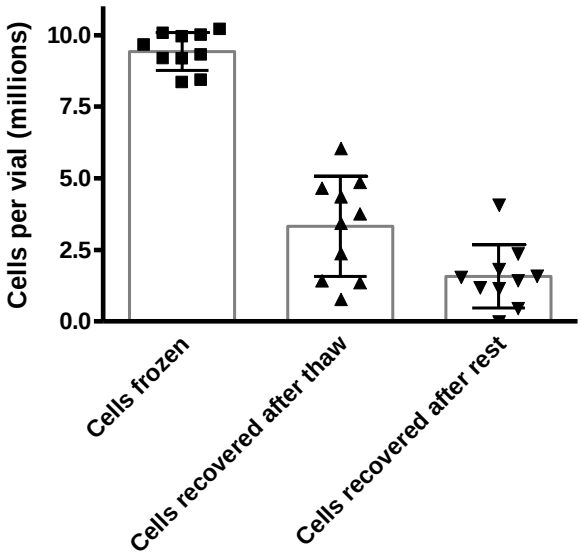

Figure 50. Number of cells recovered after thawing and overnight rest

Results are shown as mean cell numbers ± SD (error bars) from five TB-/HIV-infected patients with TB-IRIS and five TB-/HIV-infected patients who did not develop TB-IRIS (controls).

7.2.3 Protein quantitation

Total protein was quantified via modified Bradford assay. In non-IRIS samples, mean total protein recovered from control samples was 0.43 µg, 0.97 µg for *Mtb* only samples, 1.91 µg for *Mtb* + vehicle samples, and 1.77 µg for *Mtb* + PUFA samples (Figure 31). These values for protein content follow the same trend as that seen in healthy donor cells. In IRIS samples however, mean total protein recovered from control samples was 2.19 µg, 3.81 µg for *Mtb* only samples, 1.53 µg for Mtb + vehicle samples, and 1.27 µg for *Mtb* + PUFA samples. This trend is different from that seen in both healthy volunteer cells and non-IRIS patient-derived cells. Since the inter-sample variation (SD, error bars in Figure 31) is important, the differences between protein content in non-IRIS and IRIS samples per condition were not significant, and neither were the differences between protein content between the different treatment conditions ($p > 0.05$). The differences seen here may result only from inter-sample variability, which is emphasized by the small sample size. A larger sample group would help to reduce "noise" created from inherent biological variation and clarify whether this trend is in fact a significant one.

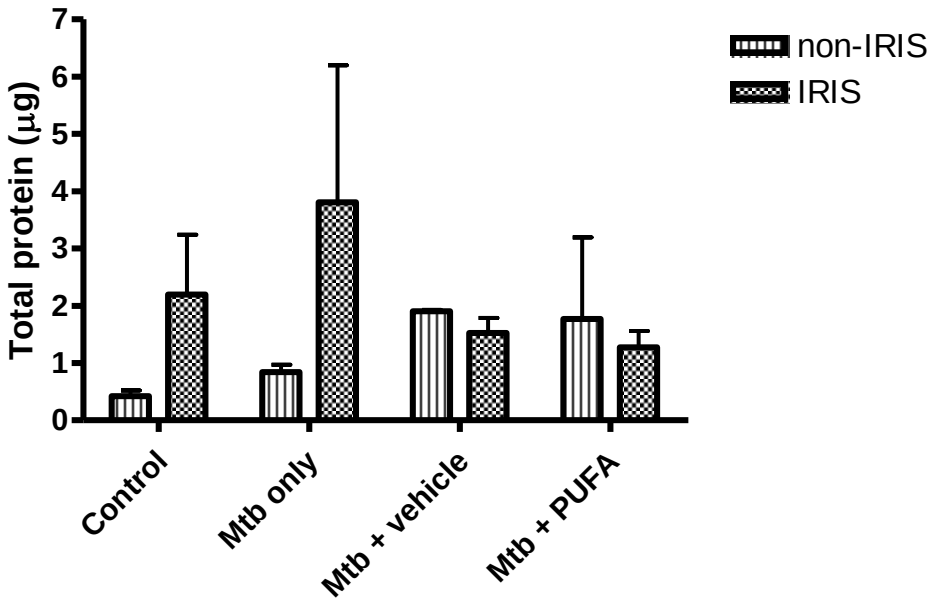

Figure 51. Total protein content in control, *Mtb* only, *Mtb* + vehicle, and *Mtb* + PUFA samples

Data are presented as means ± SD (error bars) with n = 4 for non-IRIS group samples and n = 5 for IRIS groups samples.

7.2.4 MS spectra, data quality, and protein identification

Samples were prepared in two batches with samples randomly assigned to each batch using Excel's RAND function, and were submitted to LC-MS/MS analysis in an order that was generated randomly in order to minimize batch effects.

MS spectra

The spectra obtained by discovery MS analysis on a Q Exactive LC-MS/MS are shown in Figure 52 to 6 (non-IRIS samples), and Figure 57 to 10 (IRIS samples) below. These display chromatograms from the biological replicates for each treatment condition (non-IRIS, n = 4; IRIS, n = 5). Overall, signal intensity was very low. Certain samples showed medium peptide peaks (with MS2) eluting at approximately 30 min, but these were not present in all replicates/conditions. We hypothesize that these may be specific to certain patients, as the peak is present in certain patient samples only (for example, it is seen in CL5, in all treatment conditions), and may be related to particular patient characteristics. CL5 has the lowest white cell count (WCC) of all patients ($2.67x10^9$/L at baseline), although the peak in question is also seen in CL3, which has one of the highest WCC ($11.14x10^9$/L). It is therefore more likely related to the fact that samples in which this peak appears have the lowest maximum intensity of all biological replicates, per condition. For example, in Figure 52. MS chromatogram (TIC) of non-IRIS,

control samples, the maximum intensity in CL5 is 5.81e9, which is the lowest of the four non-IRIS control replicates. This may suggest that increased signal intensity from the two greatest peaks seen in all samples (at 92.4 and 95.7 min) could be responsible for suppressing the peak at 30 min and would explain why it is only observed in samples with lower maximum signal intensity. The variation in TIC is shown in Figure 56 (non-IRIS samples) and Figure 61 (IRIS samples). TIC variation was relatively low for both sample groups.

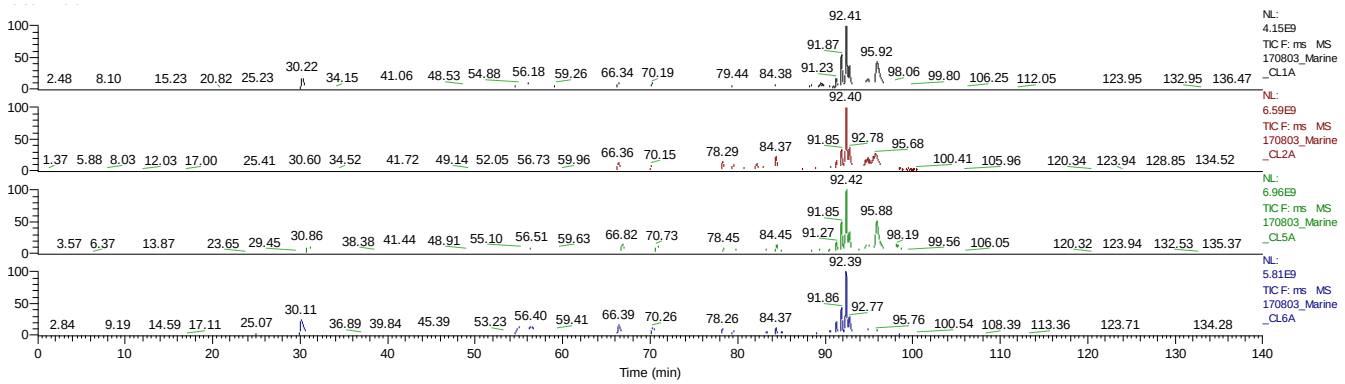

Figure 52. MS chromatogram (TIC) of non-IRIS, control samples

Spectra from top to bottom: black, CL1; red, CL2; green, CL5; blue, CL6.

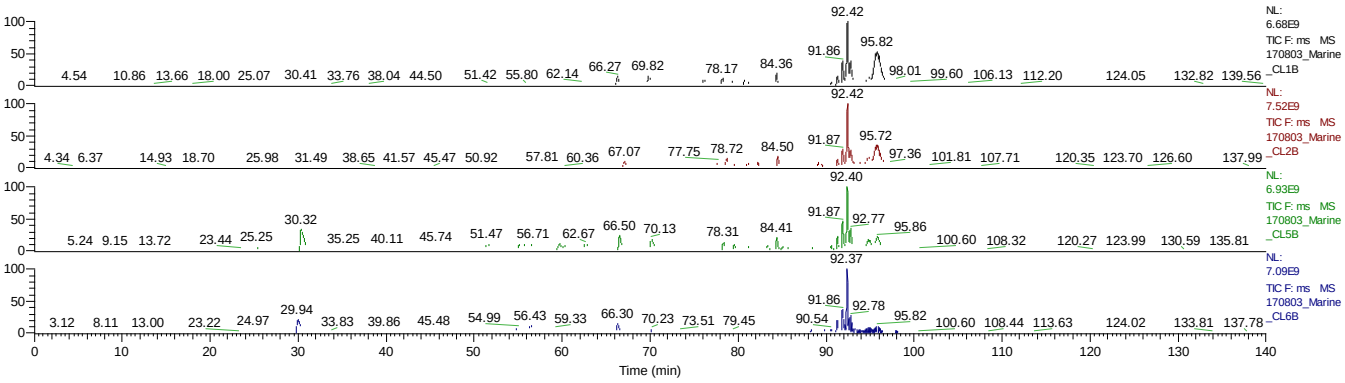

Figure 53. MS chromatogram (TIC) of non-IRIS, *Mtb* only samples

Spectra from top to bottom: black, CL1; red, CL2; green, CL5; blue, CL6.

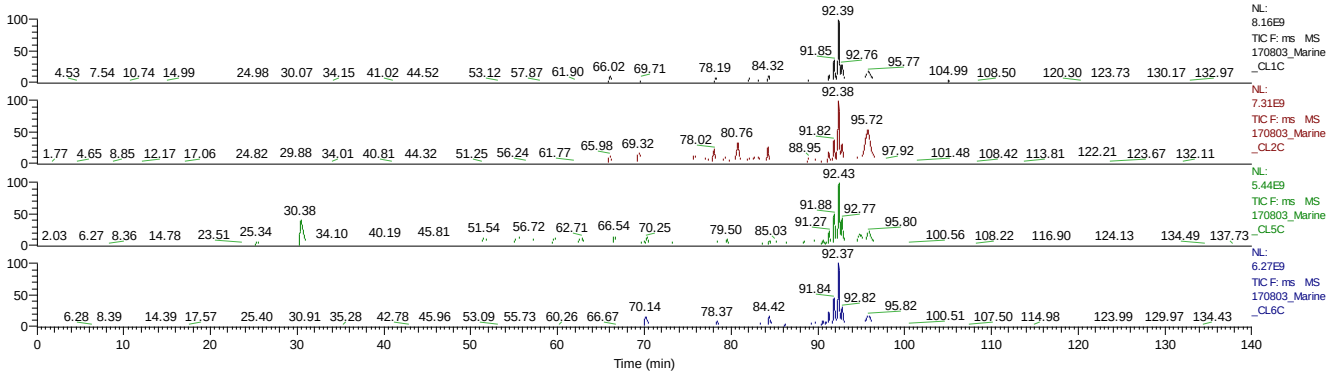

Figure 54. MS chromatogram (TIC) of non-IRIS, *Mtb* + vehicle samples

Spectra from top to bottom: black, CL1; red, CL2; green, CL5; blue, CL6.

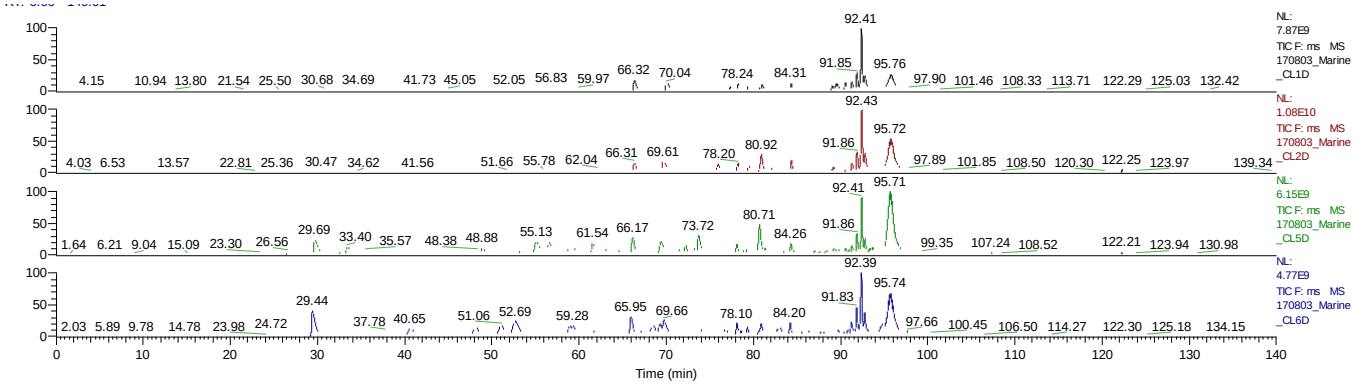

Figure 55. MS chromatogram (TIC) of non-IRIS, *Mtb* + PUFA samples

Spectra from top to bottom: black, CL1; red, CL2; green, CL5; blue, CL6.

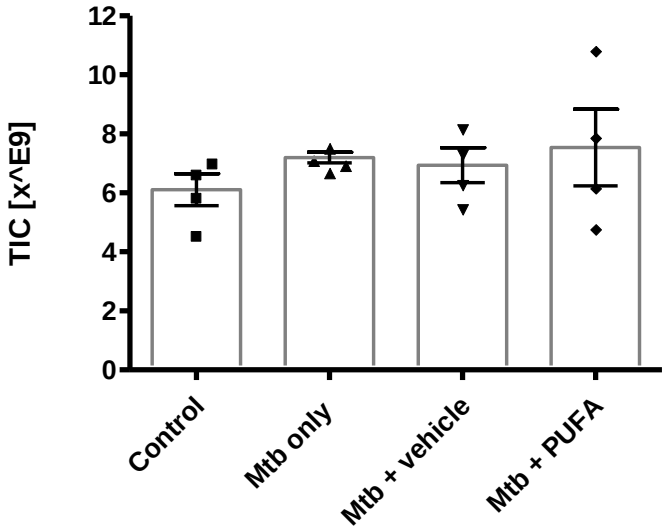

Figure 56. TIC variation in non-IRIS samples

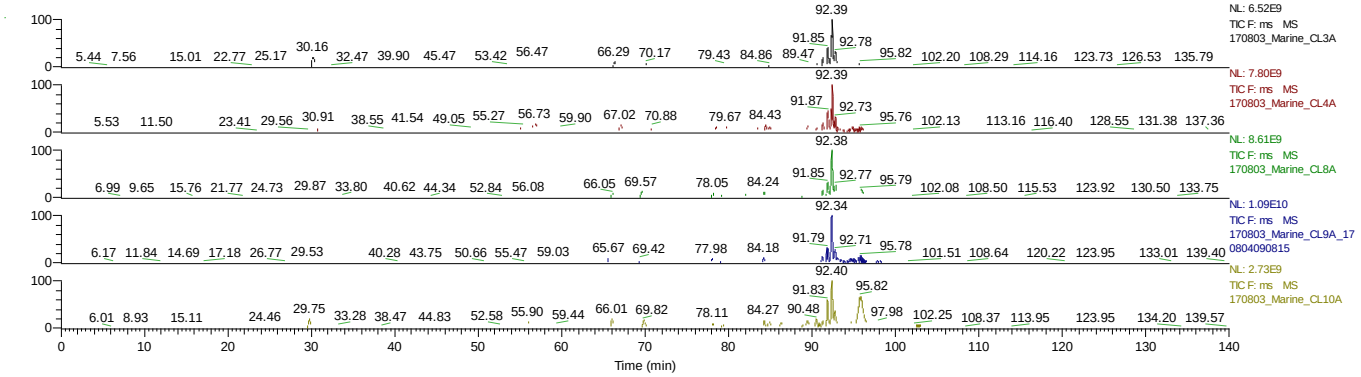

Figure 57. MS chromatogram (TIC) of IRIS, control samples

Spectra from top to bottom: black, CL3; red, CL4; green, CL8; blue, CL9; yellow, CL10.

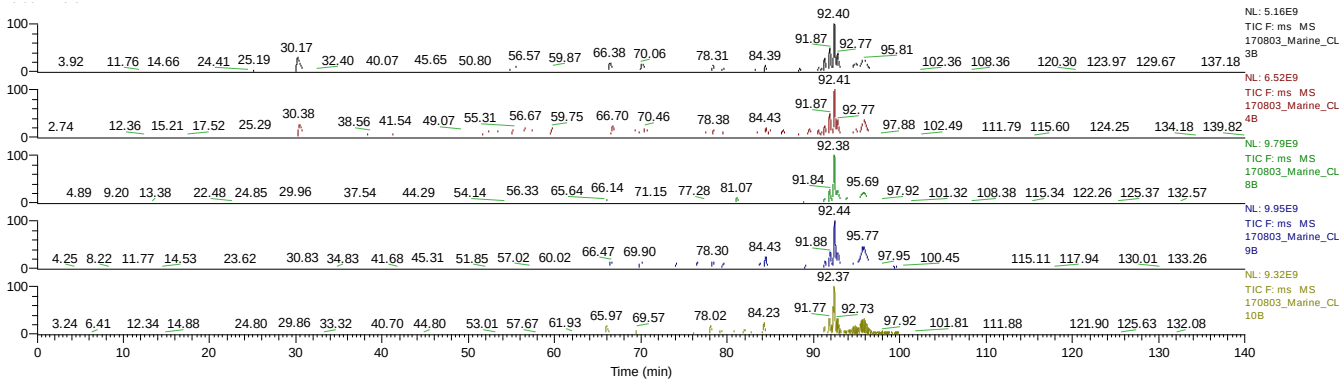

Figure 58. MS chromatogram (TIC) of IRIS, *Mtb* only samples

Spectra from top to bottom: black, CL3; red, CL4; green, CL8; blue, CL9; yellow, CL10.

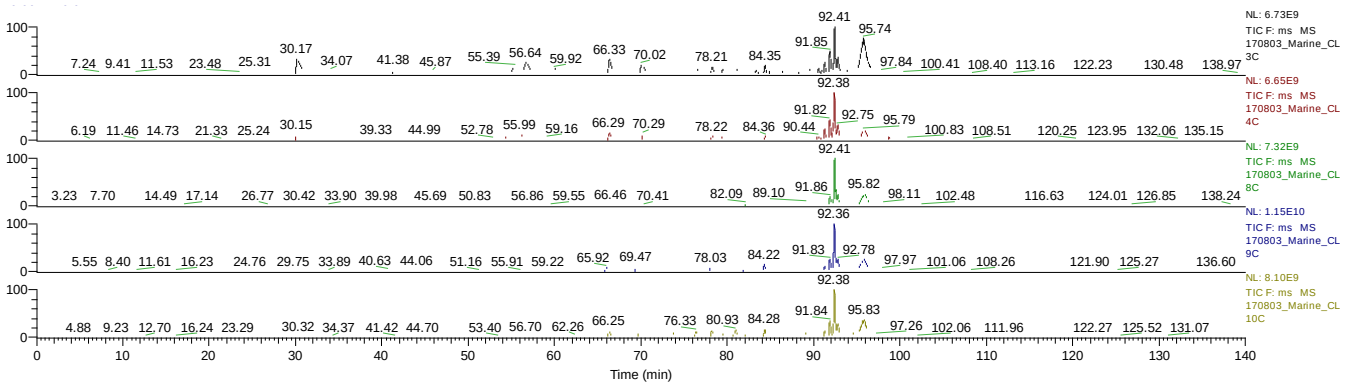

Figure 59. MS chromatogram (TIC) of IRIS, *Mtb* + vehicle samples

Spectra from top to bottom: black, CL3; red, CL4; green, CL8; blue, CL9; yellow, CL10.

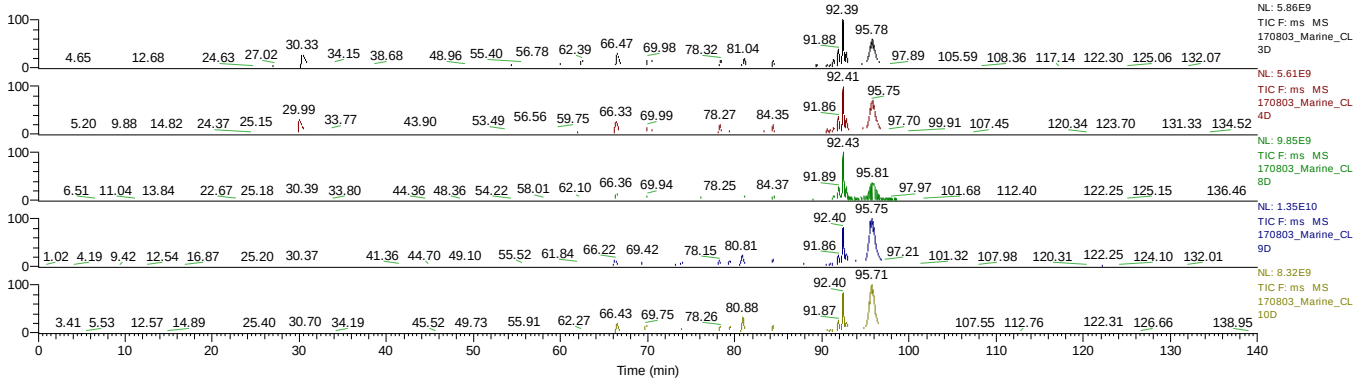

Figure 60. MS chromatogram (TIC) of IRIS, *Mtb* + PUFA samples

Spectra from top to bottom: black, CL3; red, CL4; green, CL8; blue, CL9; yellow, CL10.

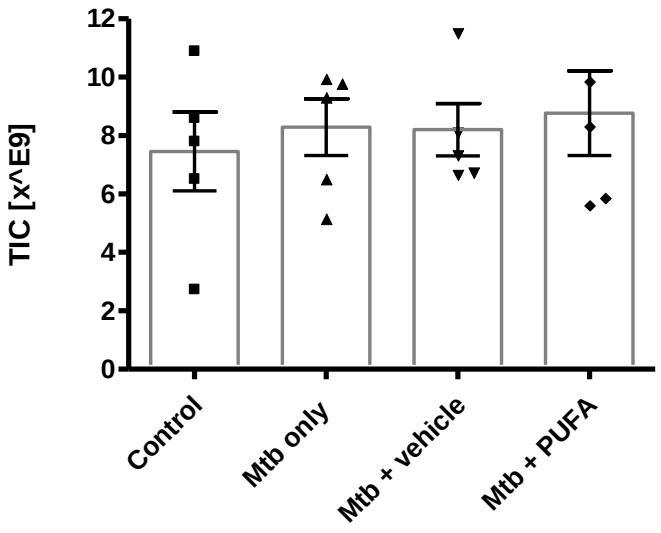

Figure 61. TIC variation in IRIS samples

The two large peaks eluting at approximately 92.4 and 95.7 min in every sample are most likely contaminants (z = 1) originating from samples processing. We identified polyethylene glycol (PEG, 415.21 Da) eluting at 92.4 min (Figure 62), as well as 44 Da transitions characteristic of PEG at 95.7 min (Figure 63). Although the presence of such contaminants may suppress signal intensity from peptides, there does not appear to be any other peptides eluting at this time, as can be seen from the lack of MS2 spectra at 92 and 95 min (Figure 62). Furthermore, the intensity of these contaminant peaks is emphasized by comparing with the very low signal obtained from peptides in our samples. Unfortunately, due to the precious nature of clinical samples, we were not able to repeat this experiment and we have therefore used results from these LC-MS/MS runs in our analyses.

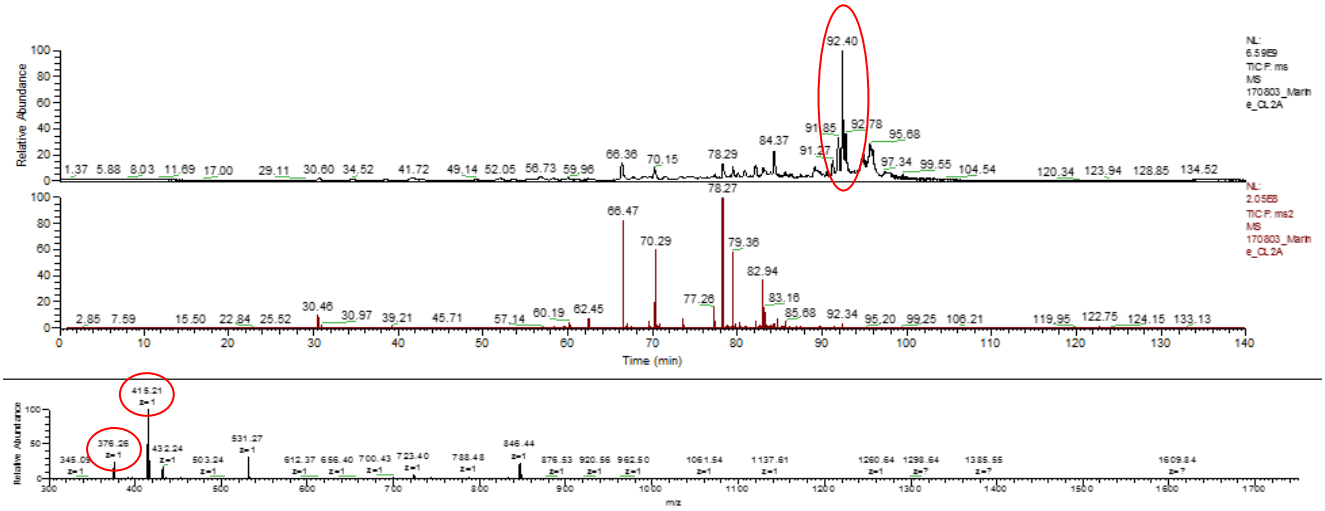

Figure 62. MS chromatogram (TIC) showing contaminant peaks at 92.4 min

Z = 1 ions observed at 92.40 min with molecular weights 376.26 and 415.21 Da are identified as PEG.

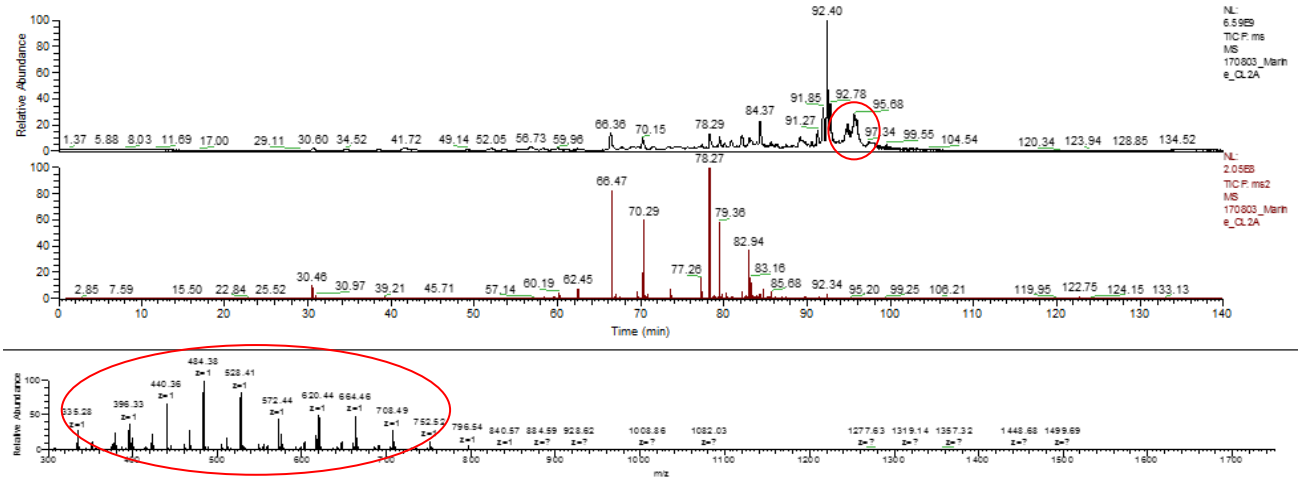

Figure 63. MS chromatogram (TIC) showing contaminant peaks at 95.7 min

Multiple transitions of 44 Da difference (z = 1) observed at 95.68 min are characteristic of PEG contamination.

Protein identification

As per Chapter 6, 'standard' MaxQuant search settings were used. The number of spectra submitted to MaxQuant was 655,769, of which 35,215 (5.37 %) were identified. There were 6,569 peptides identified, mapping to 1306 protein groups. Summarized results are presented in Table 18 below. There were more spectra submitted in this experiment than in the previous experiment (655,769 vs 607,484, Chapter 6). The number of peptides identified, however, was far lower (6,569 compared to 13,323 in the previous experiment), as was the number of protein groups (1306 vs 2083 previously, Chapter 6). The most notable difference in protein identification results is undoubtedly the significant decrease in percentage spectra identified (5.37% here compared to 16.67% previously). This decrease is most likely multi-factorial. Since the TIC were low, many MS2 spectra may have had missing peaks which could not be assigned. Furthermore, clinical samples are, by nature, heterogeneous and complex. Since the samples in this experiment were obtained from patients co-infected with HIV and TB, the degree of complexity is likely to increase when compared to samples from healthy volunteers who are not infected with either HIV or TB.

Table 18. Summary of results obtained from the peptide/protein identification search using MaxQuant standard settings.

Parameter	Result
Protein groups identified	1306
Protein groups identified with >2 unique peptides	937
Reverse hits	12
% contaminants	3.29
Peptides identified	6,569
Spectra submitted	655,769
% spectra identified	5.37
Modified peptides	400
% no missed cleavages	61,9

MaxQuant was unable to process samples CL5D (CL5, *Mtb* + PUFA) and CL6C (CL6, *Mtb* + vehicle), as the .raw files were of low quality (< 1 GB). These samples were therefore excluded from further analysis.

Digestion efficiency

Tryptic digestion efficiency was satisfactory (61.9% no missed cleavages) and highly comparable to the previous experiment (61.8%, Chapter 6). Results are shown in Figure 64 below.

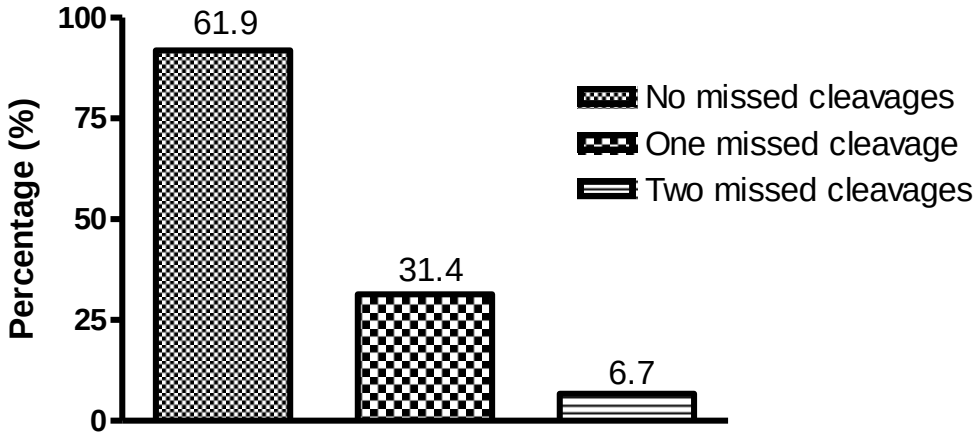

Figure 64. Tryptic digestion efficiency (missed cleavages)

Distribution of LFQ intensities and correlation between biological replicates

Protein groups were loaded to Perseus for further analysis. A total of 1306 protein groups were identified, of which 908 were left after excluding proteins only identified by site, reverse hits, potential contaminants, and proteins identified with fewer than two unique peptides. Of these, 230 were *Mtb* proteins and 678 were human proteins. Total LFQ values were then transformed by log2 and the distribution of the data was visualized through histograms (Figure 65). This data shows positive skewing to the right, and although we imputed missing values from the normal distribution, this indicates that this method may not be the most appropriate approach. To circumvent this problem, we focused primarily on qualitative analyses (presence/absence of proteins) to derive biological significance from this data.

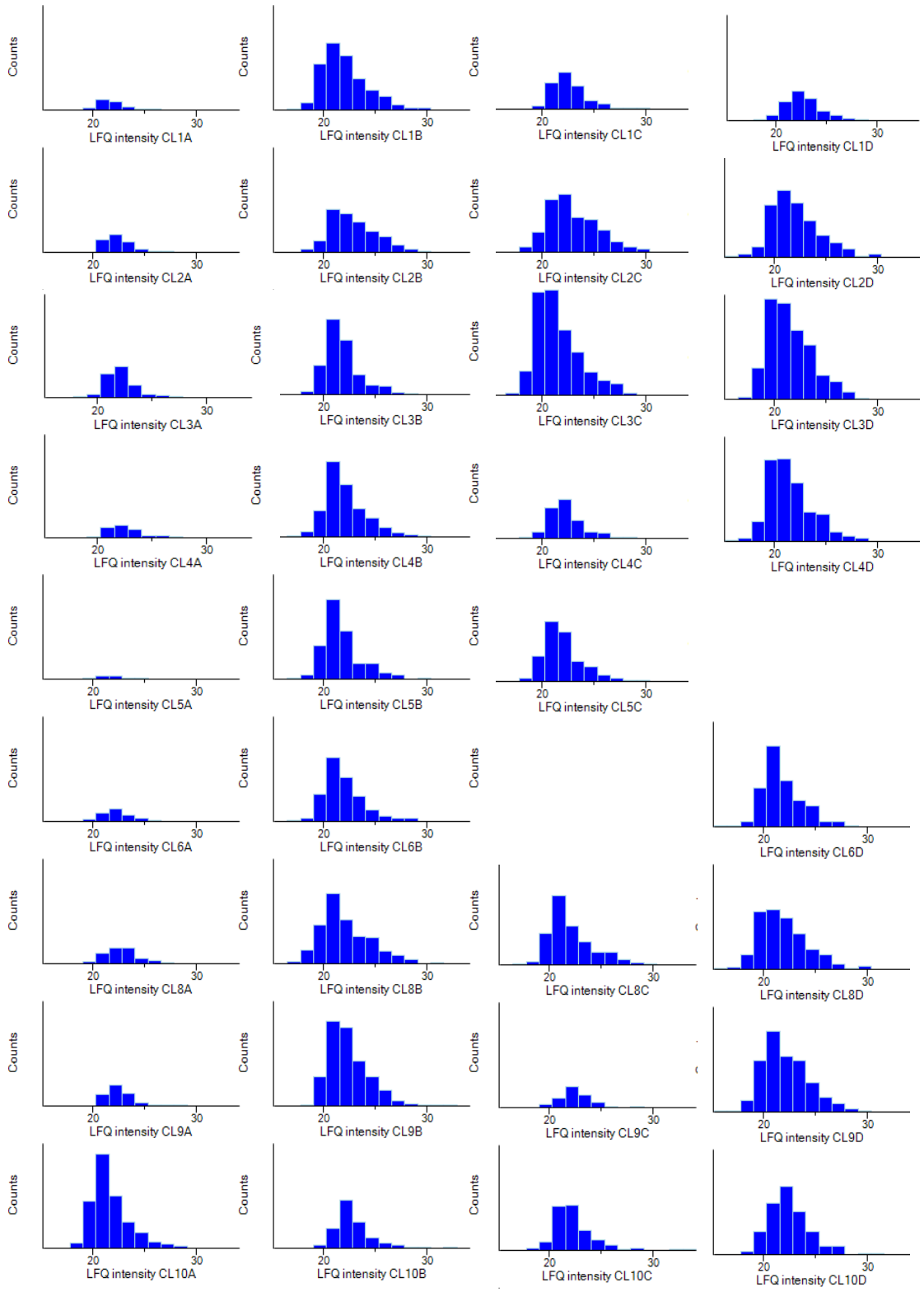

Figure 65. Distribution histograms of log2-transformed protein intensities

log2 LFQ values were plotted to assess data distribution. Left to right: control, *Mtb* only, *Mtb* + vehicle, and *Mtb* + PUFA samples. Top to bottom: CL1 to CL10 (CL6C and CL5D are excluded). Protein counts are lower in the control samples as these did not include any *Mtb* proteins.

Scatter plots and R^2 values (Pearson correlation) were generated for each set of biological replicates per condition. The correlation between samples from the non-IRIS groups for each treatment condition is shown in Figure 66 and that of samples from the IRIS group in shown in Figure 67. Overall, the correlation between biological replicates was not as strong as that between healthy volunteer replicates. In the non-IRIS group, control samples were most poorly correlated (Pearson correlation between 0.281 and 0.769, Figure 66) and *Mtb* + PUFA samples were most closely correlated (Pearson correlation between 0.584 and 0.702). The same trend was observed in the IRIS group (Figure 67) where Pearson correlation values for controls were between 0.129 and 0.700, and between 0.311 and 0.739 for n-3 PUFA-treated samples.

Poor correlation between biological replicates is most likely due to increased sample complexity, contributed by the patients' co-infection with HIV and TB. Furthermore, as can be seen in Table 17, patient characteristics related to disease and the immune system varied vastly (CD4+ count, viral load, and WCC). This suggests that PBMCs isolated from these patients may have very different responses to cryopreservation, *in vitro* culture, treatment with n-3 PUFA, and re-stimulation with *Mtb* WCL. These biological differences, which create 'noise', would be much less prominent if the sample size was greater. Repeating this experiment with a greater number of samples would therefore be beneficial to reducing noise and highlighting real differences arising from treatment rather than biological variation.

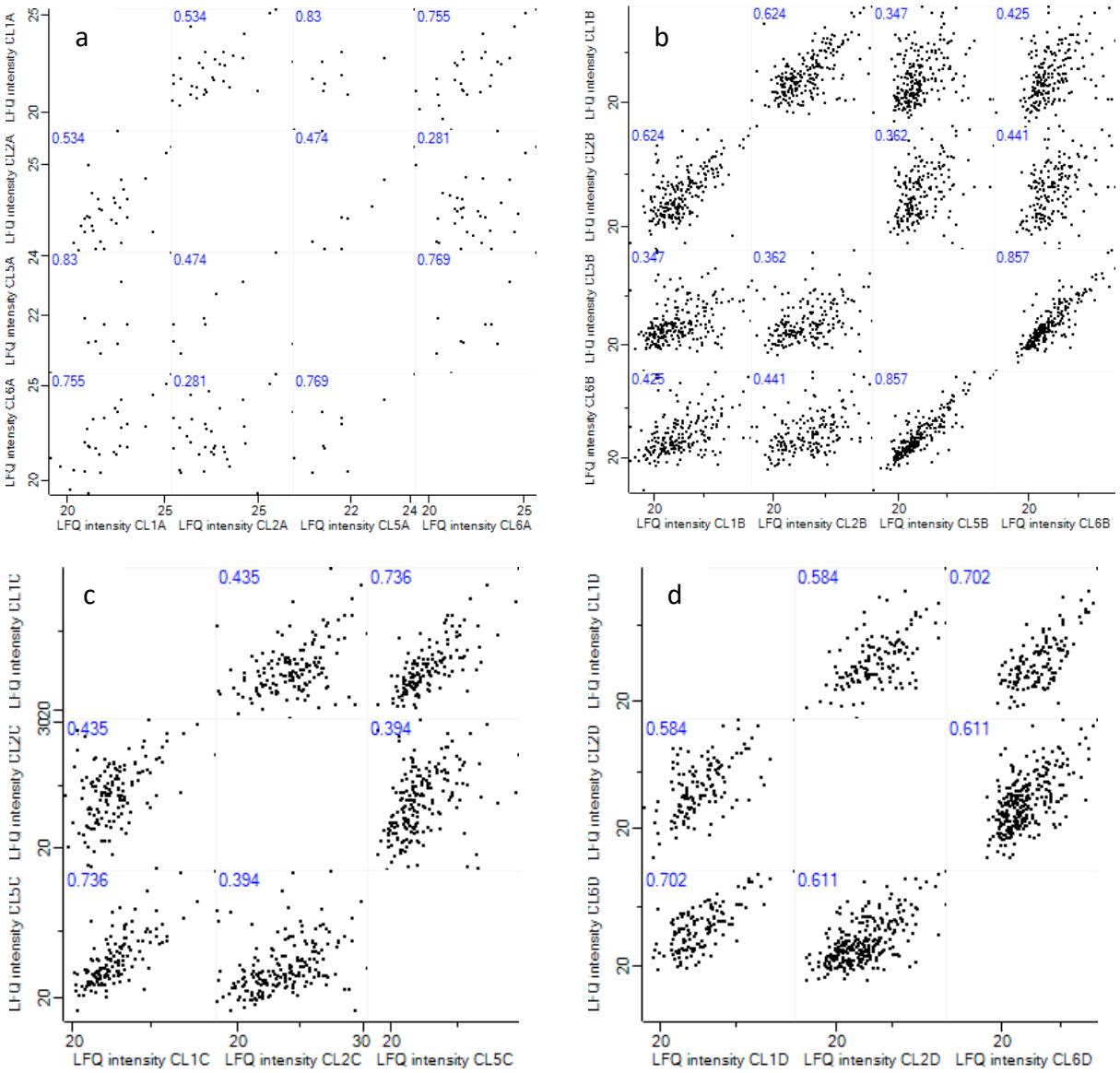

Figure 66. Scatter plots showing correlation between abundance of protein groups identified in control, *Mtb* only, *Mtb* + vehicle, and *Mtb* + PUFA biological replicates from the non-IRIS group

log2 LFQ values from each experimental sample were plotted against those from other experimental samples. Numeric values at the top of each graph indicate the Pearson correlation value for each comparison. a, controls; b, *Mtb* only samples; c, *Mtb* + vehicle; and d, *Mtb* + PUFA samples.

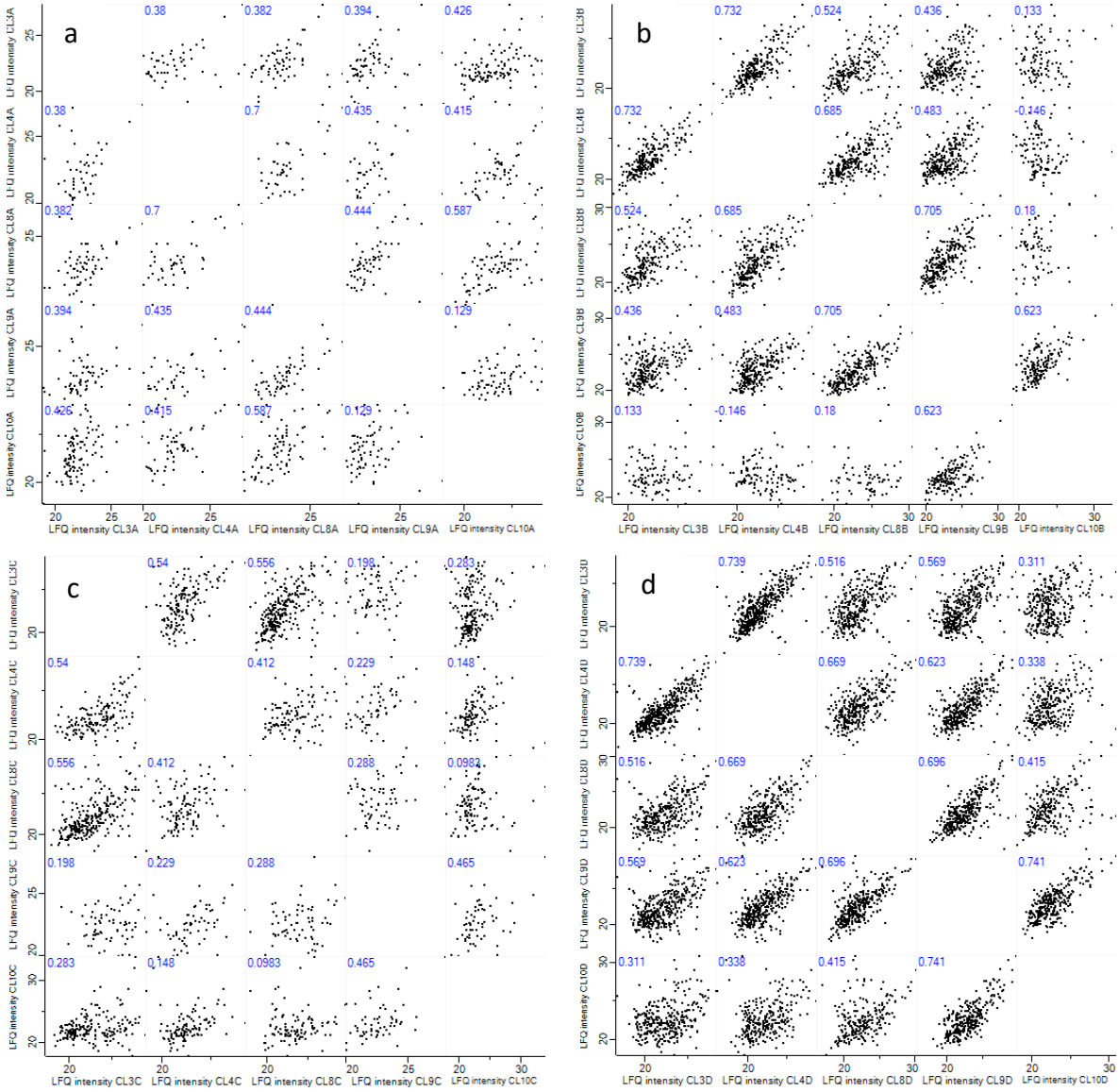

Figure 67. Scatter plots showing correlation between abundance of protein groups identified in control, *Mtb* only, *Mtb* + vehicle, and *Mtb* + PUFA biological replicates from the IRIS group

log2 LFQ values from each experimental sample were plotted against those from other experimental samples. Numeric values at the top of each graph indicate the Pearson correlation value for each comparison. a, controls; b, *Mtb* only samples; c, *Mtb* + vehicle; and d, *Mtb* + PUFA samples.

Hierarchical clustering

Hierarchical clustering revealed weak clustering of samples by treatment condition, in both the non-IRIS and IRIS group samples (Figure 68). In the non-IRIS group (Figure 68 a), control samples (A) clustered together (right, labelled CL1 to CL6A). However, samples from the other three conditions did not cluster separately from each other. The proteins highlighted in orange box 1 seem to be over-expressed in all conditions re-stimulated with *Mtb* WCL, but not in control samples. These proteins may therefore be specific to the cells' response to *Mtb* challenge. Orange box 2 highlights proteins over-expressed specifically in samples *Mtb* only (B), *Mtb* + vehicle (C), and *Mtb* + PUFA samples (D) from CL1 and CL2. In addition, these four samples clustered separately from all others. It was observed that CL1 and CL2 had the lowest baseline CD4+ cell counts with 5 and 4 cells/mm^3, respectively, whereas the mean was 71.4 cell/mm^3. This low CD4+ cell count may affect the cellular response to *ex vivo* re-stimulation with *Mtb* WCL and lead to the slightly different protein expression pattern observed here. Furthermore, orange box 3 shows increased protein expression unique to samples CL1B and CL2D.

In the IRIS group (Figure 68 a), controls (A) also clustered together on the right, with the exception of CL10. Surprisingly, sample CL4C (*Mtb* + vehicle) also clustered with the controls. Orange box 4 defines protein expression that in increased in all samples re-stimulated with *Mtb* WCL, and box 5 highlights over-expression specific to certain samples (*Mtb* only, *Mtb* + vehicle, and *Mtb* + PUFA). These differential responses may be sample-specific and patient-related, as there is no indication in the metadata available to us of what may cause such differences in protein expression and clustering.

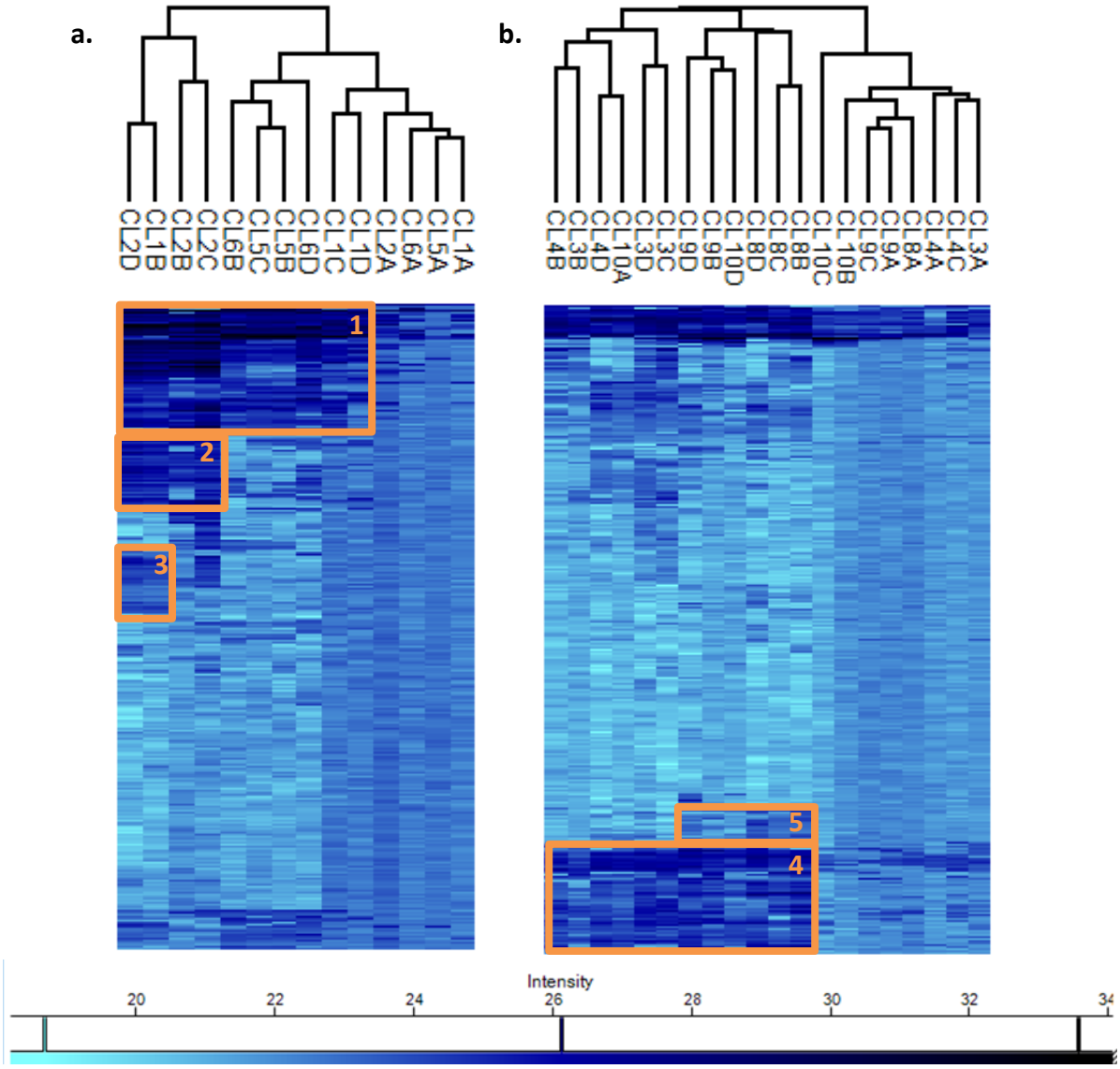

Figure 68. Hierarchical clustering analysis of human protein expression profiles for non-IRIS and IRIS group samples, using log_2 LFQ values

a. Non-IRIS group, b. IRIS group. Treatment condition codes: A, control; B, *Mtb* only; C, *Mtb* + vehicle; D, *Mtb* + PUFA.

Principal component analysis

A principal component analysis (PCA) was performed to further investigate clustering. In non-IRIS samples (Figure 69), control samples (yellow) clustered together and away from all other samples re-stimulated with *Mtb* (ellipse 1). This is consistent with a predominantly coordinated response to *Mtb* antigens, as is expected from non-IRIS patient-derived PBMCs. There was no obvious clustering observed in samples from the other three conditions, even when principal components other than PC1 and PC3 were considered. However, certain samples from the same individual seemed to cluster

more closely thus creating three subsets: CL1C and CL1D (ellipse 2); CL2B, CL2C, CL2D, and CL1C (ellipse 3); as well as CL5C, CL6B, and CL6D (ellipse 4).

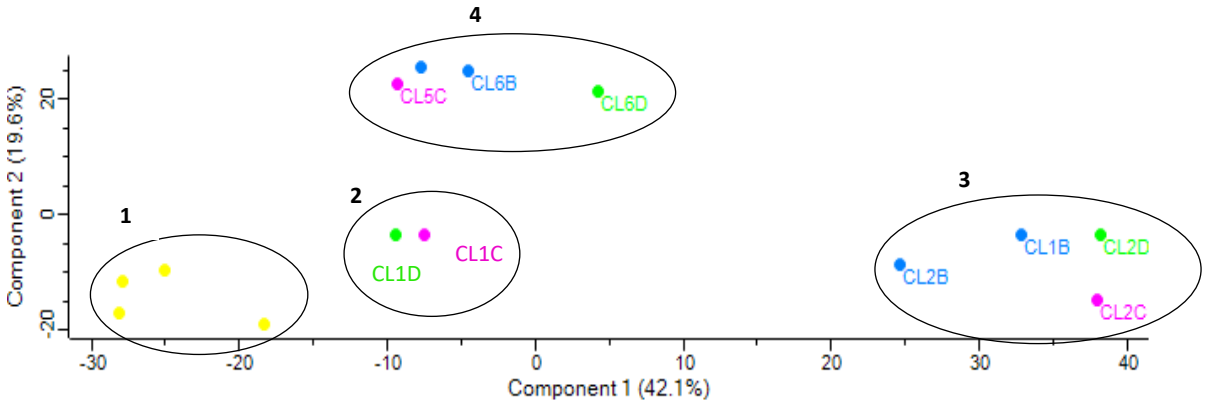

Figure 69. Principal component analysis of protein expression profiles for non-IRIS group samples

Yellow, control samples; blue, *Mtb* only samples; magenta, *Mtb* + vehicle samples; and green, *Mtb* + PUFA samples. Principal components 1 and 2 are represented on the x- and y-axis, respectively, and account for 42.1 and 19.6% of the total variance, respectively.

Clustering was far less defined in the IRIS group (Figure 70). Four of the five controls clustered together with the exception of CL10. CL9B, CL9C, CL4C, and CL10C also clustered with the control samples (ellipse 1). There was no clear clustering in the other samples, suggesting a high degree of patient-related variability in cellular response to re-stimulation with *Mtb* WCL and treatment with the vehicle or n-3 PUFA. We also investigated plots obtained when comparing other principal components, but clustering did not improve. This is consistent with previous proteomic data that suggests that PBMCs derived from patients with TB-IRIS lack coordinated responses to *Mtb* antigens.[166]

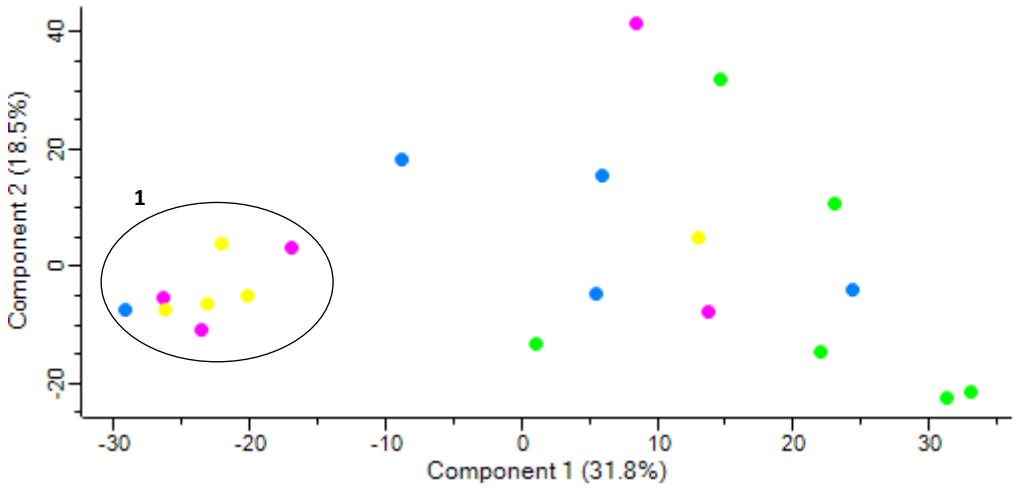

Figure 70. Principal component analysis of protein expression profiles for IRIS groups samples

Yellow, control samples; blue, *Mtb* only samples; magenta, *Mtb* + vehicle samples; and green, *Mtb* + PUFA samples. Principal components 1 and 2 are represented on the x- and y-axis, respectively, and account for 31.8 and 18.5% of the total variance, respectively.

Finally, we compared all samples across both the non-IRIS and IRIS groups to assess whether samples from these two patient groups clustered separately (Figure 71), but found that these two groups of samples did not cluster away from each other. This is most likely due to the inherent biological variability in the data, poor quality of MS data, and small sample size.

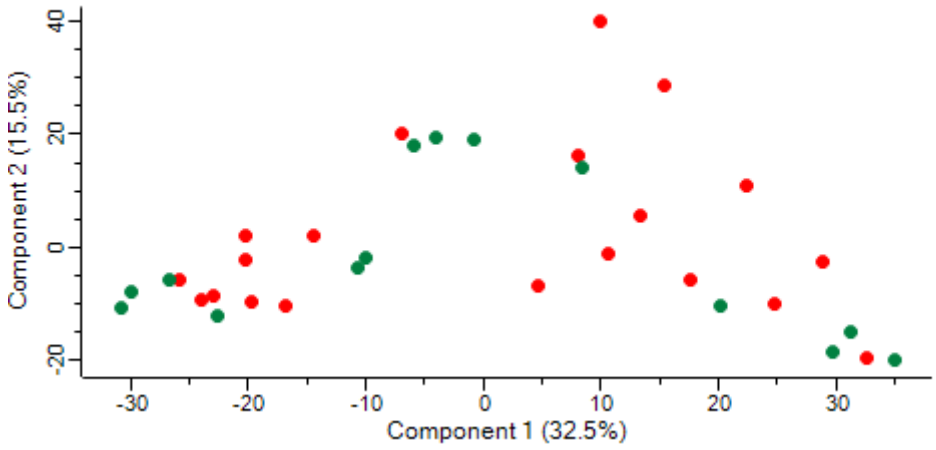

Figure 71. Principal component analysis of protein expression profiles for both non-IRIS and IRIS groups samples

Green, non-IRIS group samples; red, IRIS group samples. Principal components 1 and 2 are represented on the x- and y-axis, respectively, and account for 32.5 and 15.5% of the total variance, respectively.

Cellular component GO analysis

To confirm that we had successfully isolated the PBMC secretome, the 678 human proteins identified across all samples and conditions were added to STRING, thus creating a network of 678 nodes and 10,008 edges. The top four enriched GO terms for cellular component revealed that approximately 67% of proteins identified were extracellular (Table 9), with very small false discovery rates.

Table 19.Top four enriched cellular component GO terms

GO term ID	GO term description	Count in gene set	False discovery rate
GO:0070062	extracellular exosome	438	1.35e-223
GO:0031988	membrane-bounded vesicle	452	1.7e-199
GO:0031982	vesicle	453	7.21e-195
GO:0044421	extracellular region part	453	3.9e-188

7.3 Conclusions

The current chapter aimed to present and assess patient characteristics, cell culture data, quality of MS chromatograms and protein identification, and sample clustering. Protein identifications were lower than those of the previous experiment involving healthy volunteer cells (Chapter 6), as was the percentage of spectra identified. We expect that protein quantitation via Bradford assay may be resulting in over-estimation of the protein concentration, with downstream effects on data generated via MS analysis. Going forward in future experiments, use of a more sensitive protein quantitation method should be considered. Similarly, correlation of protein identification between the biological replicates was weaker than that observed in the previous experiment. Furthermore, PCA and hierarchical clustering was also weak. This may be due to the fact that the samples are derived from TB/HIV-infected individuals, who may present significant differences in their response to the disease as well as disease status and progression. Because of the high degree of variability in this dataset, and the non-normal distribution of protein expression, biological analyses must rely primarily on qualitative observations such as the presence and absence of proteins from certain datasets. This is further explored in Chapter 8.

Chapter 8

Secretome analysis of TB-IRIS patient-derived PBMCs: Part II

8.1 Aim

This chapter follows on from Chapter 7, with the aim of investigating the PBMC secretome of PBMCs derived from TB- and HIV-infected patients who developed TB-IRIS, and compare it to that of PBMCs from patients co-infected with *Mtb* and HIV but who did not go on to develop TB-IRIS. The current chapter investigates the biological significance of the data generated in Chapter 7.

8.2 Biological results

8.2.1 Shared and unique protein groups identified

We performed a presence/absence analysis on the data to investigate shared and unique protein groups identified. This analysis was done using data without imputed values, and a protein was considered 'absent' from a specific treatment condition if it had an LFQ intensity value of zero in all samples for that particular condition. Of the 488 quantifiable proteins identified in the non-IRIS group, 83 (17%) were common to all four conditions (Figure 72). There were 23 proteins unique to the *Mtb* only samples, 25 to the *Mtb* + vehicle controls, and 35 to the *Mtb* + PUFA samples. Interestingly, there were 235 proteins (48.2%) common to the *Mtb* only, *Mtb* + vehicle, and *Mtb* + PUFA sample groups, and this is consistent with the PCA plots in Chapter 7. This suggests that these proteins may be part of the response to re-stimulation with *Mtb* WCL as these three sample groups were cultured with *Mtb* WCL whereas the controls were not. This therefore confirms that re-stimulation with Mtb WCL elicited the expected immune response. From this analysis, we can tell that controls from this non-IRIS group had markedly different protein expression profiles that *Mtb* only, *Mtb* + vehicle, and *Mtb* + PUFA samples. This trend was not observed in healthy donor PBMCs and may therefore be specific to PBMCs isolated from HIV- and TB-infected patients, consistent with the healthy donor PBMCs being *Mtb*-naïve.

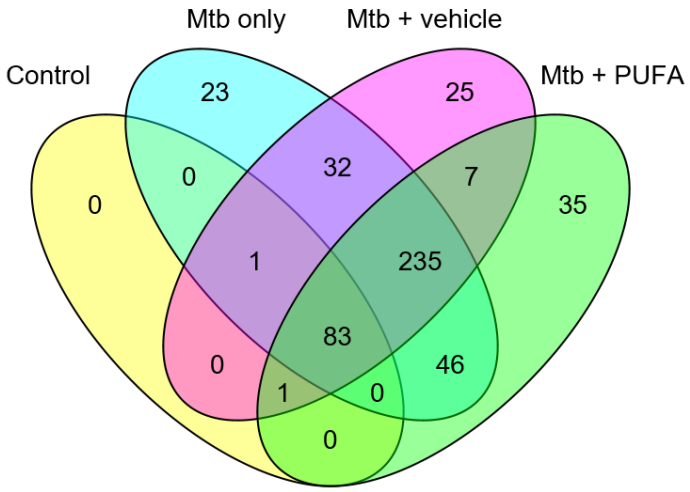

Figure 72. Shared and unique proteins identified in control, *Mtb* only, Mtb + vehicle, and Mtb + PUFA samples in the non-IRIS group

In the IRIS group, 657 proteins identified were quantifiable, of which 289 (43.9%) were common to all conditions (Figure 73. Shared and unique proteins identified in control, *Mtb* only, *Mtb* + vehicle, and *Mtb* + PUFA samples in the IRIS group). There were two proteins unique to the controls, 15 to the *Mtb* only samples, 29 to *Mtb* + vehicle, and 103 to *Mtb* + PUFA samples. In this group, most proteins were common to all four treatment conditions.

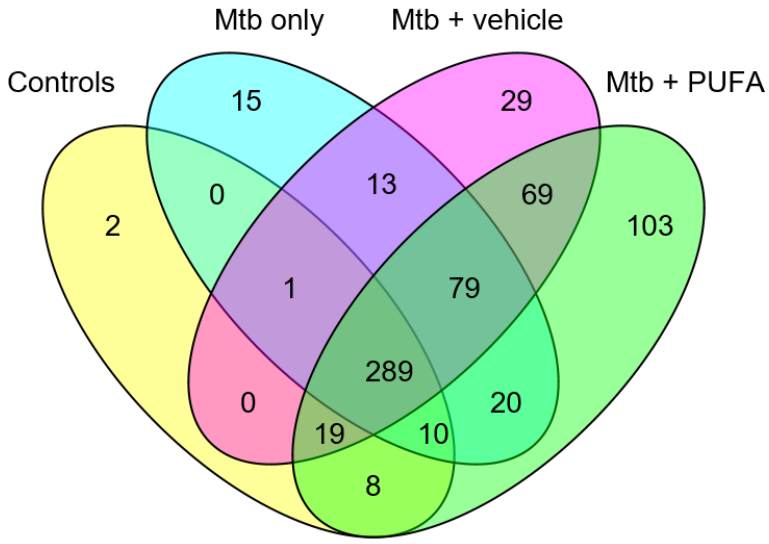

Figure 73. Shared and unique proteins identified in control, *Mtb* only, *Mtb* + vehicle, and *Mtb* + PUFA samples in the IRIS group

8.2.2 Comparing non-IRIS and IRIS sample groups

Controls

We also investigated proteins quantifiable in each condition and compared those identified in the non-IRIS group with those of the IRIS group. With regards to controls, a total of 330 proteins were quantifiable, of which 245 were quantified only in the samples from the IRIS group, and 1 in samples from the non-IRIS group (Figure 74). This important difference in proteins identified suggests that PBMCs from patients with IRIS secrete more proteins than their counterparts from non-IRIS patients. This is to be expected, since patients with TB-IRIS experience increased inflammation even at baseline, and thus produce more proteins as part of the immune response.

To further investigate this, we loaded the list of 245 proteins quantifiable only in IRIS samples to STRING. A network comprising 238 nodes and 1,197 edges was produced. The top four enriched GO terms for biological process and listed in Table 20. These terms relate to the negative regulation of apoptosis, as well as the immune response and response to stress. These results therefore suggest the increased activation of the immune system and stress response in PBMCs from the IRIS group, even at baseline (i.e., before re-stimulation with *Mtb* WCL or other treatment), rather than an increase in cell death. Most notably, IL-1β was quantified only in IRIS samples. This potent pro-inflammatory cytokine has been linked to aberrant inflammation in TB-IRIS before,[50] and it is interesting to see that it was not quantified in the non-IRIS group, suggesting that IL-1β was probably present in the non-IRIS group but at a level below the limit of detection/quantitation of the instrument. This result correlates well with the study conducted by Tadokera *et al.*,[50] which investigated cytokine levels in PBMC culture supernatants using Luminex. Levels of IL-1β were significantly greater in samples from IRIS patients ($p < 0.0001$, n = 20 IRIS patients, and 19 non-IRIS controls).

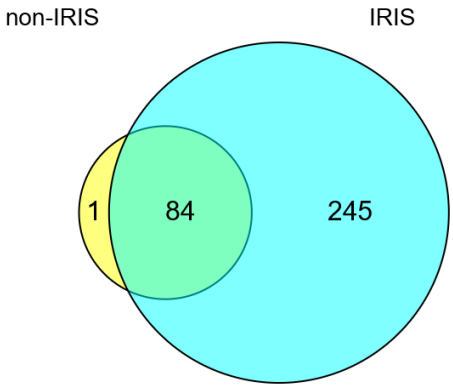

Figure 74. Proteins quantifiable in control samples from the non-IRIS and IRIS groups

Table 20. Top four enriched GO terms for biological process in proteins only quantifiable in control samples from the IRIS group

GO pathway ID	Description	Gene	False discovery
GO:0043066	negative regulation of apoptotic process	42	8.34e-14
GO:0060548	negative regulation of cell death	43	1.33e-13
GO:0002684	positive regulation of immune system process	38	1.6e-11
GO:0006950	response to stress	82	1.6e-11

Next, we performed a PCA using only control samples from both the non-IRIS and IRIS groups (Figure 75). The two groups clustered separately from one another, suggesting differences in PBMC status at baseline, as these samples were not yet perturbed with any stimulus. It must be noted that this may be partially driven by the fact that 245 out 350 proteins were quantified only in IRIS group samples. However, this result also correlates with the literature and findings that several markers appear to be dysregulated at baseline and two weeks after ART initiation in patients who go on to develop TB-IRIS. This includes differences in the number and distribution of killer immunoglobulin receptors,[167] increased plasma IL-6, IL-12, CRP, IL-18, IL-1β, TNF-α, and IL-8 levels,[43,50,168] increased CSF cytokine, chemokine, and MMP levels,[169] increased and imbalanced C1q and C1-INH levels,[152] increased NK cell degranulation capacity,[170] and increased TLR2 levels.[171] Therefore, the differences in protein expression observed here between the non-IRIS and IRIS groups may result from such changes. The outlier to the right, CL10, has the highest viral load (1,597,770 copies/mL, mean = 491,990.90 copies/mL) and the lowest BMI (15.89, mean = 22.66). These factors may contribute to the different protein expression profile observed here.

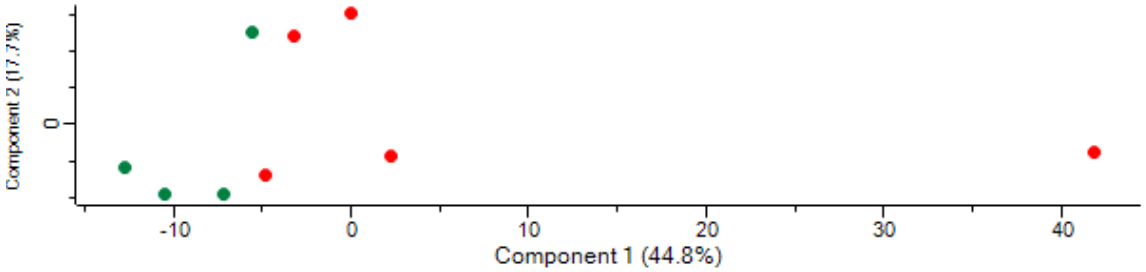

Figure 75. Principal component analysis of protein expression profiles for control samples from both the non-IRIS and IRIS groups

Green, non-IRIS group samples; red, IRIS groups samples.

Finally, we performed Student's t-tests to identify differential protein expression amongst the 84 proteins shared between the non-IRIS and IRIS groups, but no proteins were considered significantly differentially expressed.

Mtb only samples

The same comparison was made for *Mtb* only samples. Of the 472 proteins quantified, 375 were common to both groups (Figure 76). There were 45 proteins unique to non-IRIS, but there was no enriched network formed when this list was loaded to STRING. The 52 proteins unique to the IRIS group formed a network comprising 52 nodes and 69 edges with two enriched GO terms for biological process, although the false discovery rates were relatively high for these terms (Table 21). The term "viral process" is particularly relevant here, as these samples were obtained from HIV-positive patients. In addition, two pro-inflammatory mediators and key players in the immune response were identified only in IRIS samples and these are listed in Table 21 below.

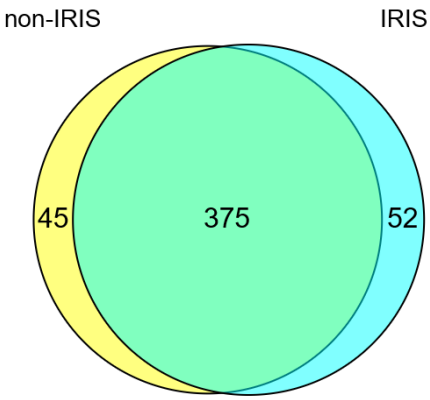

Figure 76. Proteins quantifiable in Mtb only samples from the non-IRIS and IRIS groups

Table 21. Top four enriched GO terms for biological process in proteins only quantifiable in Mtb only samples from the IRIS group

GO pathway ID	Description	Gene count	False discovery
GO:0044403	symbiosis, encompassing mutualism through parasitism	11	1.65e-2
GO:0016032	viral process	10	2.53e-2

IL-16 is an important cytokine known to promote migration of CD4+ lymphocytes, monocytes, and eosinophils, as well as stimulate IL-2 receptor and HLA-DR4 expression in T cells. In addition, it enhances CD4+ T cell responses to IL-2 and IL-15, and can suppress HIV transcription. Since PBMCs were isolated from HIV-positive patients, it is not unexpected to see IL-16. However, identification of IL-16 only in IRIS samples suggests that it is present at a higher level than in non-IRIS samples where levels may fall below the limit of detection/quantitation.

IL-6 is another cytokine that was quantifiable only in *Mtb* only samples from the IRIS group. Similarly to IL-1β, secretion of IL-6 was shown to be up-regulated in cell culture supernatants ($p < 0.0001$, n = 20 non-IRIS controls and 19 IRIS patients) and in TB-IRIS patient sera ($p = 0.0002$, n = 20 non-IRIS controls and 20 IRIS patients).[50] Furthermore, in the same study, Tadokera *et al*.[50] investigated the induction of genes in patient-derived PBMCs cultured in the presence/absence of heat-killed *Mtb* H37Rv after 6 and 24 h. At the 6-h time-point, *IL-6* was induced >100-fold in *Mtb*-stimulated samples, and induction was greater in IRIS patient samples, with p-value < 0.05 after Bonferroni multiple testing

correction (MTC). Similar results were obtained at the 24 h time-point. Our proteomic results therefore correlate well with the gene expression work done by Tadokera *et al*.

Table 22. Key pro-inflammatory proteins quantified only in *Mtb* only samples from the IRIS group

Protein ID	Gene	Protein name	Role
Q14005	IL-16	Interleukin 16	stimulates a migratory response in leucocytes, induces IL-2 receptor expression in T cells
P05231	IL-6	Interleukin 6	induces acute phase response, response to gram-negative/-positive bacteria

We also performed a PCA to investigate clustering of non-IRIS and IRIS samples re-stimulated with *Mtb* WCL (Figure 77). There was no clear clustering observed, and IRIS group samples seem to be more variably distributed across the plot, whereas non-IRIS samples formed two distinct groupings. Other principal components were investigated but did not lead to more distinct clustering.

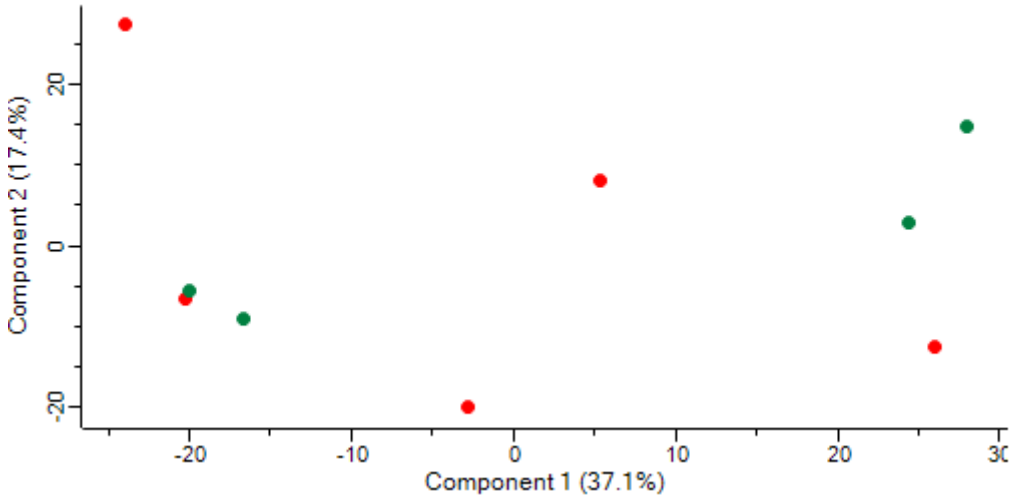

Figure 77. Principal component analysis of protein expression profiles for *Mtb* only samples from both the non-IRIS and IRIS groups

Green, non-IRIS groups samples; red, IRIS group samples.

As with control samples, no proteins were found to be significantly differentially expressed here.

Mtb + vehicle samples

When comparing vehicle control samples from the non-IRIS and IRIS group, we found 546 quantifiable proteins, 337 of which were common to both groups (Figure 78). Again, there were more proteins unique to the IRIS group than the non-IRIS group (162 vs 47, respectively). The 47 proteins unique to non-IRIS samples formed an enriched network with 35 edges in STRING. The top four enriched GO terms for biological process indicate the effect of the vehicle (0.2% ethanol) on processes such as fatty acid β oxidation, and regulation of homeostasis particularly with regards to body fluids. Ethanol is known to have an inhibitory effect on fatty acid oxidation and stimulate hepatic fatty acid synthesis.[172,173]

The 162 proteins quantified only in IRIS vehicle controls formed a STRING network with 641 edges, with the following enriched GO terms for biological process: mRNA metabolic process (GO:0016071), RNA splicing (GO:0008380), and mRNA processing (GO:0006397). It is unclear why these terms are enriched in the set of proteins quantified only in IRIS samples as these are considered part of the cell's 'house-keeping'. As with *Mtb* only sample, IL-16 was quantified only in samples from the IRIS group.

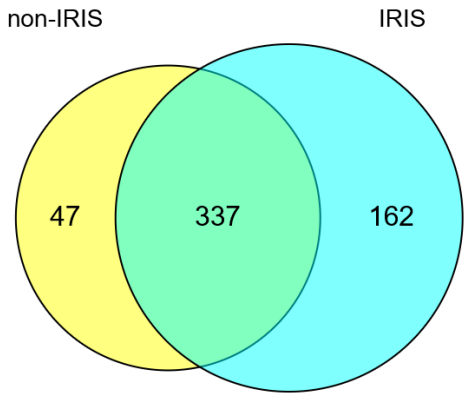

Figure 78. Proteins quantifiable in *Mtb* + vehicle samples from the non-IRIS and IRIS groups

The PCA did not reveal any significant clustering, as shown in Figure 79 below.

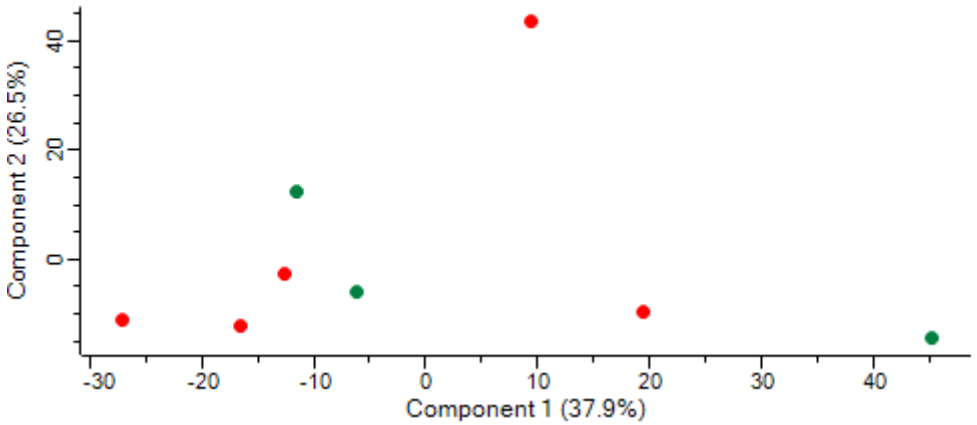

Figure 79. Principal component analysis of protein expression profiles for *Mtb* + vehicle samples from both the non-IRIS and IRIS groups

Green, non-IRIS groups samples; red, IRIS groups samples.

After performing Student's t-tests, we found no proteins significantly differentially expressed.

Mtb + PUFA samples

Of the 606 quantifiable proteins identified in *Mtb* + PUFA samples, 398 were common to the non-IRIS and IRIS groups. The nine proteins unique to the non-IRIS group did not form an enriched STRING network. Interestingly, IL-1α (present at 0.537 ppm) was quantified in non-IRIS samples. This cytokine is produced by activated macrophages and is associated with the inflammatory response. We uploaded the 199 proteins quantified uniquely in samples from the IRIS group, and produced a network with 911 edges. As in vehicle controls, the top four enriched GO terms for biological process were mRNA splicing (GO:0000398), RNA splicing (GO:0008380), and mRNA processing (GO:0006397).

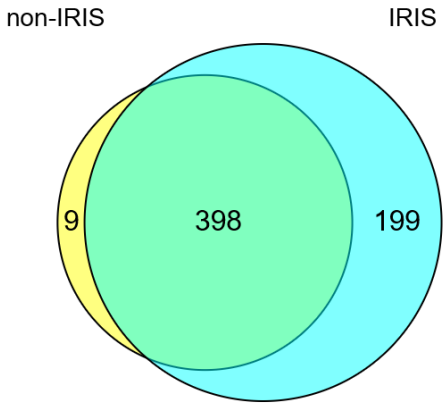

Figure 80. Proteins quantifiable in *Mtb* + PUFA samples from the non-IRIS and IRIS groups

Finally, the PCA did not reveal any clustering of non-IRIS and IRIS groups samples, as can be seen in Figure 81.

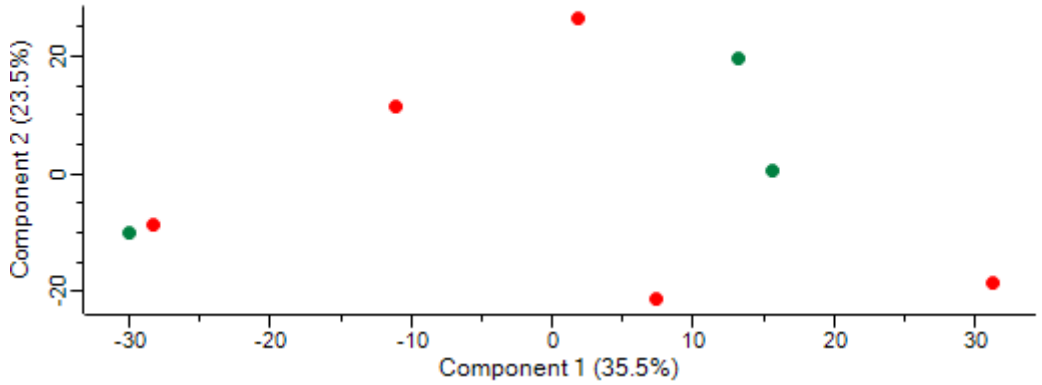

Figure 81. Principal component analysis of protein expression profiles for Mtb + PUFA samples from both the non-IRIS and IRIS groups

Green, non-IRIS group samples; red, IRIS groups samples.

Finally, as with other treatment conditions, no proteins were found to be significantly differentially expressed here, after MTC.

8.2.3 Comparing treatment conditions

Controls vs *Mtb* only samples

To investigate the effects of re-stimulating patient-derived PBMCs with *Mtb* WCL, we compared the proteins identified in control and *Mtb* only samples, for each patient group. A Venn diagram showing the overlap of proteins identified in control an *Mtb* only samples from the non-IRIS group is shown in Figure 82 below. There were 336 proteins quantifiable only in *Mtb* only samples, suggesting that re-stimulation with *Mtb* WCL may be promoting increased expression of proteins as part of the immune response. This follows the trend observed in healthy donor samples.

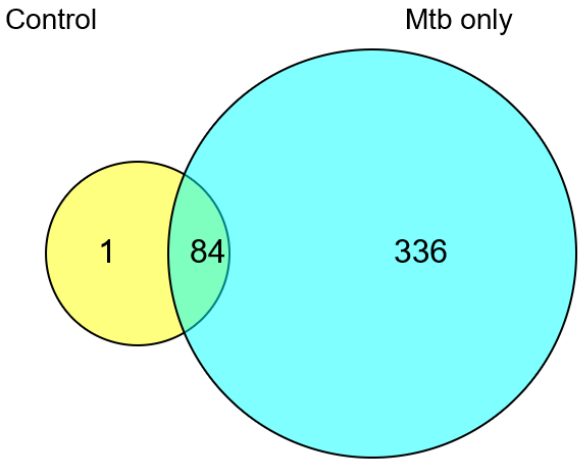

Figure 82. Proteins identified in control and *Mtb* only samples from the non-IRIS group

The 84 (19.95%) proteins common to both conditions comprised 15 histone proteins and were associated with histone H4-K20 demethylation (GO:0035574) and RNA binding (GO:0003723). The presence of histone proteins may indicate cell death occurring during culture, but as these proteins were common to both control and *Mtb* only samples, it is likely that this is regular cell death associated with *in vitro* culturing rather than directly related to re-stimulation with *Mtb* WCL.

The 336 proteins unique to *Mtb* only samples were associated with the four GO terms listed in Table 23. These terms confirmed the activation of the immune response by in vitro re-stimulation, and this was further supported by enriched KEGG pathways also listed in Table 23. IL-1α and IL-1β were also quantified only in *Mtb* only samples.

Table 23. Enriched GO terms for biological process and KEGG pathways in proteins only quantifiable in *Mtb* only samples from the non-IRIS group

GO pathway ID	Description	Gene	False discovery
	Biological process		
GO:0006950	response to stress	121	2.8e-18
GO:0002684	positive regulation of immune system process	55	3.32e-17
GO:0065008	regulation of biological quality	109	3.92e-17
GO:0002376	immune system process	84	6.72e-16
	KEGG pathways		
05130	Pathogenic Escherichia coli infection	11	5.22e-08
05100	Bacterial invasion of epithelial cells	12	1.11e-07

We performed Student's t tests to compare protein expression in control and Mtb only samples from the non-IRIS group. When Benjamini-Hochberg multiple testing correction (MTC) was applied, no proteins were considered significantly differentially expressed, but when the permutation-based FDR MTC method was used, the expression of two proteins was considered significantly different (Table 24).

Table 24. Differentially expressed proteins in *Mtb* only and control samples from the non-IRIS group

Protein ID	Gene	Protein name	Role	P-value	Fold-change*
P07237	P4HB	Protein disulfide-isomerase	redox homeostasis, response to oxidative stress, IL-12 signaling pathway[174]	2.64e-4	-3.52
Q9UI08	EVL	Ena/VASP-like protein	cytoskeletal remodeling, cell migration[175]	5.09e-4	+1.49

*Direction of fold-change: *Mtb* only/control samples.

When the same comparison is made with samples from the IRIS group, we notice that many more proteins are common to both conditions (300 proteins, 57%, Figure 83). We hypothesize that this may be caused by the overly active immune response seen in IRIS patients, even before re-stimulation. To validate this hypothesis, we further investigated the 300 proteins common to both conditions and the proteins unique to each condition in STRING. The GO terms most enriched in proteins common to both conditions are listed in Table 25 and include response to stress and regulation of apoptosis.

These terms describe a generalized cellular response to stimulus and suggest that PBMCs isolated from IRIS patients may be subject to differentially regulated apoptotic pathways when exposed to re-stimulation of the immune response, as GO terms relating to regulation of apoptosis were not enriched in non-IRIS samples.

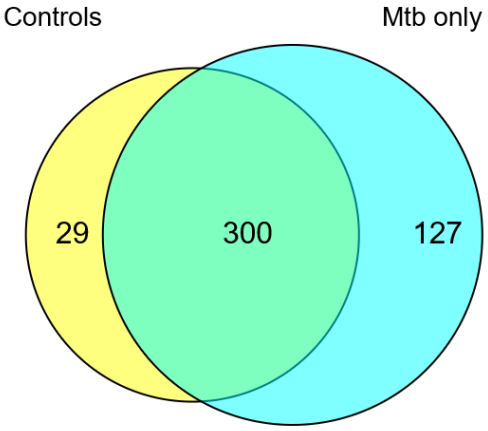

Figure 83. Proteins identified in control and *Mtb* only samples from the IRIS group

Table 25. Enriched GO terms for biological process in proteins common to both control and *Mtb* only samples from the IRIS group

GO pathway ID	Description	Gene count	False discovery rate
GO:0065008	regulation of biological quality	124	1.27e-28
GO:0006950	response to stress	123	8.29e-23
GO:0010941	regulation of cell death	79	8.29e-23
GO:0042981	regulation of apoptotic process	74	3.61e-21

The 29 proteins unique to the control samples were analyzed using STRING, but did not form an enriched network and were therefore not investigated further.

Finally, the 127 proteins unique to *Mtb* only samples produced a highly enriched STRING network, with enriched GO terms such as “symbiosis, encompassing mutualism through parasitism” (GO:0044403). In a previous analysis, this term was enriched in IRIS samples when comparing *Mtb* only samples from the non-IRIS and IRIS group. It is therefore a term that appears to be specific to the

IRIS samples after re-stimulation of the immune response. Notable proteins present in these samples are listed in Table 26. V-type proton ATPase subunit B (ATP6V1B2) and Ras-related protein Rab-7a (Rab7A) are both important in the maturation and acidification of the phagosome, as well as the fusion of the phagosome and lysosome. Rab7a appears to be particularly important in the context of *Mtb* infection, as *Mtb* is known to arrest phagosome/lysosome fusion at the stage at which Rab7 would normally be recruited. Seto *et al.*[176] demonstrated that Rab7 is transiently recruited and removed from phagosomes containing *Mtb.* When Rab7 is released from this complex, recruitment of other factors such as cathepsin D and RILF is inhibited, thereby arresting phagolysosome fusion. It is therefore proposed that *Mtb* dysregulates the activity of certain Rab GTPases, thereby disrupting phagosome maturation, and enabling intracellular survival.

Table 26. Key proteins unique to *Mtb* only samples from the IRIS group

Protein ID	Gene	Protein name	Role
P21281	ATP6V1B2	V-type proton ATPase subunit B,	Phagosome acidification
P51149	RAB7A	Ras-related protein Rab-7a	Phagosome maturation and acidification, phagosome/lysosome fusion

We performed t-tests to compare protein expression between the *Mtb*-stimulated and control samples but no proteins were considered significantly differentially expressed after MTC.

Mtb + vehicle vs *Mtb* + PUFA samples

Non-IRIS group

Next, we investigated the effects of pre-treating PBMCs with n-3 PUFA before re-stimulating with *Mtb* WCL by comparing protein expression from *Mtb* + vehicle and *Mtb* + PUFA samples using a Venn diagram (Figure 84). Of the 465 proteins quantified across *Mtb* + vehicle and *Mtb* + PUFA samples, 326 (70.11%) were common to both conditions, 58 were unique to *Mtb* + vehicle samples, and 81 were unique to *Mtb* + PUFA samples. From this analysis, we expected to see a greater number of proteins associated with inflammation expressed in the *Mtb* + vehicle samples, and more proteins associated with resolution of inflammation in the *Mtb* + PUFA samples.

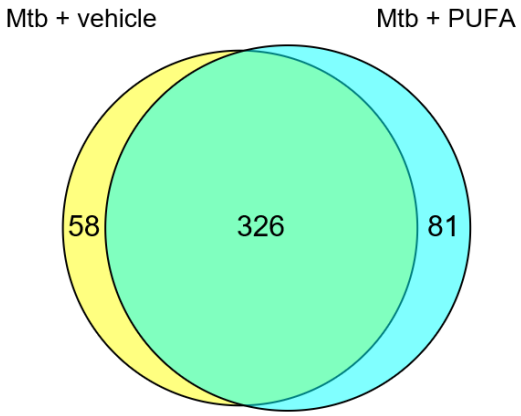

Figure 84. Proteins identified in *Mtb* + vehicle and *Mtb* + PUFA samples from the non-IRIS group

Mtb + vehicle (non-IRIS group)

To verify this hypothesis, we analyzed the 58 proteins quantified only in *Mtb* + vehicle samples using STRING. A network of 58 nodes and 78 edges was formed with several enriched GO terms, as listed in Table 13. The two enriched KEGG pathway terms relate to the inflammatory response to bacterial infection, and include several key pro-inflammatory mediators. In this dataset, we identified IL-6, ARPC3 and ARPC5, CDC42, and ASC. ASC, or apoptosis-associated speck-like protein containing a CARD (also referred to as PYCARD, Q9ULZ3), a key mediator of apoptosis and inflammation, is an adapter protein involved in the macromolecular formation of the NLRP3 inflammasome, along with pro-caspase 1. Caspase 1 then drives the production of IL-1β and IL-18.[177] The fact that ASC was only quantified in *Mtb* + vehicle samples and not *Mtb* + PUFA samples implies that its expression in *Mtb*-stimulated PBMCs was lowered by PUFA pre-treatment. This observation is supported by the recent study by Sui *et al.* who demonstrated that DHA could inhibit NLRP3 inflammasome expression in hepatocytes by inhibiting NF-κB activity. Another study published similar results, reporting EPA and DHA's ability to inhibit caspase 1 and IL-1β through inhibition of NLRP3 and interaction with GPR40 and protein-β-arrestin-2.[178]

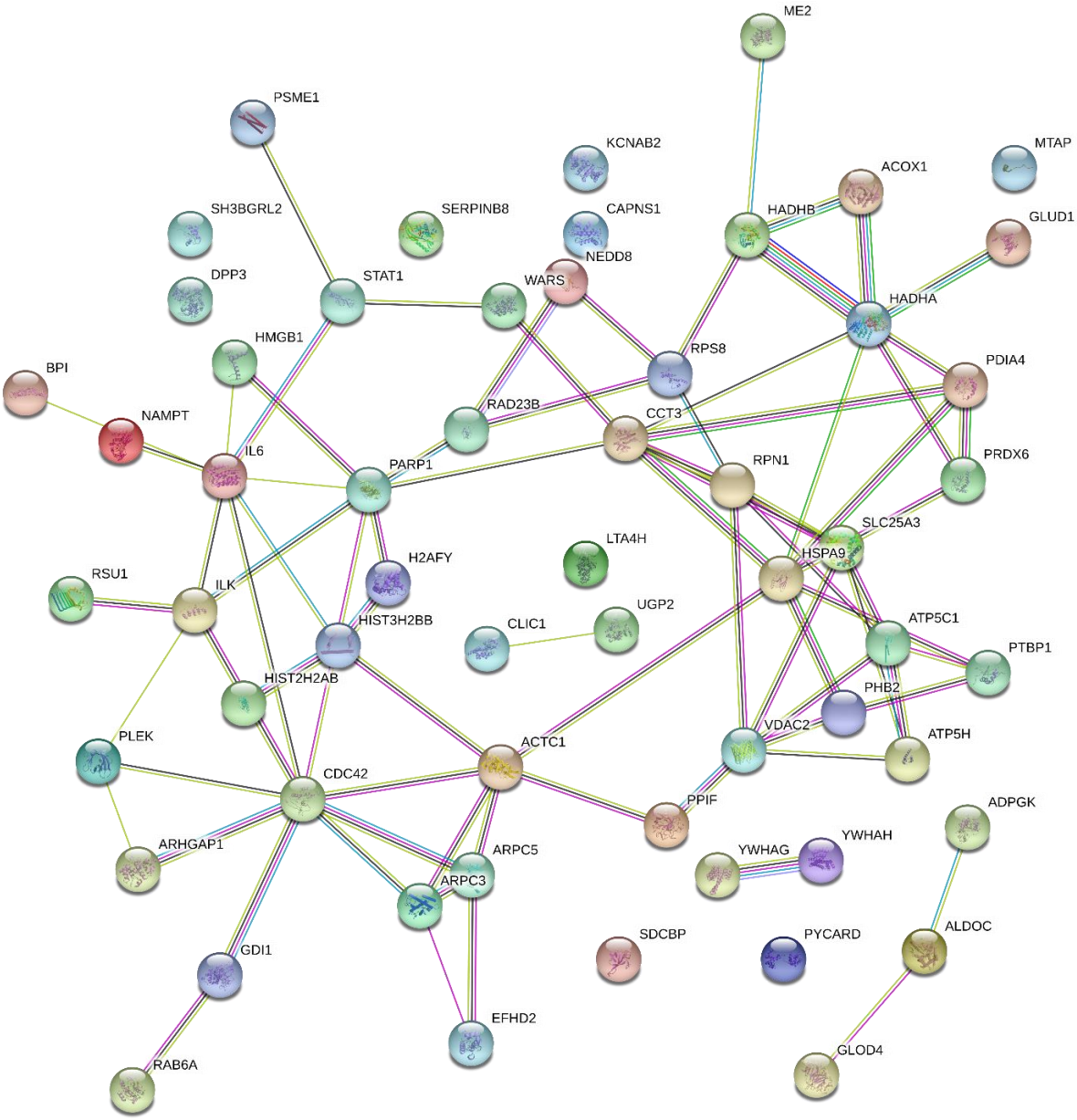

Figure 85. STRING network of 58 proteins quantifiable only in *Mtb* + vehicle samples (non-IRIS group)

Table 27. Enriched GO terms for biological process and KEGG pathway in proteins only quantifiable in *Mtb* + vehicle samples (non-IRIS group)

GO pathway ID	Description	Gene	False discovery
	Biological process		
GO:0007264	small GTPase mediated signal transduction	10	0.0312
GO:0019752	carboxylic acid metabolic process	11	0.0312
GO:0042981	regulation of apoptotic process	14	0.0312
	KEGG pathway		
05132	Salmonella infection	5	0.000958
05100	Bacterial invasion of epithelial cells	4	0.00785

Mtb + PUFA (non-IRIS group)

The 81 proteins identified only in *Mtb* + PUFA samples produced a STRING network with 81 nodes and 89 edges (Figure 86), with enriched GO terms listed in Table 28.

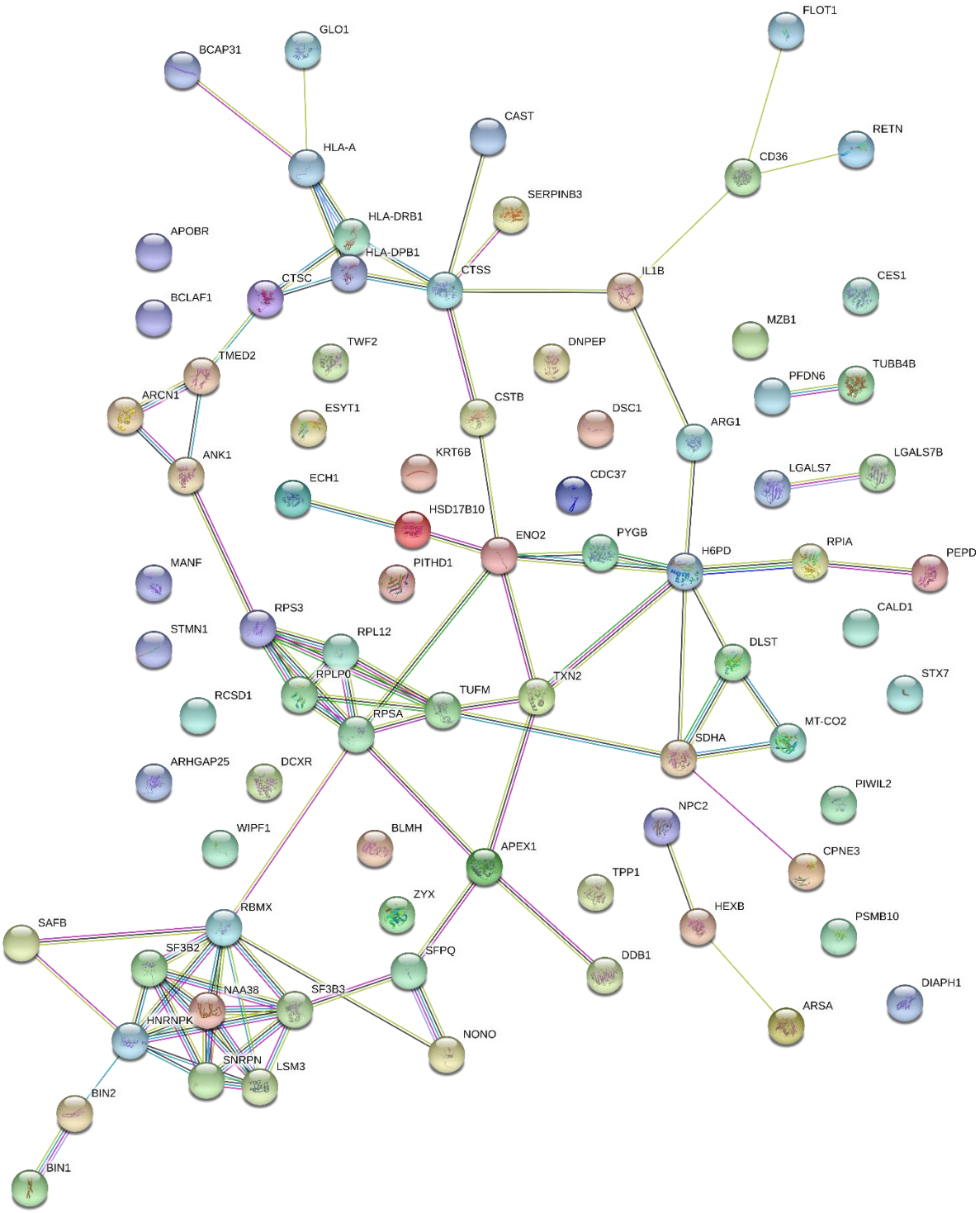

Figure 86. STRING network of 81 proteins quantifiable only in *Mtb* + PUFA samples (non-IRIS group)

Table 28. Enriched GO terms for biological process and KEGG pathway in proteins only quantifiable in *Mtb* + PUFA samples (non-IRIS group)

GO pathway ID	Description	Gene	False discovery
	Biological process		
GO:0002474	antigen processing and presentation of peptide	6	0.00609
GO:0016032	viral process	13	0.00609
GO:0016071	mRNA metabolic process	12	0.00609
GO:0051704	multi-organism process	23	0.00609
	KEGG pathway		
04145	Phagosome	7	0.000435
03040	Spliceosome	6	0.000875
04142	Lysosome	6	0.000875

The most enriched term for biological process was "antigen processing and presentation of peptide antigen via MHC class I". This was a surprising result, as the effects of n-3 PUFA supplementation on antigen presentation are well documented, and such fatty acids are understood to inhibit antigen presentation.[179–181] It is unclear why the same effects are not observed here, but it must be noted that any observations made in the current experiment are those resulting from treatment with n-3 PUFA *and* stimulation with *Mtb* WCL. We were unable to find precedent in the literature for the combined effects of these two perturbation agents.

T-tests performed did not reveal any significantly differentially expressed proteins when comparing the Mtb + vehicle and Mtb + PUFA samples from the non-IRIS group.

IRIS group

We repeated the comparison of *Mtb* + vehicle and *Mtb* + PUFA samples for the IRIS group. Of the 913 proteins quantified, 456 (49.94%) were common to both conditions while 43 were unique to *Mtb* + vehicle samples, and 141 were unique to *Mtb* + PUFA samples (Figure 87). We noted that there were many more proteins quantified for these two conditions in the IRIS group than in the non-IRIS group (913 vs 465, respectively, Figure 84). This may suggest exacerbated responses from the IRIS patient-derived cells. Similarly, there are more proteins unique to *Mtb* + PUFA samples in this group (141 vs 81 in the non-IRIS group).

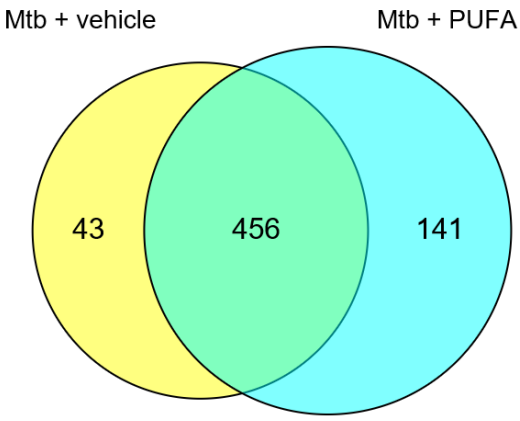

Figure 87. Proteins identified in *Mtb* + vehicle and *Mtb* + PUFA samples from the IRIS group

Mtb + vehicle (IRIS group)

The 43 proteins unique to Mtb + vehicle samples in the IRIS group did not form an enriched network in the STRING protein interaction database. Several proteins in this dataset were also uniquely quantified in Mtb + vehicle samples from the non-IRIS group (such as ASC and IL-6). This is consistent with previous proteomic work by Bell et al.,[166] which suggests that PBMCs derived from TB-IRIS patients showed an uncoordinated inflammatory response to the *Mtb* antigen stimulation.

Mtb + PUFA (IRIS group)

The 141 proteins uniquely identified here formed a STRING network comprising 139 nodes and 266 edges (Figure 88). The enriched GO terms for biological process are listed in Table 29. Enriched GO terms for biological process in proteins only quantifiable in *Mtb* + PUFA samples (IRIS group). The term "component organization" may refer to the formation of lipid rafts, and interaction of n-3 PUFA with lipid rafts and other membrane components. This is also consistent with the reported proteomic effects of prednisone on Mtb-stimulated PBMCs from TB-IRIS patients, which showed increased cellular organization.[166] Protein kinase C-α (PKCα, P17252) was identified here, and is an important kinase involved in the regulation of apoptosis, inflammation, and cell proliferation, differentiation, and migration. N-3 PUFA are known to modulate the effects of PKCα in various ways, such as inhibiting activation by blocking recruitment of PKCα,[182] and modulating IL-2 gene expression by inducing membrane translocation of PKCα.[183]

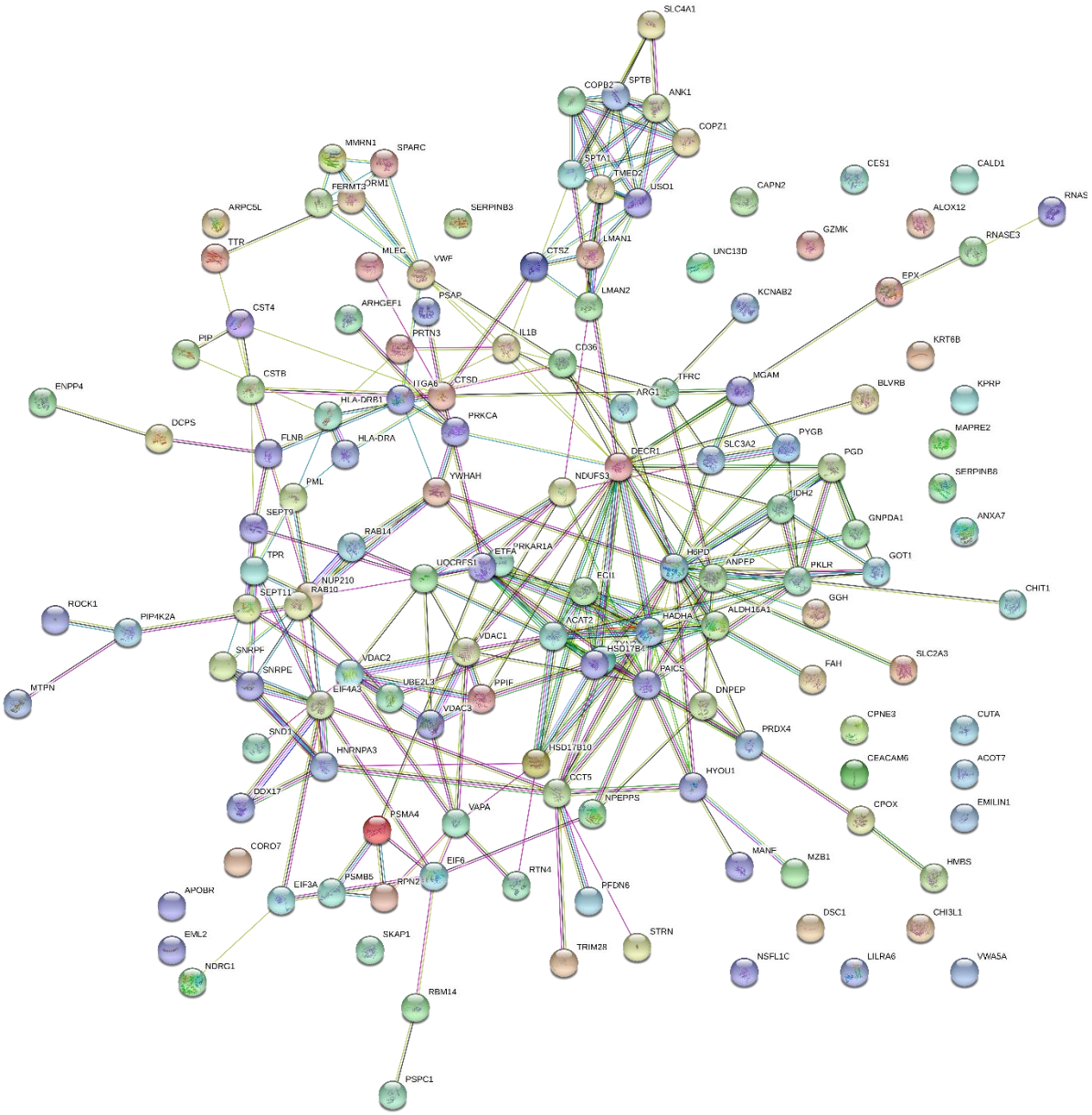

Figure 88. STRING network of 139 proteins quantifiable only in *Mtb* + PUFA samples (IRIS group)

Table 29. Enriched GO terms for biological process in proteins only quantifiable in *Mtb* + PUFA samples (IRIS group)

GO pathway ID	Description	Gene	False discovery
	Biological process		
GO:0044281	small molecule metabolic process	38	1.97e-05
GO:0048193	Golgi vesicle transport	11	0.00225
GO:0051128	regulation of cellular component organization	33	0.00225
GO:0051704	multi-organism process	23	0.00609

We performed t-tests and identified 20 proteins that are considered significantly differentially expressed (permutation-based FDR MTC applied), 15 of which were down-regulated in *Mtb* + PUFA samples (Table 30) and five were up-regulated (Table 31). CDC42 is associated with Fc-γ receptor-mediated phagocytosis, which has previously been implicated in TB-IRIS.[166] Previous proteomic analysis of *Mtb*-simulated PBMCs from non-IRIS and IRIS patients highlighted a deficit in Fc-γ receptor-mediated phagocytosis in PBMCs from IRIS patients, implying a defect in antigen clearance in these patients. Our findings, which suggest n-3 PUFA mediates up-regulation of Fc-γ receptor-mediated phagocytosis components, may therefore be significant, as this is a normal response to *Mtb* antigens in active TB patients.

Two of the five down-regulated proteins are associated with the integrin pathway, which mediates responses at the cell surface such as signal transduction, cell migration, and cell adhesion. Several down-regulated proteins are associated with the immune response (PSMB2, A1AT, AGA, CD11, CD18, HLA-DRB1, CLTC, and CPN1), particularly neutrophil degranulation, antigen presentation, cell migration, and signalling pathways. Since these proteins are down-regulated in *Mtb* + PUFA samples, this suggests that pre-treatment with n-3 PUFA may be causing the observed effect in PBMCs re-stimulated with *Mtb* WCL. This may therefore support the beneficial role of n-3 PUFA treatment in relieving inflammation in TB-IRIS patients.

Table 30. Down-regulated proteins in *Mtb* + PUFA samples from the IRIS group

Protein ID	Gene	Protein name	Function*	P-value	Fold-change**	q value
P04179	SOD2	Superoxide dismutase [Mn], mitochondrial	Removal of superoxide radicals, oxidative stress, IL-12 signaling pathways	4.49e-03	-3.62	0.0444
Q04837	SSBP1	Single-stranded DNA-binding protein, mitochondrial	DNA replication, mitochondrial organization	3.04e-03	-3.39	0.0633
P00505	GOT2	Aspartate aminotransferase, mitochondrial	Amino acid metabolism, cellular uptake of long-chain fatty acids	1.52e-03	-3.20	0.0568
P49721	PSMB2	Proteasome subunit beta type-2 (PSMB2)	NIK/NF-κB, TNF-α, and T cell receptor signaling pathways	4.50e-03	-2.97	0.0422
P01009	SERPINA1	Alpha-1-antitrypsin (A1AT)	Acute phase response, coagulation, neutrophil/platelet degranulation	2.16e-03	-2.62	0.0607
Q9Y2B0	CNPY2	Protein canopy homolog 2	Low-density lipoprotein clearance	3.22e-03	-2.56	0.0585
P20933	AGA	N(4)-(beta-N-acetylglucosaminyl)-L-asparaginase	Peptidase, neutrophil degranulation	4.43e-03	-2.55	0.4689
Q13011	ECH1	Delta(3,5)-Delta(2,4)-dienoyl-CoA isomerase, mitochondrial	Fatty acid beta oxidation	3.03e-03	-2.37	0.0691
P05107	ITGB2	Integrin beta-2 (CD18)	Inflammatory response, leukocyte recruitment and adhesion, dimer with CD11	2.78e-03	-2.33	0.0711
P20073	ANXA7	Annexin A7	Autophagy, cell proliferation, calcium/water homeostasis	4.25e-03	-2.09	0.4965

P62310	LSM3	U6 snRNA-associated Sm-like protein LSm3	mRNA processing and splicing	4.15e-03	-1.94	0.0563
P20701	ITGAL	Integrin alpha-L (CD11)	Inflammatory response, leukocyte migration, phagocytosis, dimer with CD18	9.29e-04	-1.73	0.0200
Q07493	HLA-DRB1	HLA class II histocompatibility antigen, DRB1-15 beta chain	Antigen processing and presentation via MHC class II, IFN-γ-mediated signaling, T cell stimulation and signaling	4.23e-03	-1.64	0.0528
Q00610	CLTC	Clathrin heavy chain 1	Antigen processing and presentation via MHC class II, plasma membrane organization, autophagy	2.99e-03	-1.29	0.0640
P07384	CAPN1	Calpain-1 catalytic subunit	Neutrophil degranulation, cell proliferation, macroautophagy	5.38e-04	-1.06	0.0400

**From UniProt (www.uniprot.org)*

**Fold-change: *Mtb* + PUFA/*Mtb* + vehicle

Table 31. Up-regulated proteins in *Mtb* + PUFA samples from the IRIS group

Protein ID	Gene	Protein name	Function*	P-value	Fold-change**	q value
P60953	CDC42	Cell division control protein 42 homolog	Fc-γ receptor-mediated phagocytosis, integrin pathway	3.36e-03	+1.32	0.0543
P49321	NASP	Nuclear autoantigenic sperm protein	Cell proliferation, DNA replication	2.59e-03	+1.49	0.0914
O75995	SASH3	SAM and SH3 domain-containing protein 3	B and T cell proliferation, production of IFN-γ, IL-10, IL-2, and IL-4	2.64e-03	+1.87	0.08
P08567	PLEK	Plekstrin	Integrin pathway, platelet activation/degranulation	1.94e-04	+2.14	0
P31946	YWHAB	14-3-3 protein beta/alpha	MAPK cascade, membrane organization	8.94e-04	+2.57	0.0267

**From UniProt (www.uniprot.org)*

***Fold-change: *Mtb* + PUFA/*Mtb* + vehicle

8.3 Conclusions

In this experiment, we aimed to i) identify differences in the secretome of PBMCs from non-IRIS and IRIS patients treated under various conditions, and ii) investigate the effects of re-stimulation with *Mtb* WCL and pre-treatment with n-3 PUFA on PBMCs derived from non-IRIS and IRIS patients. Although most of the analyses performed were qualitative based on presence/absence analyses rather than differential expression analyses, we were able to deduce some conclusions.

In control samples (PBMCs cultured *ex vivo* without external stimulus), cells from the non-IRIS and IRIS group produced different results. IRIS group cells secreted a greater number of proteins than their non-IRIS counterparts, and both groups clustered separately when protein expression was subjected to PCA. This was in line with previous reports in the literature of differing inflammatory marker levels both at baseline (ART initiation) and after two weeks. In *Mtb* only samples, key inflammatory mediators were identified only in the IRIS group samples, suggesting a greater inflammatory response in this group. However, there were no significantly differentially expressed proteins identified between non-IRIS and IRIS group samples, across all treatment conditions, and PCA did not reveal clustering in any of the treatment conditions other than controls.

When we compared control and *Mtb* only samples within each patient group, we found that PBMCs re-stimulated with *Mtb* WCL secreted more proteins than their unstimulated counterparts. This observation was true in both the non-IRIS and IRIS groups, although the difference in protein groups quantified was much smaller in IRIS group samples, suggesting that the inflammatory response induced by re-stimulation was already present at baseline. This is to be expected as TB-IRIS is characterized by aberrant inflammatory responses.

When comparing *Mtb* + PUFA and *Mtb* + vehicle samples, we observed that several pro-inflammatory proteins were quantifiable only in *Mtb* + vehicle samples and not *Mtb* + PUFA samples, suggesting that pre-treatment of *Mtb*-stimulated PBMCs with n-3 PUFA may have caused down-regulation of these inflammatory mediators. Although t-tests performed on non-IRIS group samples did not reveal any significantly up-/down-regulated proteins, we identified 20 differentially expressed proteins in the IRIS group samples. Several proteins down-regulated in *Mtb* + PUFA samples were associated with

pathways relating to inflammation and the immune response, further supporting the hypothesis that n-3 PUFA may lead to the resolution of TB-IRIS-associated inflammation.

This experiment holds several limitations. The sample size was small, and inherent biological variation or "noise" is therefore much more prominent. The fact that we did not include a PUFA only control also partly hampers our ability to tease out which effects observed arise from n-3 PUFA treatment and which may be due to re-stimulation with *Mtb* WCL. Finally, we must make the assumption that the presence/absence of proteins observed is an accurate reflection of the cells' biological state in the various samples, and not sampling error. Although some of these limitations are inherent to label-free MS-based proteomics, a larger sample size may lead to more accurate and relevant results.

Chapter 9

Conclusion

9.1 Summary of findings

As outlined in Chapter 2, the current study aimed to (i) investigate the effects of re-stimulating healthy donor and IRIS/non-IRIS patient-derived PBMCs with *Mtb* WCL, (ii) investigate the effects of n-3 PUFA pre-treatment on *Mtb* WCL-stimulated healthy donor and patient-derived PBMCs, and (iii) identify any differences in the responses of non-IRIS and IRIS patients-derived PBMCs to *Mtb* WCL stimulation and n-3 PUFA treatment. These research aims were fulfilled through the use of label-free, MS-based proteomic methods. Although this study could not provide complete answers for these three statements, we were able to shed some light on the effects of n-3 PUFA in the context of TB-IRIS, as summarized here.

In Chapter 4, we aimed to optimise the cell culture platform and ensure that cell isolation, preservation, and culture conditions were appropriate for cell survival. We showed that PBMCs isolated from healthy donors could be cultured for 48 h with *Mtb* WCL, with and without the addition of n-3 PUFA or the vehicle, with no significant decrease in cell survival. We also tested cell survival in the presence of n-3 PUFA at three different concentrations, including twice the concentration used later on in the study, in order to confirm that n-3 PUFA treatment was not harmful to PBMCs. This preliminary work enabled us to test the effects of re-stimulation with *Mtb* WCL and pre-treatment with n-3 PUFA in an *in vitro* cell model that is partly representative of TB-IRIS.

The following chapter (Chapter 5) describes an experiment that was designed to test the sample processing methods, and to evaluate technical and biological variation, as well as reproducibility. Through this experiment, we confirmed that we had isolated the PBMC secretome, and optimized the sample processing methods. Correlation between the technical replicates was satisfactory, and the PCA showed that samples could be differentiated based on their protein expression profile in response to *Mtb* WCL re-stimulation.

Next, we investigated the changes associated with the re-stimulation of PBMCs with *Mtb* WCL, and pre-treatment with n-3 PUFA (Chapter 6). We identified over 2000 protein groups, 727 of which were secreted human proteins, including three interleukins. Contrary to studies reported in the literature,

we did not observe significant dysregulation of protein expression in PBMCs re-stimulated with *Mtb* WCL. However, we identified possible reasons for this (discussed in Chapter 6), which include low TIC in *Mtb* only samples compared to control samples. We also identified several proteins from the complement and coagulation pathways quantified in *Mtb* + vehicle samples but not quantifiable in *Mtb* + PUFA samples. This may suggest down-regulation of these pathways by n-3 PUFA in *Mtb* WCL-stimulated PBMCs, and supports the hypothesis that n-3 PUFA may be exerting an anti-inflammatory effect in this context.

In Chapters 7 and 8, we repeated the previous experiment using PBMCs derived from TB- and HIV-infected patients who developed TB-IRIS, compared with those from patients co-infected with TB and HIV but who did not go on to develop TB-IRIS. We first compared the secretome of PBMCs from non-IRIS and IRIS patients treated under various conditions and observed that protein expression differed between these two groups. IRIS group cells secreted a greater number of proteins than cells from the non-IRIS group, and expressed more inflammatory mediators (such as IL-1β, identified in control samples). In *Mtb* WCL-stimulated samples, key proteins associated with inflammation were identified uniquely in IRIS group samples (such as IL-6 and IL-16, identified in *Mtb*-stimulated samples), suggesting a greater inflammatory response in this group.

Finally, we investigated the effects of re-stimulation with *Mtb* WCL and pre-treatment with n-3 PUFA on PBMCs derived from non-IRIS and IRIS patients. Re-stimulation with *Mtb* WCL induced increased protein expression in both the non-IRIS and IRIS group, several pathways relating to the immune response and bacterial invasion were up-regulated in these samples, and inflammatory mediators IL-1α and IL-1β were identified. We did not find any significantly dysregulated proteins when comparing n-3 PUFA-treated cells with their vehicle-treated counterparts from the non-IRIS group. However, when the same comparison was made with IRIS group samples, we observed that n-3 PUFA-treated cells secreted many more proteins, and we identified 20 proteins that were significantly dysregulated in this treatment group. Several of these were associated with the integrin pathway, which mediates responses at the cell surface such as signal transduction, cell migration, and cell adhesion, and one protein associated with Fc-γ-mediated phagocytosis (CDC42). Encouragingly, eight of the 15 down-regulated proteins were associated with inflammation and the immune response (PSMB2, A1AT, AGA, CD11, CD18, HLA-DRB1, CLTC, and CPN1). This further supports the hypothesis that n-3 PUFA may potentially lead to the resolution of TB-IRIS-associated inflammation.

The data obtained showed that PBMCs re-stimulated with *Mtb* WCL mount an immune response, that is at least partly mitigated by pre-treatment with n-3 PUFA. This was true for healthy donor samples, as well as non-IRIS and IRIS patient-derived samples. However, since most of the analyses performed were qualitative, based on presence/absence analyses, rather than quantitative, the data would need to be confirmed by targeted MS analysis in a larger cohort. The current study therefore provides positive reinforcement for the theory that n-3 PUFA may hold benefits for patients suffering from TB-IRIS-associated inflammatory symptoms.

9.2 Discussion of problems and limitations

The main flaws and limitations in the current work should be acknowledged here to inform future work.

Sample size

As mentioned in the text, the number of samples investigated in the present study is limited (healthy volunteers, n = 8; patients, n = 10). With a small sample group, biological variability may mask treatment-specific trends in the data, and prevent from drawing definite conclusions. This would easily be improved by increasing the sample size. The appropriate sample size could be calculated using a power equation to ensure results obtained are significant.

TIC variation and MS data quality

Some of the experiments performed here yielded lower quality MS data than would be desired, and would have warranted repeat submissions. However, due to constraints relating to time and machine use and sample availability, this was not always possible. This may have affected our ability to perform quantitative analyses, as seen in Chapter 6.

PUFA-only control

The four treatment conditions tested included an untreated and unstimulated control, as well as a vehicle control. However, inclusion of a PUFA-only control would have been useful to compare the effect of n-3 PUFA in *Mtb*-stimulated cells with that in cells not stimulated with *Mtb* WCL. This would have allowed us to tease out the effects of both these perturbations, rather than observation of the compound effects of n-3 PUFA treatment *and Mtb* stimulation.

Complex nature of TB-IRIS

In the current study, we have tested n-3 PUFA in what may be referred to as an *in vitro* model of TB-IRIS. "All models are wrong, but some are useful", as the statistician George Box once said, and in our case this is particularly pertinent. TB-IRIS is a complex, system-wide disorder that includes several factors not accounted for in the present work. These include the presence of live *Mtb* and HIV, anti-TB and ART drugs (and possibly prednisone), and interaction with different cells types not present in this sample (other PBMCs which would have depleted here, particularly adherent monocytes and macrophages, and other blood components). Clinical work would therefore provide a much holistic view of the TB-IRIS system and its response to n-3 PUFA treatment.

Interaction with prednisone

Finally, as prednisone is currently the drug used to relieve TB-IRIS-associated symptoms, the interaction of n-3 PUFA with prednisone (and other anti-TB and ART drugs) would be particularly relevant, and has not been addressed in the current work.

9.3 Summary of contributions

The current work provides preliminary *in vitro* data for the use of n-3 PUFA in TB-IRIS patients. The use of n-3 PUFA in treating patient-derived PBMCs may be related to dietary supplementation *in vivo* and included in a clinical trial. Since the safety of dietary n-3 PUFA consumption has been researched extensively and proven, there is no danger to the patient, and our work has shown its potential benefits in the relief of TB-IRIS-associated symptoms.

9.4 Suggestions for further research

Prednisone is a corticosteroid currently used in the treatment of TB-IRIS. It has broad anti-inflammatory activity. Since n-3 PUFA and prednisone exert anti-inflammatory effects through different mechanisms, there may be possible synergism when both are used concurrently. This has important implications for TB-IRIS, as patients being treated with prednisone could gain extra benefits from dietary supplementation with n-3 PUFA. This is an area which should be investigated further in the future, at the *in vitro* level initially. Briefly, the same experiment described here could be repeated with the addition of prednisone (in the form of prednisolone, or dexamethasone as in the work performed by Bell *et al*.[166]) to the cell culture. Additionally, further experiments using PBMC samples from patients with IRIS under prednisone treatment could be performed to assess the responses of IRIS patient-derived, prednisone-exposed PBMCs to re-stimulation with *Mtb* and treatment with n-3

PUFA. This may shed light on the modulation of the immune response by prednisone and n-3 PUFA in the context of TB-IRIS.

In terms of the next step in this work, targeted proteomic work involving a larger cohort may be needed to verify and validate the results from this preliminary study. If this follow-up study confirms our results, clinical work may be warranted. The preliminary *in vitro* data shown here suggests that clinical use of n-3 PUFA in patients with TB-IRIS may relieve inflammation. A clinical trial that includes dietary supplementation with n-3 PUFA would be needed to confirm this hypothesis *in vivo*. N-3 PUFA are safe immuno-modulatory agents, have been used successfully in the treatment of other inflammatory diseases, and can easily be obtained from the diet. They carry the added advantage of cost-efficiency as can be found in affordable products such as tinned sardines. This is particularly relevant in the South African context and would help reduce the number of medications administered to patients with TB-IRIS.

References

1. WHO. *Global tuberculosis report 2017*. (2017).
2. WHO. *South Africa - Tuberculosis profile 2016*. (2017). doi:10.1080/03071845709419205
3. Comas, I. *et al.* Out-of-Africa migration and Neolithic coexpansion of Mycobacterium tuberculosis with modern humans. *Nat. Genet.* **45,** 1176–1182 (2014).
4. Abdallah, A. M. *et al. Type VII secretion--mycobacteria show the way. Nature reviews. Microbiology* **5,** (2007).
5. WELLS, W. F., RATCLIFFE, H. L. & Crumb, C. On the Mechanics of Droplet Nuclei Infection. II. Quantitative Experimental Air-borne Tuberculosis in Rabbits. *Am. J. Hyg.* **47,** 11–28 (1948).
6. Fennelly, K. P. & Jones-lópez, E. C. Quantity and quality of inhaled dose predicts immunopathology in. **6,** 1–13 (2015).
7. Cambier, C. J., Falkow, S. & Ramakrishnan, L. Host evasion and exploitation schemes of Mycobacterium tuberculosis. *Cell* **159,** 1497–1509 (2014).
8. Vergne, I., Chua, J., Singh, S. B. & Deretic, V. CELL BIOLOGY OF *MYCOBACTERIUM TUBERCULOSIS* PHAGOSOME. *Annu. Rev. Cell Dev. Biol.* **20,** 367–394 (2004).
9. Armstrong, B. Y. J. A. & Hart, A. P. D. A. RESPONSE OF CULTURED MACROPHAGES TO MYCOBAC- TERIUM TUBERCULOSIS , W I T H OBSERVATIONS ON FUSION OF LYSOSOMES W I T H PHAGOSOMES (Received for publication 27 April 1971) Downloaded from jem . rupress . org on September 24 , 2015 When large foreign bodi. **134,** (1971).
10. Manca, C., Paul, S., Barry, C. E., Freedman, V. H. & Kaplan, G. Mycobacterium tuberculosis catalse and peroxidase activities and resistance to oxidative killing in human monocytes in vitro. *Infect. Immun.* **67,** 74–79 (1999).
11. Behar, S. M. *et al.* Apoptosis is an innate defense function of macrophages against Mycobacterium tuberculosis. *Mucosal Immunol* **4,** 279–287 (2011).
12. Cooper, A. M. & Khader, S. A. The role of cytokines in the initiation, expansion, and control of cellular immunity to tuberculosis. *Immunol. Rev.* **226,** 191–204 (2008).
13. Jouanguy, E. *et al.* A human IFNGR1 small deletion hotspot associated with dominant susceptibility to mycobacterial infection. *Nat Genet* **21,** 370–378 (1999).
14. Kolls, J. K. & Khader, S. A. The role of Th17 cytokines in primary mucosal immunity. *Cytokine Growth Factor Rev.* **21,** 443–448 (2010).
15. Tang, J., Yam, W.-C. & Chen, Z. Mycobacterium tuberculosis infection and vaccine development. *Tuberculosis* **98,** 30–41 (2016).
16. Gold, M. C., Napier, R. J. & Lewinsohn, D. M. MR1-restricted mucosal associated invariant T (MAIT) cells in the immune response to *Mycobacterium tuberculosis*. *Immunol. Rev.* **264,** 154–166 (2015).
17. Russell, D. G. Who puts the tubercle in tuberculosis? *Nat. Rev. Microbiol.* **5,** 39–47 (2007).
18. Rayasam, G. V. & Balganesh, T. S. Exploring the potential of adjunct therapy in tuberculosis. *Trends Pharmacol. Sci.* **36,** 506–513 (2015).

19. WHO. *Global Tuberculosis Report 2016*. (2016).

20. Lange, C. & Mori, T. Advances in the diagnosis of tuberculosis. *Respirology* **15,** 220–240 (2010).

21. Cheon, S. A. *et al.* Recent tuberculosis diagnosis toward the end TB strategy. *J. Microbiol. Methods* **123,** 51–61 (2016).

22. Organization, W. H. Use of tuberculosis interferon-gamma release assays (IGRAs) in low- and middle-income countries : policy statement. (2011).

23. WHO & The World Health Organization. *Treatment of tuberculosis: guidelines*. *4Th Edition* (2010). doi:10.1164/rccm.201012-1949OC

24. Vilchèze, C. & Jacobs, W. R. The mechanism of isoniazid killing: clarity through the scope of genetics. *Annu. Rev. Microbiol.* **61,** 35–50 (2007).

25. Campbell, E. a. E. A. *et al.* Structural mechanism for rifampicin inhibition of bacterial rna polymerase. *Cell* **104,** 901–12 (2001).

26. Zhang, Y., Wade, M. M., Scorpio, A., Zhang, H. & Sun, Z. Mode of action of pyrazinamide: Disruption of Mycobacterium tuberculosis membrane transport and energetics by pyrazinoic acid. *J. Antimicrob. Chemother.* **52,** 790–795 (2003).

27. TB DOTS Strategy Coordination. National Tuberculosis Management Guidelines 2014. 1–120 (2014).

28. Unaids. *UNAIDS fact sheet July 2017*. (2017).

29. UNAIDS. *UNAIDS Country factsheet South Africa 2016*. *AIDSinfo* (2016).

30. GLobal Health Observatory. WHO | HIV/AIDS. *WHO* (2017). Available at: http://www.who.int/gho/hiv/en/. (Accessed: 23rd November 2017)

31. UNAIDS. *Global Aids Update 2016*. (2016).

32. Reeves, J. D. & Doms, R. W. Human immunodeficiency virus type 2. *J. Gen. Virol.* **83,** 1253–1265 (2002).

33. Splettstoesser, T. HI virion structure. *Wikimedia Commons* (2014).

34. Esté, J. A. & Telenti, A. HIV entry inhibitors. *Lancet* **370,** 81–88 (2007).

35. Charpentier, C., Nora, T., Tenaillon, O., Clavel, F. & Hance, A. J. Extensive recombination among human immunodeficiency virus type 1 quasispecies makes an important contribution to viral diversity in individual patients. *J. Virol.* **80,** 2472–82 (2006).

36. Simon, V., Ho, D. D. & Abdool Karim, Q. HIV/AIDS epidemiology, pathogenesis, prevention, and treatment. *Lancet (London, England)* **368,** 489–504 (2006).

37. World Health Organization. Guidelines Guideline on When To Start Antiretroviral Therapy and on Pre-Exposure Prophylaxis for Hiv. *World Heal. Organ.* 78 (2015). doi:978 92 4 150956 5

38. Maddocks, S. *et al.* Gene expression in HIV-1 / Mycobacterium tuberculosis co-infected macrophages is dominated by M . tuberculosis. *Tuberculosis* **89,** 285–293 (2009).

39. Tiberi, S. *et al.* The cursed duet today: Tuberculosis and HIV-coinfection. *Press. Medicale* **46,** e23–e39 (2017).

40. Getahun, H., Harrington, M., O'Brien, R. & Nunn, P. Diagnosis of smear-negative pulmonary tuberculosis in people with HIV infection or AIDS in resource-constrained settings: informing urgent policy changes. *Lancet (London, England)* **369,** 2042–9 (2007).

41. Shelburne, S. *et al.* Immune reconstitution inflammatory syndrome: Emergence of a unique syndrome during highly active antiretroviral therapy. *Medicine (Baltimore).* **81,** 213–227 (2002).

42. Murdoch, D. M., Venter, W. D. F. & Feldman, C. Incidence and risk factors for the immune reconstitution inflammatory syndrome in HIV patients in South Africa : a prospective study. *AIDS* **22,** (2008).

43. Narendran, G. *et al.* Paradoxical Tuberculosis Immune Reconstitution Inflammatory Syndrome (TB-IRIS) in HIV Patients with Culture Confirmed Pulmonary Tuberculosis in India and the Potential Role of IL-6 in Prediction. *PLoS One* **8,** (2013).

44. Muller, M. *et al.* Immune reconstitution inflammatory syndrome in patients starting antiretroviral therapy for HIV infection: a systematic review and meta-analysis. *Lancet Infect. Dis.* **10,** 251–261 (2010).

45. French, M. A. H., Mallal, S. A. & Dawkins, R. L. Zidovudine-induced restoration of cell-mediated immunity to mycobacteria in immunodeficient HIV-infected patients. *Aids* **6,** 1293–1298 (1992).

46. Bourgarit, A. *et al.* Explosion of tuberculin-specific Th1-responses induces immune restoration syndrome in tuberculosis and HIV co-infected patients. *AIDS* **20,** F1–F7 (2006).

47. Vignesh, R. *et al.* TB-IRIS After Initiation of Antiretroviral Therapy Is Associated With Expansion of Preexistent Th1 Responses Against Mycobacterium tuberculosis Antigens. *J. Acquir. Immune Defic. Syndr.* **64,** 241–248 (2013).

48. Meintjes, G. *et al.* Type 1 Helper T Cells and FoxP3-positive T Cells in HIV – Tuberculosis-associated Immune Reconstitution Inflammatory Syndrome. *Am. J. Respir. Crit. Care Med.* **178,** 1083–1089 (2008).

49. Sutherland, J. S. *et al.* Polyfunctional CD4(+) and CD8(+) T cell responses to tuberculosis antigens in HIV-1-infected patients before and after anti-retroviral treatment. *J. Immunol.* **184,** 6537–6544 (2010).

50. Tadokera, R. *et al.* Hypercytokinaemia accompanies HIV-tuberculosis immune reconstitution inflammatory syndrome. *Eur. Respir. J.* **37,** 1248–1259 (2011).

51. Worsley, C. M., Suchard, M. S., Stevens, W. S., Rie, A. Van & Murdoch, D. M. Multi-analyte profiling of ten cytokines in South African HIV-infected patients with Immune Reconstitution Inflammatory Syndrome (IRIS). *AIDS Res. Ther.* 1–7 (2010).

52. Sharma, S. K. & Soneja, M. HIV & immune reconstitution inflammatory syndrome (IRIS). *Indian J. Med. Res.* 866–877 (2011).

53. Lawn, S., Myer, L., Bekker, L. & Wood, R. Tuberculosis-associated immune reconstitution disease: Incidence, risk factors and impact in an antiretroviral treatment service in South Africa. *Aids* **21,** 335–341 (2007).

54. Shelburne, S. A. *et al.* Incidence and risk factors for immune reconstitution inflammatory syndrome during highly active antiretroviral therapy. *AIDS* **19,** 399–406 (2005).

55. Price, P. *et al.* Polymorphisms in cytokine genes define subpopulations of HIV-1 patients who experienced immune restoration diseases. *AIDS* **16,** 2043–7 (2002).

56. Meintjes, G. *et al.* Adult antiretroviral therapy guidelines 2014. *South. Afr. J. HIV Med.* **15,** 121–143 (2014).

57. Meintjes, G. *et al.* Randomized placebo-controlled trial of prednisone for paradoxical TB-associated IRIS. *AIDS* **24,** 2381–2390 (2011).

58. Elliott, A. M. *et al.* Use of Prednisolone in the Treatment of HIV-positive Tuberculosis Patients. *Q. J. Med.* **85,** 855–860 (1992).

59. Volkow, P., Cornejo, P., Zinser, J., Ormsby, C. & Reyes-Teran, G. Life-threatening exarcebation of Kaposi's sarcoma after prednisone treatment for immune reconstitution inflammatory syndrome. *AIDS* **22,** 663–665 (2008).

60. Calder, P. C. Marine omega-3 fatty acids and inflammatory processes: Effects, mechanisms and clinical relevance. *Biochim. Biophys. Acta* **1851,** 469–484 (2014).

61. Mori, T. a & Beilin, L. J. Omega-3 fatty acids and inflammation. *Curr. Atheroscler. Rep.* **6,** 461–467 (2004).

62. Kim, W. *et al.* Regulatory activity of polyunsaturated fatty acids in T-cell signaling. *Prog. Lipid Res.* **49,** 250–261 (2010).

63. Sigma-Aldrich. Omega-3 Fatty Acids and Heart Disease | Sigma-Aldrich. *BioFiles* (2007). Available at: https://www.sigmaaldrich.com/technical-documents/articles/biofiles/omega-3-fatty-acids.html. (Accessed: 23rd November 2017)

64. Hidaka, B. H. *et al.* Omega-3 and omega-6 Fatty acids in blood and breast tissue of high-risk women and association with atypical cytomorphology. *Cancer Prev. Res. (Phila).* **8,** 359–64 (2015).

65. Calder, P. C. Polyunsaturated Fatty Acids , Inflammation , and Immunity. *Lipids* **36,** 1007–1024 (2001).

66. Proudman, S. M. *et al.* Fish oil in recent onset rheumatoid arthritis: a randomised, double-blind controlled trial within algorithm-based drug use. *Ann. Rheum. Dis.* **74,** 89–95 (2015).

67. Belluzzi, A. in *Inflammatory Bowel Diseases* 36–38 (1999).

68. Emelyanov, A. *et al.* Treatment of asthma with lipid extract of New Zealand green-lipped mussel: A randomised clinical trial. *Eur. Respir. J.* **20,** 596–600 (2002).

69. Guida, B. *et al.* Energy-restricted, n-3 polyunsaturated fatty acids-rich diet improves the clinical response to immuno-modulating drugs in obese patients with plaque-type psoriasis: A randomized control clinical trial. *Clin. Nutr.* **33,** 399–405 (2014).

70. Sharma, A. *et al.* Novel Omega-3 Fatty Acid Epoxygenase Metabolite Reduces Kidney Fibrosis. *Int. J. Mol. Sci.* **17,** 751 (2016).

71. Heydari, B. *et al.* Effect of Purified Omega-3 Fatty Acids on Reducing Left Ventricular Remodeling After Acute Myocardial Infarction (Omega-Remodel Study: a Double-Blind Randomized Clinical Trial). *J. Am. Coll. Cardiol.* **65,** A1083 (2015).

72. Beretta, L. Proteomics from the clinical perspective: many hopes and mch debate. *Nat. Methods* **4,** 785–786 (2007).

73. Bachi, A. & Bonaldi, T. Quantitative proteomics as a new piece of the systems biology puzzle. *J. Proteomics* **71,** 357–367 (2008).

74. Cho, W. C. S. Proteomics Technologies and Challenges. *Genomics, Proteomics Bioinforma.* **5,** 77–85 (2007).

75. Yates, J. R., Ruse, C. I. & Nakorchevsky, A. Proteomics by Mass Spectrometry: Approaches, Advances, and Applications. *Annu. Rev. Biomed. Eng.* **11,** 49–79 (2009).

76. Schwamborn, K. & Caprioli, R. M. Molecular imaging by mass spectrometry — looking beyond classical histology. *Nat. Rev. Cancer* **10,** 639–646 (2010).

77. Aebersold, R. & Mann, M. Mass spectrometry-based proteomics. *Nature* **422,** 198–207 (2003).

78. Michalski, A. *et al.* Mass spectrometry-based proteomics using Q Exactive, a high-performance benchtop quadrupole Orbitrap mass spectrometer. *Mol. Cell. Proteomics* **10,** M111.011015 (2011).

79. Altelaar, A. F. M., Munoz, J. & Heck, A. J. R. Next-generation proteomics: towards an integrative view of proteome dynamics. *Nat. Rev. Genet.* **14,** 35–48 (2012).

80. Urgen Cox, J. *et al.* Andromeda: A Peptide Search Engine Integrated into the MaxQuant Environment. *J. Proteome Res* **10,** 1794–1805 (2011).

81. Elias, J. E. & Gygi, S. P. Target-decoy search strategy for mass spectrometry-based proteomics. *Methods Mol. Biol.* **604,** 55–71 (2010).

82. Hoedt, E., Zhang, G. & Neubert, T. A. in *Advances in experimental medicine and biology* **806,** 93–106 (2014).

83. Unwin, R. D. Quantification of proteins by iTRAQ. *Methods Mol. Biol.* **658,** 205–15 (2010).

84. Arike, L. & Peil, L. Spectral counting label-free proteomics. *Methods Mol. Biol.* **1156,** (2014).

85. Cox, J. *et al.* Accurate Proteome-wide Label-free Quantification by Delayed Normalization and Maximal Peptide Ratio Extraction, Termed MaxLFQ. *Mol. Cell. Proteomics* **13,** 2513–2526 (2014).

86. Tyanova, S. *et al.* The Perseus computational platform for comprehensive analysis of (prote) omics data. (2016). doi:10.1038/nmeth.3901

87. Szklarczyk, D. *et al.* The STRING database in 2017: quality-controlled protein-protein association networks, made broadly accessible. *Nucleic Acids Res.* **45,** D362–D368 (2017).

88. Mi, H., Muruganujan, A., Casagrande, J. T. & Thomas, P. D. Large-scale gene function analysis with the PANTHER classification system. *Nat. Protoc.* **8,** 1551–1566 (2013).

89. Millán, P. P. Network generation and analysis through Cytoscape and PSICQUIC. *EMBL-EBI Tutor.* (2014).

90. Böyum, A. A one-stage procedure for isolation of granulocytes and lymphocytes from human blood. General sedimentation properties of white blood cells in a 1g gravity field. *Scand. J. Clin. Lab. Invest. Suppl.* **97,** 51–76 (1968).

91. Healthcare, G. Isolation of mononuclear cells. *Methods* 1–20 (2014). doi:10.1002/9780470151808.sc02a00s2

92. Riedhammer, C., Halbritter, D. & Weissert, R. Peripheral Blood Mononuclear Cells: Isolation, Freezing, Thawing, and Culture. *Methods Mol. Biol.* 53–61 (2015). doi:10.1007/7651

93. Hoft, D. F. *et al.* Investigation of the relationships between immune-mediated inhibition of mycobacterial growth and other potential surrogate markers of protective Mycobacterium tuberculosis immunity. *J. Infect. Dis.* **186,** 1448–1457 (2002).

94. Ehrhardt, R. O. *et al.* Maximizing PMBC Recovery and viability: A method to optimize and streamline peripheral blood mononuclear cell isolation, cryopreservation, and thawing. (2015).

95. Kleeberger, C. A. *et al.* Viability and Recovery of Peripheral Blood Mononuclear Cells Cryopreserved for up to 12 Years in a Multicenter Study. **6,** 14–19 (1999).

96. Nazarpour, R. *et al.* Optimization of Human Peripheral Blood Mononuclear Cells (PBMCs) Cryopreservation. *Int. J. Mol. Cell. Med.* **1,** 88–93 (2012).

97. Ramachandran, H. *et al.* Optimal Thawing of Cryopreserved Peripheral Blood Mononuclear Cells for Use in High-Throughput Human Immune Monitoring Studies. *Cells* 313–324 (2012). doi:10.3390/cells1030313

98. Kutscher, S. *et al.* Overnight Resting of PBMC Changes Functional Signatures of Antigen Specific T- Cell Responses: Impact for Immune Monitoring within Clinical Trials. *PLoS One* **8,** (2013).

99. Kuerten, S. *et al.* Resting of Cryopreserved PBMC Does Not Generally Benefit the Performance of Antigen-Specific T Cell ELISPOT Assays. *Cells* **1,** 409–27 (2012).

100. Skuladottir, I. H. & Petursdottir, Æ. D. H. The Effects of Omega-3 Polyunsaturated Fatty Acids on TNF- a and IL-10 Secretion by Murine Peritoneal Cells In Vitro. *Lipids* 699–706 (2007). doi:10.1007/s11745-007-3081-1

101. Nauroth, J. M. *et al.* Docosahexaenoic Acid (DHA) and Docosapentaenoic Acid (DPAn-6) Algal Oils Reduce Inflammatory Mediators in Human Peripheral Mononuclear Cells In Vitro and Paw Edema In Vivo. *Lipids* 375–384 (2010). doi:10.1007/s11745-010-3406-3

102. Zhao, Y. & Joshi-Barve, S. Eicosapentaenoic acid prevents LPS-induced TNF-α expression by preventing NF-κB activation. *J. Am. Coll. Nutr.* **23,** 71–8 (2004).

103. Skolimowska, K. H. *et al.* Altered Ratio of IFN- c / IL-10 in Patients with Drug Resistant Mycobacterium tuberculosis and HIV- Tuberculosis Immune Reconstitution Inflammatory Syndrome. **7,** (2012).

104. Bell, L. High throughput proteomic analysis of Mycobacterium tuberculosis associate Immune Reconstitution Inflammatory Syndrome (TB-IRIS). (2012).

105. Mosmann, T. Rapid colorimetric assay for cellular growth and survival: Application to proliferation and cytotoxicity assays. *J. Immunol. Methods* **65,** 55–63 (1983).

106. Makridakis, M. & Vlahou, A. Secretome proteomics for discovery of cancer biomarkers. *J. Proteomics* **73,** 2291–2305 (2010).

107. Brown, K. J. *et al.* Advances in the proteomic investigation of the cell secretome. *Expert Rev. Proteomics* **9,** 337–345 (2012).

108. Shin, J. S. *et al.* Serum starvation induces G1 arrest through suppression of Skp2-CDK2 and CDK4 in SK-OV-3 cells. *Int. J. Oncol.* **32,** 435–439 (2008).

109. Hasan, N. M., Adams, G. E. & Joiner, M. C. Effect of serum starvation on expression and phosphorylation of PKC-α and p53 in V79 cells: Implications for cell death. *Int. J. cancer* **80,** 400–405 (1999).

110. Levin, V. A. *et al.* Different changes in protein and phosphoprotein levels result from serum starvation of high-grade glioma and adenocarcinoma cell lines. *J. Proteome Res.* **9,** 179 (2010).

111. Mbeunkui, F., Fodstad, O. & Pannell, L. K. Secretory protein enrichment and analysis: an optimized approach applied on cancer cell lines using 2D LC− MS/MS. *J. Proteome Res.* **5,** 899–906 (2006).

112. Makridakis, M. *et al.* Analysis of secreted proteins for the study of bladder cancer cell aggressiveness. *J. Proteome Res.* **9,** 3243–3259 (2010).

113. Bradford, M. M. A rapid and sensitive method for the quantitation of microgram quantities of protein utilizing the principle of protein-dye binding. *Anal. Biochem.* **72,** 248–254 (1976).

114. Qiu, P., Wheater, M. K., Qiu, Y. & Sosne, G. Thymosin β(4) inhibits TNF-α-induced NF-κB activation, IL-8 expression, and the sensitizing effects by its partners PINCH-1 and ILK. *FASEB J.* **25,** 1815–1826 (2011).

115. Paulussen, M., Landuyt, B., Schoofs, L., Luyten, W. & Arckens, L. Thymosin beta 4 mRNA and peptide expression in phagocytic cells of different mouse tissues. *Peptides* **30,** 1822–1832 (2009).

116. Gutierrez-Pabello, J. A., Mcmurray, D. N. & Garry, L. Upregulation of Thymosin β -10 by Mycobacterium bovis Infection of Bovine Macrophages Is Associated with Apoptosis. 4–11 (2002). doi:10.1128/IAI.70.4.2121

117. Suradej, B., Pata, S., Kasinrerk, W. & Cressey, R. Glucosidase II exhibits similarity to the p53 tumor suppressor in regards to structure and behavior in response to stress signals : A potential novel cancer biomarker. 2511–2519 (2013). doi:10.3892/or.2013.2721

118. Lim, Y. *et al.* Endoplasmic Reticulum Stress Pathway-Mediated Apoptosis in Macrophages Contributes to the Survival of Mycobacterium tuberculosis. **6,** (2011).

119. Gonzales, P. A. *et al.* Large-scale proteomics and phosphoproteomics of urinary exosomes. *J. Am. Soc. Nephrol.* **20,** 363–379 (2009).

120. Zanivan, S. *et al.* SILAC-based proteomics of human primary endothelial cell morphogenesis unveils tumor angiogenic markers. *Mol. Cell. Proteomics* **12,** 3599–3611 (2013).

121. Lyadova, I. V. Review Article Neutrophils in Tuberculosis : Heterogeneity Shapes the Way ? **2017,** (2017).

122. Kinoshita, T., Nohata, N., Watanabe-takano, H. & Yoshino, H. to cell migration and invasion and is directly regulated by tumor-suppressive microRNA-133a in head and neck squamous cell carcinoma. **5,** 1770–1778 (2012).

123. Ghosh, A., Tousif, S., Bhattacharya, D., Samuchiwal, S. K. & Bhalla, K. Expression of the ARPC4 Subunit of Human Arp2 / 3 Severely Affects Mycobacterium tuberculosis Growth and Suppresses Immunogenic Response in Murine Macrophages. **8,** (2013).

124. Singh, R., Sharma, M., Sarkar, C., Singh, M. & Chauhan, S. Transcription factor C / EBP - β mediates downregulation of dipeptidyl - peptidase III expression by interleukin - 6 in human glioblastoma ... *FEBS J.* (2014). doi:10.1111/febs.12728

125. Qualls, J. E. *et al.* Arginine Usage in Mycobacteria-Infected Macrophages Depends on Autocrine-Paracrine Cytokine Signaling. *Sci. Signal.* **3,** ra62-ra62 (2010).

126. Buschow, S. I. *et al.* MHC class II-associated proteins in B-cell exosomes and potential functional implications for exosome biogenesis. *Immunol. Cell Biol.* **88,** 851 (2010).

127. Bonnard, C. *et al.* Mitochondrial dysfunction results from oxidative stress in the skeletal muscle of diet-induced insulin-resistant mice. *J. Clin. Invest.* **118,** 789 (2008).

128. Mahesh, P. P., Retnakumar, R. J. & Mundayoor, S. Downregulation of vimentin in macrophages infected with live Mycobacterium tuberculosis is mediated by Reactive Oxygen Species. *Nat. Publ. Gr.* 1–12 (2016). doi:10.1038/srep21526

129. Romeo, J. *et al.* Moderate alcohol consumption and the immune system: A review. *Br. J. Nutr.* S111-115 (2007). doi:10.1017/S0007114507838049

130. Prunotto, M. *et al.* Proteomic analysis of podocyte exosome-enriched fraction from normal human urine. *J. Proteomics* **82,** 193–229 (2013).

131. He, P.-P. *et al.* MicroRNA-590 attenuates lipid accumulation and pro-inflammatory cytokine secretion by targeting lipoprotein lipase gene in human THP-1 macrophages. *Biochimie* **106,** 81–90 (2014).

132. Rousseau, A., Michaud, A., Chauvet, M. T., Lenfant, M. & Corvol, P. The hemoregulatory peptide N-acetyl-Ser-Asp-Lys-Pro is a natural and specific substrate of the N-terminal active site of human angiotensin-converting enzyme. *J. Biol. Chem.* **270,** 3656–3661 (1995).

133. Bernstein, K. E. *et al.* A modern understanding of the traditional and nontraditional biological functions of angiotensin-converting enzyme. *Pharmacol. Rev.* **65,** 1–46 (2013).

134. Vowinkel, T. *et al.* Apolipoprotein A-IV inhibits experimental colitis. *J. Clin. Invest.* **114,** 260–269 (2004).

135. Wong, W.-M. R. *et al.* Common variants of apolipoprotein A-IV differ in their ability to inhibit low density lipoprotein oxidation. *Atherosclerosis* **192,** 266–274 (2007).

136. Hogaboam, C. M. *et al.* Novel CXCR2-dependent liver regenerative qualities of ELR-containing CXC chemokines. *FASEB J. Off. Publ. Fed. Am. Soc. Exp. Biol.* **13,** 1565–1574 (1999).

137. Jeong, W., Yoon, H. W., Lee, S.-R. & Rhee, S. G. Identification and characterization of TRP14, a thioredoxin-related protein of 14 kDa. New insights into the specificity of thioredoxin function. *J. Biol. Chem.* **279,** 3142–3150 (2004).

138. Sun, W. *et al.* PPM1A and PPM1B act as IKKbeta phosphatases to terminate TNFalpha-induced IKKbeta-NF-kappaB activation. *Cell. Signal.* **21,** 95–102 (2009).

139. Carroll, M. C., Fathallah, D. M., Bergamaschini, L., Alicot, E. M. & Isenman, D. E. Substitution of a single amino acid (aspartic acid for histidine) converts the functional activity of human complement C4B to C4A. *Proc. Natl. Acad. Sci. U. S. A.* **87,** 6868–6872 (1990).

140. Wuyts, A. *et al.* Isolation of the CXC chemokines ENA-78, GRO alpha and GRO gamma from tumor cells and leukocytes reveals NH2-terminal heterogeneity. Functional comparison of different natural isoforms. *Eur. J. Biochem.* **260,** 421–429 (1999).

141. Jeong, W., Chang, T.-S., Boja, E. S., Fales, H. M. & Rhee, S. G. Roles of TRP14, a thioredoxin-related protein in tumor necrosis factor-alpha signaling pathways. *J. Biol. Chem.* **279,** 3151–3159 (2004).

142. Lin, X. *et al.* PPM1A functions as a Smad phosphatase to terminate TGFbeta signaling. *Cell* **125,** 915–928 (2006).

143. Schwefel, D. *et al.* Structural insights into the mechanism of GTPase activation in the GIMAP family. *Structure* **21,** 550–559 (2013).

144. Schierloh, P. *et al.* Mycobacterium tuberculosis-Induced Gamma Interferon Production by Natural Killer Cells Requires Cross Talk with Antigen-Presenting Cells Involving Toll-Like Receptors 2 and 4 and the Mannose Receptor in Tuberculous Pleurisy. *Infect. Immun.* **75,** 5325–5337 (2007).

145. Sharma, S., Sharma, M., Roy, S., Kumar, P. & Bose, M. Mycobacterium tuberculosis induces high production of nitric oxide in coordination with production of tumour necrosis factor-α in patients with fresh active tuberculosis but not in MDR tuberculosis. *Immunol. Cell Biol.* **82,** 377–382 (2004).

146. von Reyn, C. F. *et al.* Safety and immunogenicity of an inactivated whole cell tuberculosis vaccine booster in adults primed with BCG: A randomized, controlled trial of DAR-901. *PLoS One* **12,** e0175215 (2017).

147. Oliveira, E., Marinho, J. & Barbosa, T. Interferon-gamma production by mononuclear cells in Bacille Calmette-Guérin-revaccinated healthy volunteers predicted long-term antimycobacterial responses in a randomized controlled trial. *Vaccine* **31,** 3778–3782 (2013).

148. Jensen, K. *et al.* A neonatal oral Mycobacterium tuberculosis-SIV prime/intramuscular MVA-SIV boost combination vaccine induces both SIV and Mtb-specific immune responses in infant macaques. *Trials Vaccinol.* **2,** 53–63 (2013).

149. Bantscheff, M., Lemeer, S., Savitski, M. M. & Kuster, B. Quantitative mass spectrometry in proteomics: Critical review update from 2007 to the present. *Anal. Bioanal. Chem.* **404,** 939–965 (2012).

150. Kashuba, E., Bailey, J., Allsup, D. & Cawkwell, L. The kinin–kallikrein system: physiological roles, pathophysiology and its relationship to cancer biomarkers. *Biomarkers* **18,** 279–296 (2013).

151. Phillips, C. M. *et al.* Complement component 3 polymorphisms interact with polyunsaturated fatty acids to modulate risk of metabolic syndrome. *Am. J. Clin. Nutr.* **90,** 1665–73 (2009).

152. Tran, H. T. T. *et al.* Modulation of the complement system in monocytes contributes to tuberculosis-associated immune reconstitution inflammatory syndrome. *AIDS* **27,** 1725–1734 (2013).

153. Webb, D. J. & Gonias, S. L. A modified human alpha 2-macroglobulin derivative that binds tumor necrosis factor-alpha and interleukin-1 beta with high affinity in vitro and reverses lipopolysaccharide toxicity in vivo in mice. *Lab. Invest.* **78,** 939–48 (1998).

154. Kurdowska, A., Alden, S. M., Noble, J. M., Stevens, M. D. & Carr, F. K. INVOLVEMENT OF α-2-MACROGLOBULIN RECEPTOR IN CLEARANCE OF INTERLEUKIN 8–α-2-MACROGLOBULIN COMPLEXES BY HUMAN ALVEOLAR MACROPHAGES. *Cytokine* **12,** 1046–1053 (2000).

155. Chakraborty, N. *et al.* Contributions of polyunsaturated fatty acids (PUFA) on cerebral neurobiology: an integrated omics approach with epigenomic focus. *J. Nutr. Biochem.* **42,** 84–94 (2017).

156. Chapkin, R. S. *et al.* Bioactive dietary long-chain fatty acids: emerging mechanisms of action. *Br. J. Nutr.* **100,** 1152 (2008).

157. Fan, Y.-Y., McMurray, D. N., Ly, L. H. & Chapkin, R. S. Dietary (n-3) polyunsaturated fatty acids remodel mouse T-cell lipid rafts. *J. Nutr.* **133,** 1913–1920 (2003).

158. Chadwick, W., Brenneman, R., Martin, B. & Maudsley, S. Complex and Multidimensional Lipid Raft Alterations in a Murine Model of Alzheimer's Disease. *Int. J. Alzheimers. Dis.* **2010,** 1–56 (2010).

159. Ravi, S., Schilder, R. J. & Kimball, S. R. Role of precursor mRNA splicing in nutrient-induced alterations in gene expression and metabolism. *J. Nutr.* **145,** 841–6 (2015).

160. Salati, L. M. *et al.* Nutritional Regulation of mRNA Processing. *J. Nutr.* **134,** 2437S–2443 (2004).

161. Reardon, H. T. *et al.* The polypyrimidine tract binding protein regulates desaturase alternative splicing and PUFA composition. *J. Lipid Res.* **52,** 2279–86 (2011).

162. Caterina, R. De, Cybulsky, M. I., Clinton, S. K., Jr, M. A. G. & Libby, P. The Omega-3 Fatty Acid Docosahexaenoate Reduces Cytokine-Induced Expression of Proatherogenic and Proinflammatory Proteins in Human Endothelial Cells. (2016).

163. Storey, A., McArdle, F., Friedmann, P. S., Jackson, M. J. & Rhodes, L. E. Eicosapentaenoic Acid and Docosahexaenoic Acid Reduce UVB- and TNF-α-induced IL-8 Secretion in Keratinocytes and UVB-induced IL-8 in Fibroblasts. *J. Invest. Dermatol.* **124,** 248–255 (2005).

164. Spigoni, V. *et al.* N-3 PUFA increase bioavailability and function of endothelial progenitor cells. *Food Funct.* **5,** 1881–90 (2014).

165. Cox, H. S. *et al.* Epidemic Levels of Drug Resistant Tuberculosis (MDR and XDR-TB) in a High HIV Prevalence Setting in Khayelitsha, South Africa. *PLoS One* **5,** e13901 (2010).

166. Bell, L. *et al.* TB-IRIS: Proteomic analysis of in vitro PBMC responses to Mycobacterium tuberculosis and response modulation by dexamethasone. *Exp. Mol. Pathol.* **102,** 237–246 (2017).

167. Bourgarit, A. *et al.* Tuberculosis-Associated Immune Restoration Syndrome in HIV-1-Infected Patients Involves Tuberculin-Specific CD4 Th1 Cells and KIR-Negative T Cells. *J. Immunol.* **183,** 3915–3923 (2009).

168. Conesa-Botella, A. *et al.* Corticosteroid therapy, vitamin D status, and inflammatory cytokine profile in the HIV-tuberculosis immune reconstitution inflammatory syndrome. *Clin. Infect. Dis.* **55,** 1004–1011 (2012).

169. Marais, S. *et al.* Neutrophil-Associated Central Nervous System Inflammation in Tuberculous Meningitis Immune Reconstitution Inflammatory Syndrome. *Clin. Infect. Dis.* **59,** 1638–1647 (2014).

170. Pean, P. *et al.* Natural killer cell degranulation capacity predicts early onset of the immune reconstitution inflammatory syndrome (IRIS) in HIV-infected patients with tuberculosis. *Blood* **119,** 3315–3320 (2012).

171. Tan, D. B. A. *et al.* TLR2-induced cytokine responses may characterize HIV-infected patients experiencing mycobacterial immune restoration disease. *AIDS* **25,** 1455–1460 (2011).

172. Grunnet, N. & Kondrup, J. The Effect of Ethanol on the ?-Oxidation of Fatty Acids. *Alcohol. Clin. Exp. Res.* **10,** 64S–68S (1986).

173. Charles Lieber, B. S. & Schmid, R. THE EFFECT OF ETHANOL ON FATTY ACID METABOLISM; STIMULATION OF HEPATIC FATTY ACID SYNTHESIS IN VITRO *.

174. Ko, H. S., Uehara, T. & Nomura, Y. Role of Ubiquilin Associated with Protein-disulfide Isomerase in the Endoplasmic Reticulum in Stress-induced Apoptotic Cell Death. *J. Biol. Chem.* **277,** 35386–35392 (2002).

175. Mouneimne, G. *et al.* Differential Remodeling of Actin Cytoskeleton Architecture by Profilin Isoforms Leads to Distinct Effects on Cell Migration and Invasion. *Cancer Cell* **22,** 615–630 (2012).

176. Seto, S., Tsujimura, K. & Koide, Y. Rab GTPases Regulating Phagosome Maturation Are Differentially Recruited to Mycobacterial Phagosomes. *Traffic* **12,** 407–420 (2011).

177. Man, S. M. & Kanneganti, T. D. Converging roles of caspases in inflammasome activation, cell death and innate immunity. *Nat. Rev. Immunol.* **16,** 7–21 (2016).

178. Yan, Y. *et al.* Omega-3 Fatty Acids Prevent Inflammation and Metabolic Disorder through Inhibition of NLRP3 Inflammasome Activation. *Immunity* **38,** 1154–1163 (2013).

179. Shaikh, S. R. & Edidin, M. Polyunsaturated fatty acids, membrane organization, T cells, and antigen presentation. *Am. J. Clin. Nutr.* **84,** 1277–1289 (2006).

180. Shaikh, S. R. & Edidin, M. Immunosuppressive effects of polyunsaturated fatty acids on antigen presentation by human leukocyte antigen class I molecules. *J. Lipid Res.* **48,** 127–138 (2007).

181. Hughes, D. A. & Pinder, A. C. n−3 Polyunsaturated fatty acids inhibit the antigen-presenting function of human monocytes. *Am. J. Clin. Nutr.* **71,** 357s–360s (2000).

182. Denys, A., Hichami, A. & Khan, N. A. n-3 PUFAs modulate T-cell activation via protein kinase C-alpha and -epsilon and the NF-kappaB signaling pathway. *J. Lipid Res.* **46,** 752–8 (2005).

183. Kim, W. *et al.* Regulatory activity of polyunsaturated fatty acids in T-cell signaling. *Prog. Lipid Res.* **49,** 250–61 (2010).

Appendix A: Preparation and Contents of Reagents

Note: In the following appendix, 'water' refers to high-purity HPLC-MS-grade water.

Preparation of glassware

All glassware used in the preparation of reagents used in proteomics experiments were prepared in order to remove any contaminants and detergents remaining inside the glassware after normal cleaning. Glassware was washed once with water, followed by three washes with MS-grade methanol, and a final wash with water. The glassware was then left to air-dry upside down on absorbent paper.

Reagent recipes

0.05M ammonium bicarbonate (ABC)

0.0197 g ABC (Sigma, 09830) was dissolved in 5 mL water.

Denaturation buffer

In 40 mL 10 mM Tris-Cl pH 8 was dissolved 14.41 g urea and 6.088 g thiourea. The solution was mixed by inversion on a rotator for 1 h until dissolved. The denaturation buffer was stored at -20 °C in 2 mL aliquots and used within 3 months.

5% DOC stock

2.5 g DOC (Sigma, D6750) was dissolved in 25 mL water, and topped up to 50 mL, before shaking on vortex for 5 min. The solution was then mixed by inversion on a rotator for 30 min before transferring to an amber vial for long-term storage at 4 °C.

5X dithiothreitol (DTT) stock for FASP

0.185 g DTT was dissolved in 1.2 mL water.

1.5M HEPES buffer

17.8725 g HEPES (4-(2-Hydroxyethyl)piperazine-1-ethanesulfonic acid, N-(2-hydroxyethyl)piperazine-N'-(2-ethanesulfonic acid), Sigma, H3375) was dissolved in 30 mL MS-grade water. The pH was adjusted to 7.4 using 1 M NaOH, made up by dissolving 2 g NaOH (Merck Millipore, 106462) in 50 mL water and filtered through a 0.2 um filter. After pH adjustment, the HEPES solution was topped up to 50 mL with water and stored at 4 °C.

0.5 M iodoacetamide (IAA) for FASP

0.0185 g IAA (Amresco, M216) was dissolved in 2 mL UA, vortexed and covered with foil.

0.55 M IAA alkylation buffer

0.1017 g IAA was dissolved in 1 mL 0.02 M ABC.

3X RIPA lysis buffer

3X RIPA buffer was prepared by combining 5 mL 1.5 M HEPES buffer, 15 mL 5% DOC, and 15 mL 20% SDS. The solution was warmed to 40 °C on a heating plate and 1.3 g sodium chloride (NaCL, Sigma, S7653) was slowly added. The solution was transferred to amber vials in 7 mL aliquots was stored at room temperature. Just before use, 3 protease inhibitor tablets (cOmplete™ ULTRA Tablets, Mini, EDTA-free, *EASYpack*Protease Inhibitor Cocktail, Roche, 05892791001) were dissolved in 3 mL water and added to 7 mL of the 3X RIPA buffer.

20% sodium dodecyl sulphate (SDS) stock

20 g SDS (Sigma, L4390) was dissolved in 100 mL water warmed to 60 °C and mixed by magnetic stirring at low speed for 30 min. The solution was then stored at room temperature.

Trypsin

Trypsin-Ultra (MS-grade, New England Biolabs (NEB), P8101S) was reconstituted by adding 20 µL water per vial and triturating gently several times.

Trypsin-Ultra Reaction buffer

2X Trypsin-Ultra Reaction buffer (NEB), containing 50 mM Tris-CL, 20 mM $CaCl_2$ at pH8 was used in conjunction with Trypsin-Ultra (NEB, P8101S) according to the manufacturer's instructions.

1 M Tris-Cl, pH 8.5

30.29 g Trizma base (Sigma, T6066) was dissolved in 200 mL water and pH was adjusted to 8.5 using 37% hydrochloric acid (HCl, Sigma, 258148). The solution was topped up to 250 mL with water.

0.1 M Tris-Cl, pH 8.5

3 mL 1 M Tris-Cl, pH 8.5 was added to 27 mL of water and inverted to ensure mixing.

8 M urea buffer (UA)

9.6 g urea (Sigma, 33247) was added to 20 mL 0.1M Tris-Cl pH 8.5 and inverted several times to dissolve.